Analysis of Stem Cell Interactions At Single Cell Resolution

Reimer, Andreas Sven

Awarding institution:
King's College London

Analysis of Stem Cell Interactions At Single Cell Resolution

DIVISION OF GENETICS AND MOLECULAR MEDICINE

King's College London

This dissertation is submitted for the degree of

Doctor of Philosophy

Biotechnology

Andreas Reimer

Watt Laboratory

CENTRE FOR STEM CELLS & REGENERATIVE MEDICINE

London, November 2015

Contents

Let's not forget it's Name is Tangea

- Andreas Reimer

1 Abstract

As a stem cell divides, two daughter cells are produced that either possess stem cell characteristics or become a cell with a more specialized function. Cellular markers have been identified that can be used to describe the phenotype of stem cell progeny. However, the development of tools that allow the description of cellular phenotypes remains a challenge due to the complexity of cellular heterogeneity. In my thesis, I address this problem by developing a phenotyping platform that stimulates cells to either remain in a stem cell state or become a cell with a more specialized function. Multi-well plates were used to create microenvironments that resemble the natural surroundings of stem cells in tissues. High-resolution imaging technology was used to capture the cellular state after exposure to these microenvironments. High-content analysis was applied to generate a detailed description of every cell in the assay. Subsequently, mathematical modelling was used to describe the cell phenotyping profile in each environment. These profiles were then compared to characterise the cellular response to each environment. High-throughput technology was used to understand how topography features affect proliferation of pluripotent stem cells in a xeno-free environment. An algorithm was used to predict whether any given topography will support the pluripotent state. A second algorithm was used to predict an optimised topography. In the final part of my thesis, primary mouse skin fibroblasts and neural progenitor cells that were derived from human iPS cells were exposed to extrinsic cues in cellular assays. While distinct fibroblast subpopulations from neonatal mouse back skin responded to the assay irrespective of media conditions, human iPS cell-derived neural progenitor cells required the addition of extrinsic cues to induce a self-renewal response. Therefore, it is possible to produce neural progenitor cells in vitro and study stem cell characteristics that are known to occur in an in vivo context.

2 Introduction

2.1 Different kinds of stem cells

2.1.1 Pluripotency

Embryonic (ES) stem cells are derived from the inner cell mass of the blastocyst which is formed during early mammalian embryogenesis (Martin et al., 1981). ES cells are pluripotent stem cells and possess two major characteristics which make them particularly suitable for research and potential medical applications. They are capable of unlimited replication *in vitro* and are able to turn into cells from all three germ layers (Nagy et al., 1990; Thomson et al., 1998). As an ES cell divides, it either undergoes self-renewal, giving rise to an almost identical daughter cell or turns into a cell with a specialized function such as contraction in muscle cells, transmission of stimuli in neurons or binding and transporting oxygen in red blood cells (Martin et al., 1981; Nagy et al., 1990). These fundamental properties of pluripotency allow the investigation of elementary principals in developmental biology as well as enable the development of modern approaches to regenerate tissues. The regulatory networks that are responsible for maintaining pluripotency are thought to consist of internal transcription-regulated circuitries and the stem cell microenvironment. Several stimuli act in synergy to maintain the cell in a pluripotent state and prevent differentiation (

In mice, leukemia inhibitory factor (LIF) and other IL-6 family cytokines are known to induce the activation of the JAK/STAT and PI3K pathway, which in turn induces the production of the differentiation inhibitory proteins Oct-4 (POU5F1), Sox-2 and Nanog (Boiani et al., 2005). Furthermore, Nanog activity is indispensable for the maintenance of the pluripotent state through repression of pro-differentiation signals by NF-KB (Torres et al., 2008). *in vitro*, LIF requires either serum or bone morphogenic protein (BMP) for the activation of STAT3 (Ying et al., 2003). To-

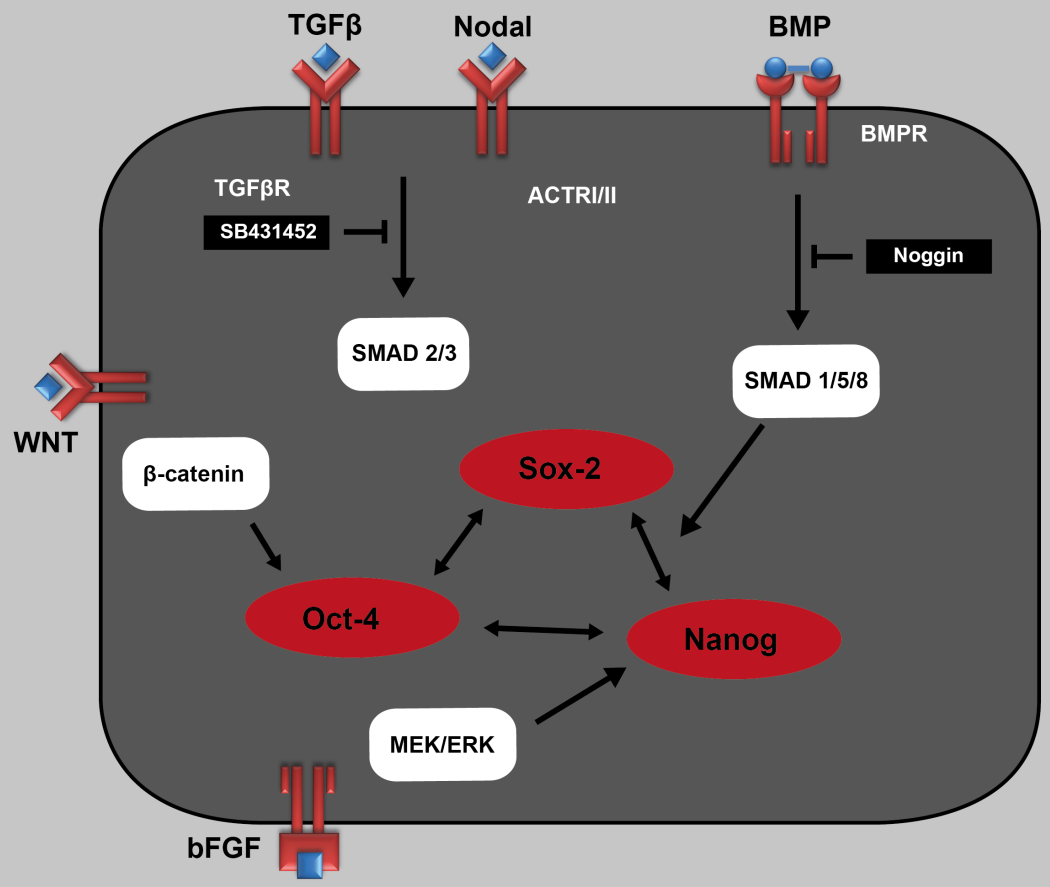

Figure 2.1: Regulatory network of puripotency in humans. hiPSC pluripotency is maintained through the positive feedback loop between Sox-2, Oct-4 and Nanog. Autocrine effects of FGF induce differentiation which is inhibited by the activation of SMADs through TGF-β and BMP. Blocking SMAD activity through Noggin and SB431452 induces differentiation into the ectoderm lineage by inhibiting self-renewal and mesoderm and endoderm differentiation. FGF2 (bFGF) and Wnt promote iPS cell self-renewal through the MEK-ERK pathway and β-catenin dependent Oct-4 activation, respectively. (Redrawn from He et al., 2009)

gether, BMP and LIF counteract the differentiation signaling of FGF via inhibition of the MAPK pathway. The WNT pathway induces Oct-4 expression via β-catenin activation, and along with the JAK/STAT pathway, is involved in the regulation of MYC. Recently, the combination of two inhibitors (2i) of the Erk pathway and of glycogen synthase kinase-3 with LIF was sufficient to maintain pluripotency in mouse embryonic stem cell cultures (Nichols and Smith, 2012).

Despite similarities in pluripotency marker expression profiles increasing evidence suggests that human pluripotent stem cells are at a different developmental stage

to mouse embryonic stem cells. The derivation of post-implantation epiblast stem cells (EpiSC), which resemble the anterior primitive streak, shows that alternative stem cells can be derived from mice (Brons et al., 2007; Kojima et al., 2014; Tesar et al., 2007; Tsakiridis et al., 2014). Human ES cells are considered more related to EpiSCs (Kojima et al., 2014). Recent studies show that it may be possible to convert human ES cells into the naive ground state of pluripotent stem cells using distinct combinations of growth factors and inhibitors (Chan et al., 2013; Gafni et al., 2013; Ware et al., 2014; Takashima et al., 2014). However, these studies lack phenotypic characterization and proof of long term stability.

2.1.2 Induction of pluripotency

In 2006, an innovative way to generate embryonic stem cell-like cells from mouse somatic cells was discovered by Yamanaka and Takahashi (Takahashi et al., 2006). 24 candidate genes, that are indispensable in the maintenance of the pluripotent state, were retrovirally transduced in different combinations into mouse embryonic fibroblasts (MEFs). Remarkably, overexpression of the four transcription factors Sox-2, Oct-4, Klf-4 and c-Myc was sufficient for the induction of pluripotent stem cells. Soon after, the methods for generating induced pluripotent stem (iPS) cells were refined, for example by omitting c-myc, which reduced the tumorigenicity in the reprogrammed cells (Nakagawa et al., 2008). Only one year after the initial discovery in mice, human iPS cells were generated using the same defined factors (Park et al., 2008) or a combination of different factors where Klf-4 and c-MYC were substituted with Lin28 and Nanog (Yu et al., 2007). Apart from fibroblasts, cells derived from each of the three germ layers, including the liver, stomach, pancreas and neural progenitors have been induced to a pluripotent state (Aoi et al., 2008; Stadtfeld et al., 2008). It has been indicated that the efficiency of reprogramming into the pluripotent state is dependent on the tissue of origin (Kim et al., 2010;

Reimer et al., 2012).

Reprogramming somatic cells into pluripotent stem cells has been one of the greatest advancements in stem cell research in the last decades (Yamanaka, 2014). iPS cells have been used to study the biology of natural genetic variations or specific mutations in inherited diseases (Merkle et al, 2013). The production of a large-scale set of iPS cell lines from healthy and patients can be used to generate cell lines that carry the identical genetic background as the donor (McKernan and Watt, 2013). These human iPS cell banks are important to understand genotype-phenotype correlations on a population scale and help advance understanding disease mechanisms and accelerate drug development.

2.1.3 Adult stem cells

In contrast to the pluripotent ability of ES cells, adult stem cells give rise to cells from the tissue they reside in. Distinct and specific microenvironments within each tissue are responsible for the regulation of different stem cell populations to maintain tissue function (He et al., 2009, Watt, 2014). For example, hematopoietic stem cells (HSCs) possess the ability to differentiate into megakaryocytes, erythrocytes, myelocytes and lymphocytes depending on the location within the bone marrow.

The skin consists of distinct layers with specific functions. Within the skin, stem cells reside in, for example, the dermis, which contains a variety of subpopulations of mesenchymal cells, with different locations and functions (Driskell and Watt, 2015). Position/function correlations within the skin have been elucidated using genetically modified mice. At E12.5 mouse dermal cells are capable of differentiating into all the different fibroblast types present in postnatal skin. However, at about E16.5 of mouse development, the dermal mesenchyme undergoes commitment to two different lineages. In late embryonic and neonatal skin, the upper dermal lineage gives rise to papillary fibroblasts, the cells of the arrector pili muscle (APM), the

dermal sheath and the dermal papilla. The lower dermal lineage gives rise to the reticular fibroblasts, which deposit most of the skin fibrillar collagen, pre-adipocytes and mature adipocytes (Driskell et al., 2013). The different fibroblast lineages are functionally significant, because the upper, papillary lineage is required for new hair follicle formation while the lower (or reticular) lineage is responsible for the first wave of dermal repair following wounding (Driskell et al., 2013).

Epidermal Wnt/β-catenin signaling causes profound changes in the underlying dermis, leading to expansion of both the upper and lower dermal lineages, de novo formation of dermal papillae and an increase in adipocyte differentiation (Collins et al., 2011; Donati et al., 2014). In addition, there is compelling evidence that Wnt/β-catenin signaling in fibroblasts regulates the composition of the dermis. β-catenin activation is necessary and sufficient to specify dermal fate in different body regions during mouse embryonic development (Atit et al., 2006; Ohtola et al., 2008). β-catenin activation has a well-characterized inhibitory effect on adipogenic differentiation (Gesta et al., 2007; Kennell and MacDougald, 2005; Longoet al., 2004; Donati et al., 2014), while being required in the dermal papilla to promote hair follicle formation and control dermal papilla activity and size (Enshell-Seijffers et al., 2010; Kaushal et al., 2015). Furthermore, it was shown recently that expression of stabilized β-catenin in fibroblasts of mouse ventral dermis at E16.5 results in progressive skin fibrosis, with thickened collagen fibres and altered collagen fibril morphology (Hamburg-Shields et al., 2015).

Culturing fibroblasts in 3D hydrogels allows clonal expansion as spheroids and can be used to study self-renewal and differentiation capacities (Figure 2.3). It has previously been shown that growing Sox-2 positive cells in the presence of serum retains cell identity and the ability to contribute to hair follicle formation in vivo after transplantation (Driskel et al., 2009).

Position/function correlations can also be observed in the intestine where rapidly

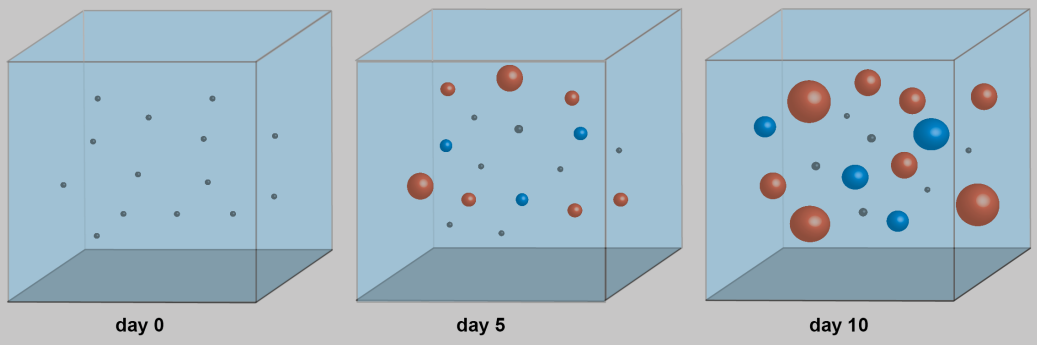

Figure 2.3: Clonal expansion of fibroblasts in 3D hydrogels. (A) Mouse back skin can be digested and flow-sorted for PDGFRα positive cells to isolate fibroblasts which may be cultured in 3D hydrogels. Cells are able to expand at clonal density forming spheres after 5 days and are further matured after 10 days.

cycling and quiescent stem cells lie in distinct positions within the base of the intestinal crypt (Li and Clevers, 2010). Regional specification also occurs during lung development leading to the development of different populations of epithelial cells that function as adult stem cells to maintain tissue homeostasis (Hogan et al., 2014).

In the brain, the subgranular zone (SGZ) of the hippocampus and the subventricular zone (SVZ) of the forebrain physically localize neural stem cells (NSCs) and maintain their functional identity. Type 1 NSCs are characterized by Sox-2, Nestin and glial fibrillary acidic protein (GFAP) expression and are thought to be quiescent stem cells (Gage, et al. 2000; Fukuda et al., 2003; Garcia et al., 2004; Suh et al., 2007). These cells give rise to self-amplifying type 2 NSCs that also express Sox-2 and Nestin but not GFAP. Similar to the SGZ two types of NSCs (type A and type B) are found in the SVZ, the other major NSC niche, which give rise to a Dcx and PSA-NCAM double positive neuroblast population (Consiglio et al., 2004). In the adult SVZ, newly formed neural progenitors migrate through the rostral migratory system and mature into GABAergic interneurons in the olfactory bulb.

2.2 What is the niche?

2.2.1 Function of the niche

The environment of a stem cell provides basic cellular necessities including mechanical support, soluble factors and a hospitable chemical environment (Lane et al., 2014). These environmental factors act in concert to regulate the fate of the stem cell. Interactions with the extracellular matrix (ECM) provide physical support and mechanical signals as well as sequestering locally and systemically produced growth factors, cytokines and other signaling molecules (Lane et al., 2014).

Before providing a description of the individual components of the stem cell environment, or niche, I will first review its functional role. The founding theory of the stem cell niche dates back to the 1970s (Schofield et al., 1978) and was first described by Raymond Schofield as: *"Physical site where stem cells reside and provide an environment that 1) Restricts stem cell entry into the cell cycle and differentiation programs 2) Integrates signals reflecting tissue and organismal state 3) Imposes stem cell features on daughter cells 4) Provides mechanisms for limiting mutational errors."*

We can affirm that the stem cell niche refers to the microenvironment which interacts with stem cells to regulate cell fate. There are two general strategies by which stem cells generate differentiated progeny (Potten et al., 1997). At one extreme, a stem cell divides asymmetrically giving rise to one stem daughter and one daughter that undergoes differentiation (Watt et al., 2000). At the other extreme, stem cells give rise to daughter cells that have a certain probability of being either stem cells or differentiated progenitor (Watt et al., 2000). At any given time, each stem cell gives rise to, on average, one committed and one stem daughter, but asymmetry is achieved on a population basis rather than at individual cell divisions (Watt et al., 2000).

Traditionally, stem cell niche factors are studied in animal models. Genetically modifying mice by replacing or disrupting an existing gene often causes changes in phenotype, including observable abnormalities in tissue architecture and biochemical characteristics (Russel et al., 1985; Zambrowicz et al., 2003). These genetically modified mice can be used to develop animal models that mimic pathological phenotypes of human diseases. However, despite remarkable scientific advances in the last decades the number of drugs against new targets has steadily declined (Lang et al., 2006; McNeish et al., 2015). One reason is that mouse models which often only allow the study of single mutations likely do not reflect the pathogenesis of complex hereditary disorders that have mutations at multiple gene loci (Nguyen et al. (2014); McNeish et al. (2015)). Thus, new strategies to study stem cell properties are required to accelerate advancements of drug discovery. Tissue engineering might allow the development of alternative strategies to improve the validity of animal models.

2.2.2 Different niche components

Stem cell niches are dynamic and highly complex and include acellular and cellular components (Lane et al., 2014; Wagers et al., 2012). A number of regulatory cues that control stem cell fate have been identified and a simplified scheme is depicted in Figure 2.4. Key components of the stem cell niche include cell-cell interactions, secretory factors, inflammation and scarring, extracellular matrix, physical factors such as shear forces and elasticity and environmental signals such as hypoxia.

Interactions within the stem cell niche are either direct, through physical contact, or indirect, through soluble factors. Direct contact can be mediated by a range of receptors such as cell-cell adhesion molecules and receptors with membrane-bound ligands (Lane et al., 2014). For example, Notch signaling acts according to the level of pathway activation both cell autonomously and non-cell autonomously mediating signaling between epidermal cells, fibroblasts and bone marrow-derived cells (Watt

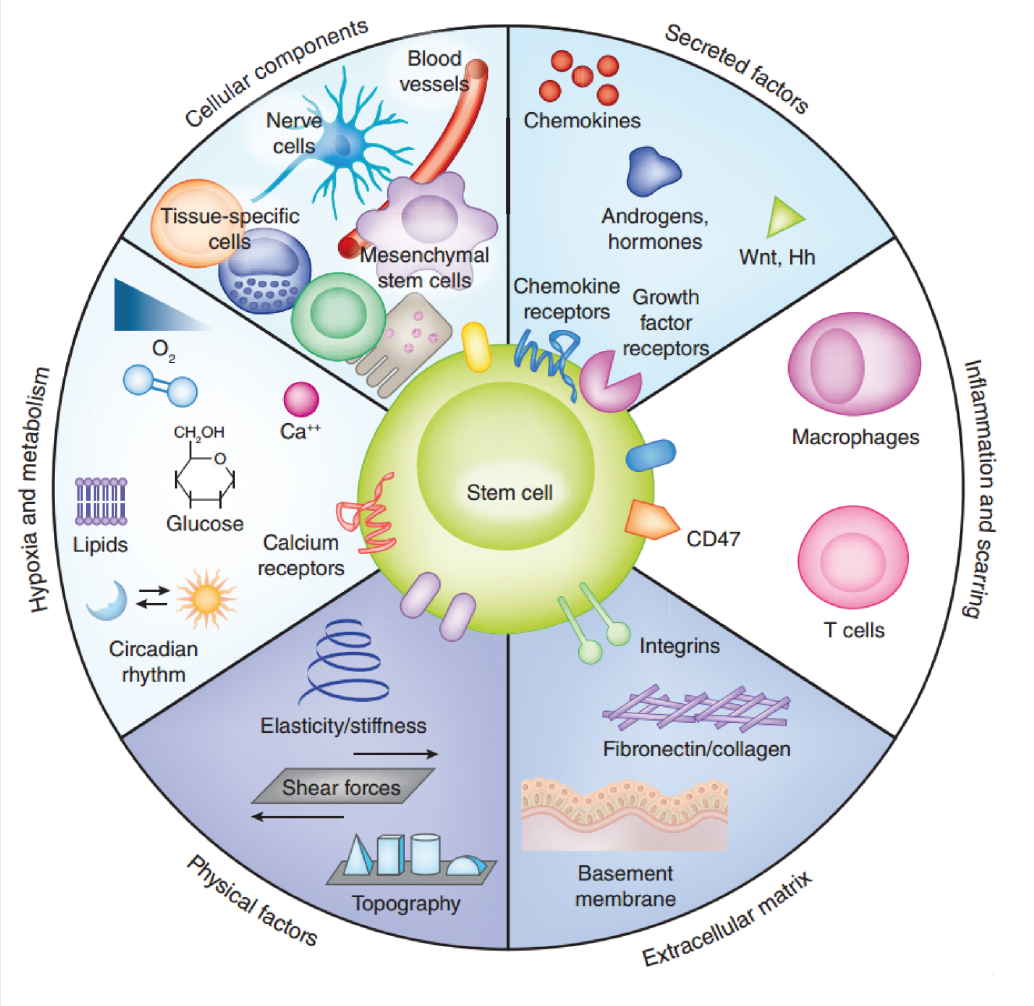

Figure 2.4: Niche Components. Heterologous cell-cell interactions often exhibit complex, bidirectional signaling and are often dependent on cell-cell contact. Secreted and membrane bound factors such as Wnt, stem cell factor (SCF) and Notch directly bind surface receptors to regulate cell fate, self-renewal and polarity. Immunological cells provide dynamic regulation of the niche during inflammation and tissue damage, which is tightly regulated through the presence of „immune privilege“ and evasion from this privilege. ECM proteins are critical for orientation and structural maintenance of the niche, but importantly provide instructive signals through ligand interaction with integrins expressed on stem cells and may also serve as reservoirs for soluble factors. Physical parameters such as shape, stiffness (or elasticity) and blood flow direct stem cell maintenance and differentiation. Many stem cell niches have altered environmental characteristics, such as hypoxia, and require tight metabolic regulation to maintain the long-term quiescence and self-renewal of stem cell populations. (Lane & Watt, 2014)

et al., 2008; Ambler et al., 2010). Experimental ablation of stem cells can be used to study the contribution of niche cells to tissue homeostasis. Laser ablation of skin tissue results in the loss of hair follicle stem cells leads to repopulation of the niche by neighboring epithelial cells that are able to sustain hair regeneration (Rompolas

et al., 2013).

Autocrine and paracrine secreted growth factors bind and activate a specific receptor located on the cell surface or inside the cell. In turn, this receptor activates signal transduction pathways that control stem cell activity (Morrison et al., 2008). These pathways include those of Wnt proteins, fibroblast growth factors (FGF) and leukemia inhibitory factors (LIF). More recently, bone morphogenic proteins (BMPs) have been identified as crucial regulator of stem cell fate (Ying et al., 2010). The induction of BMP signaling in combination with LIF sustains embryonic stem cell self-renewal *in vitro*. Wnt signaling modulates the activity of stem cells and neighboring cells. For example, activation of Wnt signaling expands all compartments of the skin and promotes hair follicle differentiation as well as stimulates melanocyte differentiation. Furthermore, stabilization of β-catenin, the Wnt effector protein, reprograms the adult dermis to a neonatal-like stage (Silva-Vargas et al., 2005; Tanimura et al., 2011; Collins et al., 2011). Although the term niche is defined as a specialized microenvironment, widely diffusible signals such as insulin and serotonin are also critically important to maintain stem cell function (Hsu et al., 2008).

The stem cell niche is a dynamic environment consisting of stem cells that occupy the niche transiently and "permanent residents" (Lane et al., 2014). Permanent cells include cells of the connective tissue, nerve cells and vascular cells. Transient stem cells include migrating immune cells and cells that respond to tissue injury as part of host responses during tissue repair and fibrosis. Modulating the function of immune cells can promote stem cell function. For example, genetically modifying HSCs improves the efficacy of HSC transplants by enhancing tolerogenic expression of surface antigens (Coleman et al., 2013).

The ECM is a key component of the stem cell niche and the composition and interaction with stem cells vary considerably (Lane et al., 2014) (see also Chapter 2.2.3). In the case of connective tissue, fibroblasts tend to be completely surrounded

by ECM proteins, which provide a scaffold that defines tissue architecture (Watt & Huck, 2013). Even in the peripheral blood stream, circulating blood cells are in contact with soluble ECM proteins such as fibronectin. The stiff structure of bones is provided by calcium phosphate that is deposited between collagen fibers. Cartilage ECM deposition is mainly composed of hyaloronan and large proteoglycan aggregates to absorb frictional stress and prevent damage to joints (Watt & Huck, 2013). Given the abundance of ECM in the body (Hynes et al., 2009), it is important to understand the underlying regulatory mechanisms. In addition to providing a structural role, extracellular matrix components also exert functional cues (see Chapter 2.2.3).

Many stem cell populations such as HSCs reside in oxygen-deprived regions (hypoxia), which is required for their survival and maintenance, carrying out glycolysis rather than mitochondrial oxidative phosphorylation (Kimura et al., 2012). Growing some mammalian cell types in culture under hypoxic conditions can be beneficial for maintaining growth and function after transplantation (Muscari et al., 2013). Hypoxia inducible factor 1α (HIF-1α) is highly elevated in these cells and its stabilization through small molecules such as dimethyloxalyl glycine or dimethyl prostaglandin E2 improve long-term HSC function in vivo (Speth et al., 2014; Forristal et al., 2013).

2.2.3 Biophysical properties of the niche

Depending on the cell type and geometry of the ECM have a profound influence on a number of cell properties including cell adhesion, migration and state (

Tan et al. used a microfabricated array with posts varying in mechanical compliance to demonstrate that not only biochemical signals but also mechanical forces regulate cell adhesion (Tan et al. 2003) (Figure 2.5 B). RhoA protein was identified as mediator of cell shape responses during lineage commitment of human mesenchy-

mal stem cells (hMSCs) (McBeath et al., 2004). If ROCK, the downstream effector of RhoA, was constitutively activated cells committed to differentiation independently of cell shape changes. Manipulating the cytoskeleton of keratinocytes affects the differentiation response indicating that cell shape is directly linked to cell fate independently of ECM composition or density (Connelly et al., 2010). Actin and serum response factor were shown to be key regulators to regulate cell shape-dependent differentiation. Furthermore, epidermal stem cell differentiation was modified through varying the concentration of hydrogel crosslinker that was conjugated with collagen fibers (Trappmann et al., 2012) (Figure 2.5 C). It is possible that stem cells respond to the mechanical force of substrate bound ECM to make cell fate decisions.

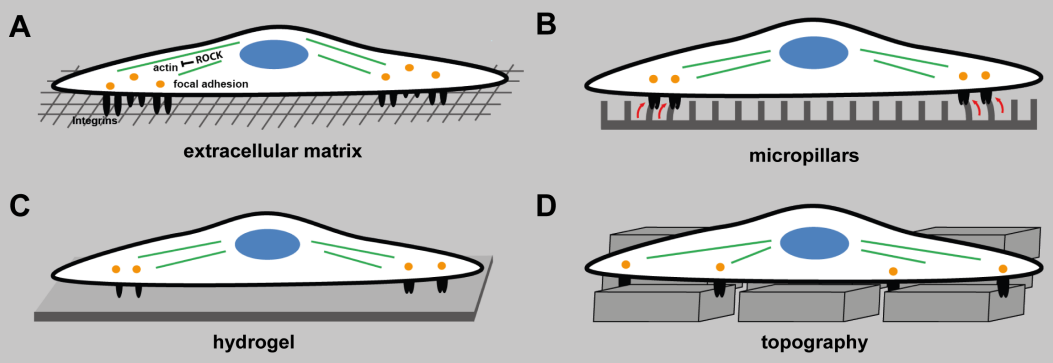

Figure 2.5: Design of biomaterial substrates to model components of the extracellular matrix. (A) Cells adhere and attach to the extracellular matrix via integrins which cluster and form focal adhesion sites and transmit mechanical signals from the environment. ROCK, the downstream mediator of RhoA, is a key mediator of actin organisation and regulator of cell migration. (B) Regulating the mechanical force by varying the mechanical compliance of micropillars affects cell adhesion (Guilak et al., 2009). (C) Varying the crosslinker concentration of hydrogels regulates cell differentiation. (D) Surface topography affects adhesion and self-renewal of human iPS cells.

Although cell culture surfaces are typically flat, there is good evidence that cells also respond to topographical features at the nano- and micro-scale (Mashinchian et al., 2015) (Figure 2.5 D). Surfaces that incorporate topographical features can support the growth and differentiation of mouse and human pluripotent stem cells in serum-containing medium (Markert et al.; Pan et al., 2013; Lue et al., 2014). By assaying cell behaviour quantitatively on a library of different topographical features

(Unadkat et al., 2009) and applying computational analysis it is possible to predict cellular responses to topographical features prior to experimental analysis (Hulsman et al., 2014).

2.2.4 What does the niche mean for pluripotent stem cells?

Undifferentiated human ES cells express a subset of integrins that are required for attachment to the ECM. The integrin $\alpha 6\beta 1$ interacts with laminins found in Matrigel (Vuoristo S et al., 2008). $\alpha 5\beta 1$ and $\alpha\nu\beta 1$ interact with fibronectin and $\alpha\nu\beta 5$ and $\alpha\nu\beta 1$ interact with vitronectin via the arginine-glycine-aspartate (RGD) binding motif (Rowland et al., 2010; Ruoslahti, 1991; Braam et al., 2008; Vuoristo et al., 2008). After the initial cell-matrix adhesion junctional complexes are formed through which mechanical forces and regulatory signals are transmitted.

Most of the current understanding on the effects of mechanical force in human stem cell fate specification is based on studies with adult human stem cells. Mechanisms underlying the regulation of pluripotent stem cell (PSC) fate remain largely elusive. Nonetheless, distinct biomaterial substrates have been used to improve the efficiency of differentiation protocols. For example, differentiating human iPS cells into neuroectodermal precursor cells in the presence of serum was more efficient on microstructured PDMS substrates compared to a flat matrigel-coated surface (Pan et al., 2013). Integrins and E-cadherins have been demonstrated to affect human PSC fate. E-cadherin mediated adhesion is required for the maintenance of the pluripotent state while enhanced integrin-mediated forces promote differentiation (Harb et al., 2008; Li et al., 2010; Chowdhury et al., 2009). Interestingly, the two opposing cell fate instructions through E-cadherin and integrin adhesion act via the same Rho-ROCK myosin II signaling complex. In contrast, integrin-activated Rho-ROCK-myosin II signaling opposes signaling by cadherin activated Rho or Rac signaling. However, it remains unclear how integrin and cadherin regulate PSC

differentiation and self-renewal through a common signaling pathway.

Using cell micropatterning technology Toh et al. recently addressed this issue by modulating the relative spatial distribution and strength of integrin and cadherin adhesion within a PSC colony (Toh et al., 2015). It was shown that localized integrin adhesion is dominant over E-cadherin signaling by recruiting the Rho-ROCK activated myosin II complex away from E-cadherin mediated cell-cell junctions, resulting in a heterogeneous cell population (Toh et al., 2015). Understanding the signaling components of how human PSCs sense physical cues from the environment would allow a more effective control of stem cell fate and potentially facilitate the development of PSC-compatible substrates.

2.2.5 Expansion of human iPS cells on substrates

The derivation and expansion of human iPS cells using traditional methods are generally associated with safety and scalability issues. Many expansion protocols rely on feeder cells to provide essential growth factors, cytokines and ECM molecules to support the self-renewal of iPS cells. However, it is difficult to ensure reproducibility of feeder-supported cultures due to the poorly defined chemical contents (Villa-Diaz et al, 2009). Potentially animal-derived pathogens associated with feeder layers increase the risk of contamination limiting the development of clinically compliant therapeutics. To overcome these limitations novel biomaterials have recently been explored. Engineered biomaterials, ranging from complex ECM-substitutes to simple UV/ozone treated polystyrene (Saha et al., 2011), are becoming progressively simpler (

Matrigel has been widely used to substitute feeder layers but due to its undefined chemical composition and being animal-derived makes it unreliable and challenging to use in large-scale production (Katon et al, 1982). Several cell adhesive ECM-proteins including the laminin isoform LN521 (Amit et al, 2004; Kalaskar et

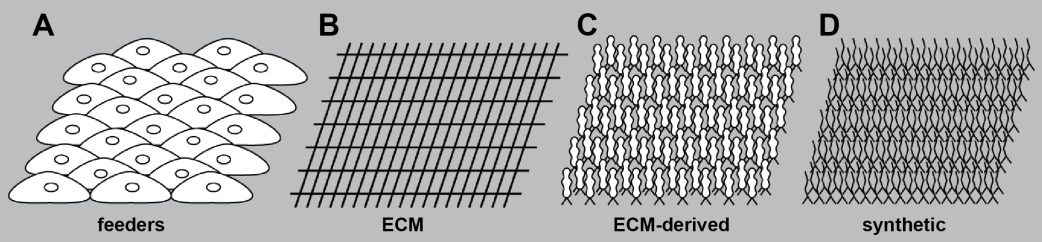

Figure 2.6: The development of PSC expansion substrates. (A) Irradiated MEF feeder layers support the growth of hPSCs by providing secretome contents. (B) Undefined ECM protein mixtures such as Matrigel can be extracted from inactivated cell lines and are routinely used for maintining hPSCs. (C) ECM-derived substrates including vitronectin derived peptides such as heparin binding peptide, GKKQRFRHRNRKG (Klim et al., 2010). (D) Synthetic polymeric substrates support the self-renewal of hPSCs. (Adapted from Tong et al., 2015.)

al, 2013) and vitronectin (Braam et al, 2008; Chen et al, 2011) have been identified as promising substrate for iPS cell expansion. But despite improved efficiency and reproducibility ECM-derived substrates are not ideal due to their large, temperature/pH-sensitive nature, making them unstable for long-term use (Wong et al, 2014).

Synthetic peptides and polymers that mimic biological motifs such as the heparin binding site have been developed to allow long term growth and scalability (Klim et al., 2010). For example, the conserved peptide fragment QHREDGS previously identified in angiopoietin-1 was responsible for endothelial cell adhesion and vascularization (Miklas et al., 2013). When tethered to a polyethylene glycol (PEG) hydrogel surface the peptide improved the adhesion of iPS cells via β51-integrin binding (Dang et al., 2014). In conjunction with newly identified chemically defined culture media (Chen et al., 2011), synthetic substrates could provide a new avenue for the large-scale production of clinical grade human iPS cells.

One major advantage of biomaterial substrates is the reduced batch-to-batch variability and enhanced scalability. Furthermore, these substrates can be implemented in high-throughput platforms to investigate simultaneous interactions with growth factors and molecular compounds (see Chapter 2). Indeed, microarray technology has revolutionized genomics and drug discovery by allowing cost effective, multi-

plexed screening of thousands of miniaturized spots (Lander et al., 2011). Miniaturizing experimental design permits high throughput parameter identification which is of great significance to identify novel biomaterials (Mei et al, 2007; Cimetta et al, 2013). Mei et al. tested a library of synthetic substrates for their ability to support pluripotency and developed structure-function relationshuman iPS between material properties and cell phenotypes (Mei et al., 2007). Substrates generated from monomers with high acrylate content were identified as optimal substrate for hESCs self-renewal, binding via $\alpha\nu\beta3$ and $\alpha\nu\beta5$ integrin to adsorbed vitronectin.

2.3 Analysis of stem cell interactions

2.3.1 High-throughput screening

High-throughput screening (HTS) is widely used in the pharmaceutical industry for drug discovery. Most commonly, a large library of compounds is assayed for basic biological or biochemical activity using automated robotic technologies. However, to enable the integration of biological complexity into large-scale screens new cellular imaging and analysis technologies need to be developed (

For example, Desbordes et al. screened a library of compounds for the ability to regulate self-renewal and differentiation of human pluripotent stem cells (PSCs) (Desbordes et al., 2008). Using automated microscopy and image analysis, the expression of the pluripotency marker Oct-4 was used to categorize compounds into promoters of self-renewal or differentiation. Further analysis has revealed potential downstream signaling factors of the self-renewal response and early lineage commitment during differentiation. HTS has also been used to elucidate specific signaling components during endoderm differentiation (Loh et al., 2014). In a series of systematic screens, Loh et al. showed that during embryonic development BMP, FGF, TGF-β, and Wnt initially establish the primitive streak and induce anteroposterior

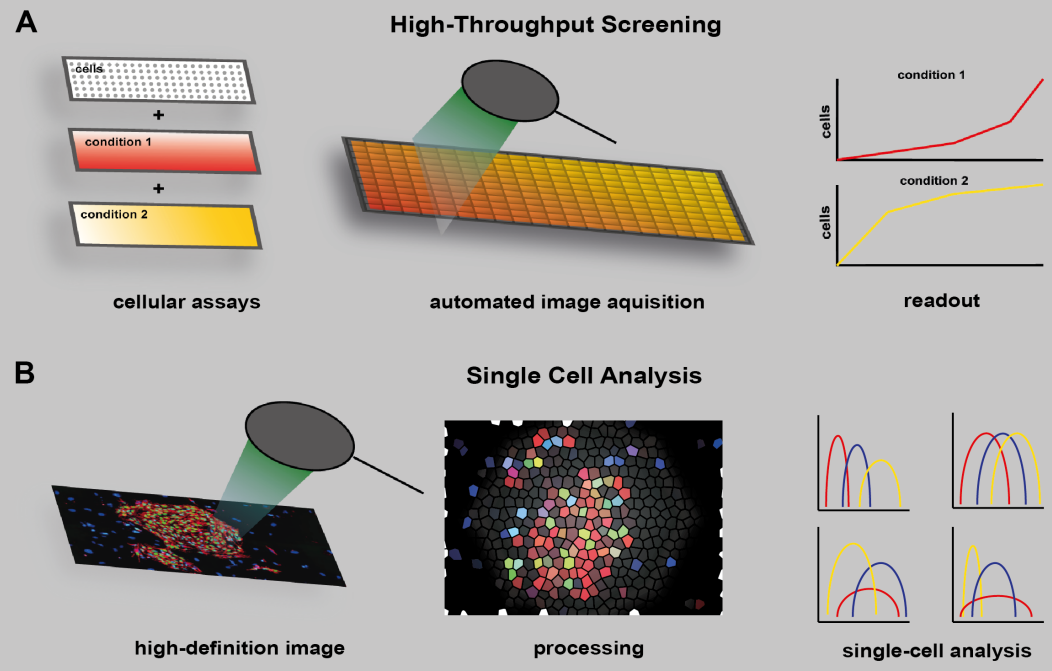

Figure 2.7: High-throughput screening to identify cellular phenotypes. (A) To generate distinct assay conditions molecular components may be added to the culture. Images for each assay condition can be aquired using automated technology to obtain simple readouts on cellular activity. (B) High-Definition images can be processed with algorithms to calculate sophisticated cellular phenotypes at the single cell resolution.

patterning. Interestingly, the screening strategy revealed that BMP and Wnt impose opposite signals depending on the time of exposure during ES cell differentiation. The addition of BMP and Wnt protein to the culture medium during the first 24 hrs specified the anteriormost primitive streak but induced an endoderm phenotype if added on day 2 and 3.

To allow the simultaneous investigation of mechanical and biological cues within the same system Gobaa et al. generated a high-throughput microwell platform (Gobaa et al, 2011, Kobel et al., 2009). Not fully cross-linked polyethylene glycol (PEG) was chemically functionalized with proteins of interest and stamped with a PDMS template to form micrpatterns in the gel (Kobel et al., 2009). Using this platform, Laminin 1 and Jagged 1, which are known NSC signaling regulators, were found to stimulate neural stem cell proliferation independently and in

a non-synergistic way. To investigate the impact of physical cues on cell behavior a high-throughput platform called Topochip was designed to identify correlations of topography cues to biological responses (Unadkat et al., 2011). Novel surface features that enhanced hMSCs proliferation or osteogenic differentiation were identified. Subsequent mathematical analysis of morphological parameters revealed correlations between surface features and cell properties such as nuclei shape (Hulsman et al., 2015).

Ranga et al. developed a screening platform that allows the modular design of stem cell microenvironments to dissect the role of niche factors (Ranga et al., 2014) in 3D hydrogels. Using robotic nanolitre liquid-dispensing technology substrate elasticity, cell-cell interaction and soluble factors were investigated in 1000 unique microenvironments. Systems-based analysis techniques allowed the identification of previously unknown relationshuman iPS between stem cell components regulating stem cell fate.

These and other complex regulatory mechanisms are difficult to dissect using traditional low-throughput experiments. Despite the ability to quickly conduct a large number of experiments simultaneously, high-throughput screens often suffer from phenotypic characterization. While the study by Desbordes et al. considered only one protein (Oct-4) for initial scoring, Loh et al. used microarray and qPCR analysis where morphological information is lost. The Topochip screening strategy on the other hand includes multiple parameters, which maximizes readout information in the initial screen.

2.3.2 Image processing

Image-based analysis is widely used to quantitate biological readouts and characterise biological processes in phenotypic screens. A change in cellular phenotype may be identified by a set of cell surface antigens which can be labelled with fluo-

rescently tagged antibodies. Cell morphology can also be detected to describe the state of a cell. For example, the mesenchymal-to-epithelial transition (MET) during reprogramming of somatic cells to iPS cells (Samavarchi-Tehrani et al., 2010) can easily be visualized without antibody labeling. In some instances, specific markers that reflect the endpoint of the assay may not be available. In such cases, morphometric descriptors can be used to cluster genetic effects or compounds based on their phenotypic signatures. Furthermore, morphometric screens can make use of more standardized dyes such as Phalloidin or DAPI that are more economical. For example, multi-parametric analysis of cytoskeletal features has been performed on mesenchymal stem cells to determine cell fate decisions (Treiser et al., 2010; Kilian et al., 2010). Yin et al. used high content analysis to develop quantitative methods describing that Drosophila haemocytes in culture are a heterogeneous mixture of five discrete morphologies (Yin et al. 2012). The group also showed that the tumor suppressor gene PTEN decreases the heterogeneity of the population leading to more rounded and elongated cell shapes. A comprehensive analysis of shape diversity through systematic RNAi screening revealed that a dynamic cross-talk between Rho and Rac can generate different cell shapes during cell migration which can lead to morphological heterogeneity in genetically identical populations (Sailem et al., 2014). Conclusively, in combination with immunohistochemistry the analysis of cell morphology can be a powerful tool to define cell state and aid to the understanding of complex interactions that occur in the stem cell environment.

2.3.3 Mathematical modelling

In any hypothesis-driven investigation, and especially in high-throughput screens, it is important to define an experimental readout and test its significance. The principal behind mathematical modeling to understand biological complexity is not new and originates from a seminal publication by Alan Turing proposing that a

pattern can emerge in an initial homogeneous mixture of two chemicals (Turing et al., 1952). Physical phenomena have been described by mathematical equations for much longer. Galileo observed that "Nature's great book is written in mathematical language" four hundred years ago. However, biological systems are more complex due to non-linear interactions of many heterogeneous species and a clearer picture is only beginning to emerge.

Various modeling approaches have been used to address specific questions about a system (Tomlin et al., 2007). Strategies for formulating modeling architectures include "Bottom-up" and "Top-down" approaches. Both strategies aim to process information and order knowledge. The "Bottom-up" approach includes the collection of data from resource data banks while the "Top-down" approach originates from experimental data (Shahzad & Loor, 2012). Designing such models requires the collection of large amounts of experimental data which was facilitated by the development high-throughput technologies. Models aid by helping to generate hypotheses and ideally should suggest new experiments that could be used to extend and refine the model (Editors, 2000). It has been suggested that a model's value should not be judged by its complexity but what can be learned from it (Mogilner et al., 2012).

3 Aims of this Thesis

The ability to model stem cell interactions with the niche has a great potential for applications in the field of regenerative medicine. Recent studies show that the stimulation of stem cells with extrinsic factors has a profound influence on the fate of stem cells (Lane et al., 2014). The ability to control stem cell fate can facilitate the development of novel strategies for tissue engineering. To develop strategies that would allow the study of stem cell responses in any given environment, a high-content imaging system was established that allows the extraction of quantitative data at single cell resolution. A high-throughput assay was established to investigate the cell fate response of pluripotent stem cells that were dissociated in distinct environments. A cell phenotyping algorithm was developed for the analysis of pluripotent stem cells in self-renewing and differentiating conditions. To understand the cell-to-substrate response of human iPS cells in a xeno-free environment, the established assay conditions were used to study surface topographies. A mathematical model was developed that allows the prediction of how stem cells would respond to any given surface structure. The high-content imaging system was also used to characterize the self-renewing ability of neural progenitor cells at single cell resolution. Finally, a three-dimensional hydrogel assay was used to characterise the function of distinct fibroblast populations and test the effect of epidermal Wnt activation on the differentiation phenotype. The following research questions were addressed:

1. How do human iPS cells respond to distinct extracellular matrix environments?
2. What is the optimal topography for the self-renewal of human iPS cells?
3. What is the effect of Sonic Hedgehog on the self-renewal ability of human iPS cell-derived neural progenitor cells?
4. What is the effect of epidermal Wnt activation on the differentiation potential of fibroblasts?

4 Materials and Methods

4.1 Materials

4.1.1 Cell lines

Cell line	Description
BOB	wild-type human iPS cell line (Yusa et al., 2011)
Flow-sortted fibroblasts	primary cells, isolated from P2-5 postnatal pubs and flow sorted using a FACS Aria II
SPC clone 2	wild-type human iPS cell line (Cocks et al., 2014)
Mouse embryonic fibroblasts (MEFs)	primary cells, isolated from embryos at CSCR, Cambridge
NPC-iPS	wild-type, derived from human iPS cell lines SPC clone 2 and BOB

4.1.2 Media, supplements and solutions

Name/Product	Composition/Company
0.05% Trypsin-EDTA	0.25% Trypsin-EDTA solution (Sigma) diluted in PBS
0.2% Triton X-100	Triton X-100 (Sigma Aldrich)
100% TritonX-100 stock	Triton X-100 diluted in 1 x PBS
4% Paraformaldehyde	dissolved in water according to manufacturer's instructions (Sigma Aldrich)

8% Paraformaldehyde	dissolved in water according to manufacturer's instructions (Sigma Aldrich)
10 x PBS (stock)	Sigma-Aldrich
Blocking buffer	10% donkey serum (Abcam), 0.05% Triton-X in PBS
Click-it EdU Assay kit	Life technologies
Essential 8 medium	Basal medium with E8 supplements (Life Technologies
Gelatin solution	0.1% (w/v) gelatin (Sigma Aldrich) in water, autoclaved
KSR medium	advanced DMEM (Life Technologies) supplemented with 20% Knockout Serum Replacer (KSR, Life Technologies), 4 ng/ml FGF (Peprotech), 1% Penicillin/Streptomycin (PAA) (100x), 50 nM β-Mercaptoethanol (Sigma Aldrich)
MEF medium	DMEM (Life Technologies) supplemented with 10% FBS (PAA) and 1% P/S (Sigma Aldrich)
N2/B27 medium	Basal medium with N2/B27 supplement (Life Technologies
Penicillin-Streptomycin (P/S)	diluted 1 to 100, Sigma Aldrich
Staining buffer	1% donkey serum (Abcam), 0.05% Triton-X in PBS
Amniomax	basal medium with supplements (Life Technologies)

Extracel-xTM hydrogel kit	Glycosan Biosystems

4.1.3 Chemicals and reagents

Product	Company
4',6'Damidino2phenylindol (DAPI)	Sigma Aldrich
CellMask	Life Technologies
Dimethylsulfoxide (DMSO)	Sigma Aldrich
EDTA (Versene)	Life Technologies
Extracel-x Hydrogel kit	Glycusan Biosystems
FGF8	Peprotech
Geltrex	Life Technologies
HBSS	Life Technologies
Laminin	Life Technologies
LipidTox	Life Technologies
Noggin	Peprotech
Phalloidin diluted 1 to 50	Life Technologies
Poly-L-ornithine hydrobromide	Sigma Aldrich
Rho-associated protein kinase inhibitor	Sigma Aldrich
Sonic hedgehog	R&D Systems
β-Mercaptoethanol	Sigma Aldrich

4.1.4 Enzymes

Name	Company
1 mg/ml collagenase IV solution	collagenase IV (Life Technologies) dissolved in water, sterile filtered

1 mg/ml dispase	dispase (SLS) dissolved in advanced DMEM, sterile filtered
Accutase	Life Technologies
Thermolysin	Sigma
TrypLE	Life Technologies

4.1.5 Labware

Product	**Company**
Cell culture dishes	BD Biosciences
Cell culture multiple-well plates	Corning
Cell strainer and mesh, 40 μm	BD Biosciences
Cryo vials	Fisher Scientific
Falcon tubes	BD Biosciences
Glass-bottom 6-well plates	IBL Baustoff + Labor GmbH
Stripettes	Appleton Woods

4.1.6 Antibodies

Product	Dilution	Species	Company
Human Mitochondria	1:100	mouse	Millipore
Nanog	1:100	goat	R&D Systems
Nestin	1:100	mouse	Abcam
Oct-4	1:100	mouse	Santa Cruz
Sox-1	1:100	goat	R&D Systems
Sox-2	1:100	goat	R&D Systems
Tra-1-60	1:100	mouse	Santa Cruz
Dlk-1	1:100	rat	MBL International
Sca	1:100	mouse	BD Biosciences
CD26	1:100	mouse	eBioscience
ITG6A	1:100	rat	BD Bioscience
Pdgfr-α	1:100	goat	R&D Systems
anti-Rfp	1:100	rabbit	Rockland

4.1.7 Instruments

Product	Company
A1R confocal microscope	Nikon
Centrifuge, 5810R	Eppendorf
FACS Aria II	BD Biosciences
Inverse microscope Eclipse	Leica DMIL with DFC 350 camera
Neubauer Counting Chamber	Thermo Scientific
Operetta High-Content Imaging System	Perkin Elmer
Thermomixer	Eppendorf

4.1.8 Software

Program	Application
Adobe Illustrator	illustrations and figures
Adobe Photoshop	image processing
Gene-E	graphs
GraphPad Prism 6.0	graphs
Harmony	image analysis
Office 2007	figures and calculations

4.2 Cell Culture

4.2.1 Preparation of feeder mouse embryonic fibroblasts

Frozen primary mouse embryonic fibroblasts (MEFs) (cells from one embryo) were thawed, added to a 15-cm culture dish and diluted to a final volume of 20 ml in culture medium (Dulbecco's Modified Eagle Medium (DMEM), Life Technologies) supplemented with 10% Fetal Bovine Serum (FBS, PAA) and incubated at 37 °C and 5% CO_2. After reaching 100% confluency, the cells were washed twice with 1 x PBS (Sigma Aldrich) and trypsinised in 5 ml 0.05% Trypsin-EDTA solution (Sigma Aldrich) for 5 minutes at 37 °C. To stop trypsinisation, 10 ml culture medium was added and the cells were resuspended to make a single cell solution and transferred to a 50-ml falcon tube. Next, the supernatant was aspirated, the cells were resuspended and reseeded in a 1:3 ratio onto fresh 15-cm culture dishes (BD Biosciences) containing 20 ml culture medium. Cells were passaged four times to make a total of 54 culture dishes. After reaching 100% confluency, the cells were trypsinised as before, resuspended and transferred to two 50-ml falcon tubes (SLS). On ice, the cells were γ-irradiated with 3000 rad to disrupt cell proliferation. After irradiation, the cells were centrifuged at 300g and 4 °C and the supernatant was aspirated.

After resuspension in freeze medium (90% FBS/ 10% dimethylsulfoxide (DMSO), Life Technologies), irradiated MEFs were frozen at -80 °C in aliquots of 7×10^5 and 1.5×10^6 cells per cryo tube (SLS). On the next day, the frozen cells were transferred to liquid nitrogen for long term storage.

4.2.2 Maintenance of human iPS cells on feeders

Human iPS cell lines BOB (Yusa et al., 2011, kind gift of Dr. Ludovic Vallier, Anne McLaren Laboratory for Regnerative Medicine, Cambridge) and SPC clone 2 (Cocks et al., 2014, kind gift of Prof. Jack Price, Institute of Psychiatry, KCL London) were cultured in advanced DMEM (Life Technologies) supplemented with 20% Knockout Serum Replacer (KSR, Life Technologies), 4 ng/ml FGF (Peprotech), 1% Penicillin/Streptomycin (PAA) (100x) and 50 nM β-Mercaptoethanol (Sigma Aldrich) on irradiated feeder MEFs. To prepare the feeder MEFs, the dish was first coated with 0.1% gelatin solution (Sigma Aldrich) and incubated at 37 °C for at least 15 minutes. Irradiated feeder MEFs were seeded at least 5 hours before the addition of stem cells. For multi-well plates, 1.5×10^6 irradiated MEFs were used and 7×10^5 for a 6 cm dish.

Stem cells were passaged every 4-6 days depending on the growth rate and the culture medium was changed every day. For passaging, the cells were washed with 1x PBS and slowly dissociated from the feeder layer by adding 2 ml dissociation solution (1mg/ml collagenase IV solution (Life Technologies)/ 1mg/ml dispase (SLS)) to each well of a 6-well plate and incubation at 37 °C and 5 % CO_2. After 45 minutes, the dissociation solution with floating stem cell colonies was transferred to a 15 ml falcon tube. Each well was then washed with 2 ml culture medium and added to the same tube. Next, the clumps were left on the bench to settle to the bottom of the tube for 2-3 minutes. The dissociation solution containing single cells and feeder MEFs was aspirated without disturbing the pellet and washed with 2 ml culture

medium. The cells were washed a total of 3 times, each time leaving the clumps to settle and aspirating the medium. At the last wash step, 1 ml culture medium was added and the clumps were carefully broken into smaller pieces using a 1-ml pipette tip by resuspending the pellet 3-10 times depending on the clump size. 4 ml culture medium was added to create a gradient with different colony sizes where smaller clumps settled slower than larger clumps. Intermediate chunks were taken up from the middle of the gradient and added drop-wise to the prepared feeder layer. The number of colonies (approximately 100 - 200) that were added to each well was adjusted such that sufficient room was allowed for each colony to attach to the feeders and expanded without growing into neighboring colonies.

4.2.3 Thawing of frozen human iPS cells

Frozen cells were thawed quickly in a 37 °C water bath until just a small amount of solution remained frozen. 1 ml pre-warmed culture medium containing 10 μM Rho-associated protein kinase (ROCK) inhibitor (Sigma Aldrich) was added slowly drop by drop and the cells were transferred into a 15-ml falcon tube containing 9 ml culture medium with 10 μM ROCK inhibitor. After centrifugation for 5 minutes at 300g, the supernatant was aspirated and the cells were resuspended in culture medium containing 10 μM ROCK inhibitor.

4.2.4 Preparation of Geltrex-coated plates

Pre-aliquoted Geltrex (Life Technologies) was defrosted on ice and resuspended in ice-cold DMEM at a ratio 1:10. 1.5 ml Geltrex solution was added to each well of a 6-well plate and incubated at 37 °C for 45 minutes and used immediately. For 96-well plates, 50 μl Geltrex solution was used per well.

4.2.5 Maintenance of human iPS cells in feeder-free conditions

Human iPS cell line SPC clone 2 was maintained in Geltrex-coated 6-well plates in Essential 8 medium according to the manufacturer's instructions. In brief, when the cells reached 70% confluency, and before colonies had begun to merge, cells were washed with HBSS (Life Technologies), treated with EDTA (Life Technologies) for 5 minutes at 37 °C and removed from the dish by gentle pipetting. Cell clumps were transferred to fresh Geltrex-coated 6-well plates at a splitting ratio of 1:6 or 1:12, depending on the growth rate.

4.2.6 Neural differentiation of pluripotent stem cells

Human iPS cells were differentiated into neural progenitor cells via embryoid bodies (EBs) as previously described (Boyer et al., 2012). Briefly, human iPS cell colonies were lifted off the feeder layer as described above and added to a 10 cm low adhesive dish (Corning) in DMEM supplemented with N2/B27 medium (Life Technologies) in the presence of 200 ng/ml Noggin (Peprotech). The medium was changed every other day during neural induction. After 7 days, EBs were transferred to a poly-L-ornithine (Sigma)/laminin (Life Technologies) (P/L) coated dish to allow neurite outgrowth and rosette formation. On day 14 after the start of differentiation, EBs containing rosettes were picked and seeded at a high density onto freshly P/L-coated 6-well plates. 1 mg/ml laminin was added to the medium to promote proliferation. After a further 7 days, cells were trypsinised with TrypLE (Life Technologies) and seeded onto P/L-coated 6-well plates in neural progenitor medium (DMEM supplemented with N2/B27, 200 ng/ml sonic hedgehog (SHH) (R&D Systems), 100 ng/ml FGF8 (Peprotech) and 1 mg/ml laminin). Thereafter, cells were passaged once a week or when necessary and fresh neural progenitor medium was added every other day.

5 Results

5.1 Effect of ECM on the self-renewal ability of human iPS cells

5.1.1 Seeding of human iPS cells

It is well established that the self-renewal of human iPS cells relies on appropriate interaction with the ECM. In the past, a variety of ECM proteins have been associated with being supportive of pluripotency. Geltrex, for example, is a basement membrane extract purified from murine Engelbreth-Holm-Swarm tumour and is commonly used as ECM substitute (Chen et al., 2011). However, it remains unclear how human iPS cells react to different ECM compositions. To test the self-renewal ability of human iPS cells to the ECM and to distinct microenvironmental signals contained in culture media, I aimed to establish a seeding strategy that allows the quantification of human iPS cell responses at the single cell level.

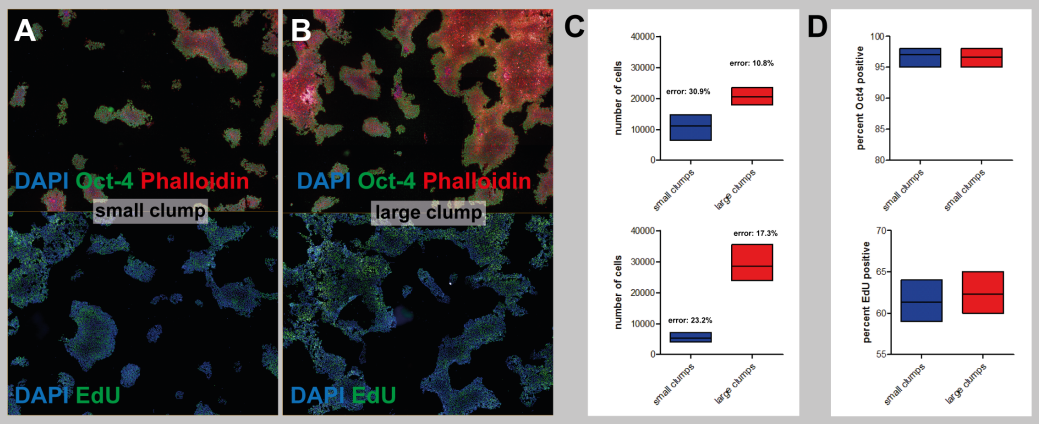

Figure 5.1.: Seeding of human iPS cells in clumps. (A) Small and (B) large iPS cell clumps were seeded in triplicates onto geltrex-coated plates. To assess the reproducibility of cell seeding the number of cells was counted (C and D). The percentages of (E) Oct-4 and (D) EdU positive cells were determined.

Human iPS cells were dissociated into clumps using EDTA (see chapter 3.2.5) and

seeded in triplicates into a 96-well plate. The cells were grown for 48 hours in an incubator and EdU was added 30 minutes before fixation to label proliferating cells. The number of pluripotent cells was quantified by Oct-4 expression. Nine high-resolution images were taken for each condition and replicate and quantified using an Operetta system (see chapter 5.2). One representative image of each sample is shown in (Figure 5.1 A and B. The error (percent standard deviation of the mean) between technical replicates was greater than 20 percent for small clumps and more than 10 percent for large clumps (

To achieve better control of cell number at the time of seeding, human iPS cell colonies were dissociated into single cells using Accutase. Cells were counted and seeded at different densities in the presence and absence of Rho-associated kinase (ROCK) inhibitor, which has previously been shown to reduce the rate of apoptosis (Saha et al., 2011). In the absence of the inhibitor, cells survived only at the highest seeding density whereas the inhibitor allowed survival of iPS cells at lower seeding densities after 48 hours Figure 5.2 A and B). In the presence of ROCK inhibitor, the cell quality at different seeding densities was further investigated. The error was less than 5% between three technical replicates at all seeding densities. The cell number and Oct-4 expression was consistent at all seeding densities (Figure 5.2 C and D). However, the intermediate seeding density showed a higher rate of proliferation compared to low and high seeding densities (Figure 5.2 E and F). It is possible that low cell numbers prevent proliferation due to reduced cell-cell contact which is known to be important in iPS cell cultures (Chen et al., 2011). The average cell size and nucleus area was greater at the lowest seeding density compared to higher seeding densities (Figure 5.2 G and H). At the same time, nuclei possessed an elongated phenotype if the seeding density was low. Thus, a reduced rate of proliferation can be associated with a change in cellular and nuclear morphology.

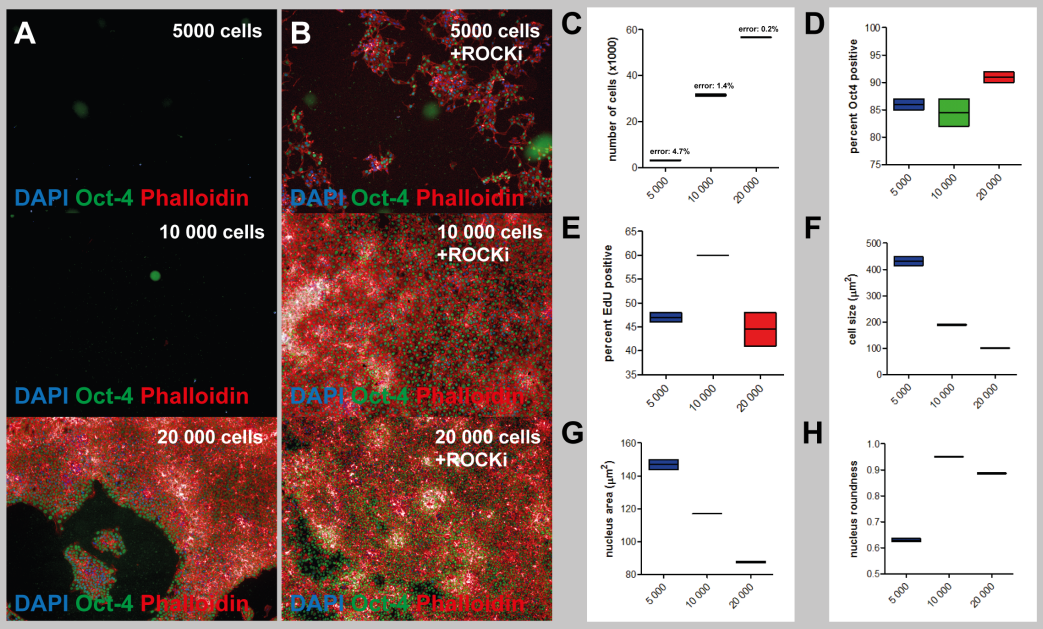

Figure 5.2.: Seeding of human iPS cells as single cells. Dissociated human iPS cells were seeded (A) in the absence and (B) in the presence of ROCK inhibitor at the indicated cell number. After 48 hours in culture, cells were fixed and stained with DAPI and Oct-4. (C) The number of cells was counted. (D) Percentage of Oct-4 positive cells. (E) Percentage of EdU positive cells. The change in cell morphology was determined by calculating (F) cell size, (G) nucleus size and (H) nucleus roundness.

5.1.2 Loss of pluripotency factor Oct-4 in standard media condition

Human iPS cells differentiate spontaneously if self-renewal factors such as basic FGF are removed from the media (Singh et al., 2012). To test the ability of human iPS cells to survive and grow in the absence of FGF, one well of a 6-well plate was left without media change on the day of routine passaging. Two days later, cells were assessed for proliferation and pluripotency. EdU was added to the culture 30 minutes before fixation to detect proliferating cells (Salic et al., 2008) and Oct-4 was used to detect pluripotent cells (Adachi et al., 2012). Using an Operetta system, 32 high-resolution images were taken to capture cellular responses (Figure 5.3 A-C). Images were processed using Harmony software and standard algorithms applied to quantify the number of EdU and Oct-4 positive cells (see Chapter 5.3). A total of

32,215 cells were analysed. 20.7% of the cells were Oct-4 negative of which only a small fraction (9%) proliferated (Figure 5.3 D). On the other hand, 28% of Oct-4 positive cells were EdU-positive (see section 4.1), indicating that the removal of self-renewal factors induces differentiation and limits cell cycle progression.

To determine whether removal of self-renewal factors resulted in a change in nuclear morphology, the nucleus area was calculated for every cell. I was able to show that the mean nucleus area was significantly smaller in Oct-4 negative cells compared to Oct-4 positive cells (Figure 5.3 E and F) when the medium was not changed for two days. Overall, the mean nuclear area was significantly smaller in cultures with media change (Figure 5.3 E). Furthermore, EdU positive cells had a larger cell nucleus compared to EdU negative cells irrespective of Oct-4 expression. A threshold was set at 80 μm^2 according to the mean nuclear area of the controls to investigate the difference in Oct-4 expression in small and large nuclei. I found that 40 percent of the cells with a small nucleus were Oct-4 positive while more than 80% of cells with a large nucleus were Oct-4 positive.

5.1.3 Self-renewal and differentiation of human iPS cells on matrices

To test whether changing the matrix concentration and media conditions would affect the self-renewal capacity of human iPS cells, cells were dissociated into single cells using Accutase (see chapter 2.8) and plated at a low seeding density (3000 cells per well of a 96-well plate) in E8. To assess the effect of ECM on the self-renewal ability of iPS cells, four different matrices were prepared. The lowest matrix was 25% (0.25 GX) of standard geltrex solution (1 GX) and the highest was double the standard geltrex solution (2 GX). During the first 24 hours, cells attached to the matrix and formed cell clusters through migration and proliferation. Four hours after cell seeding, no difference in cell morphology was observed between the matrices

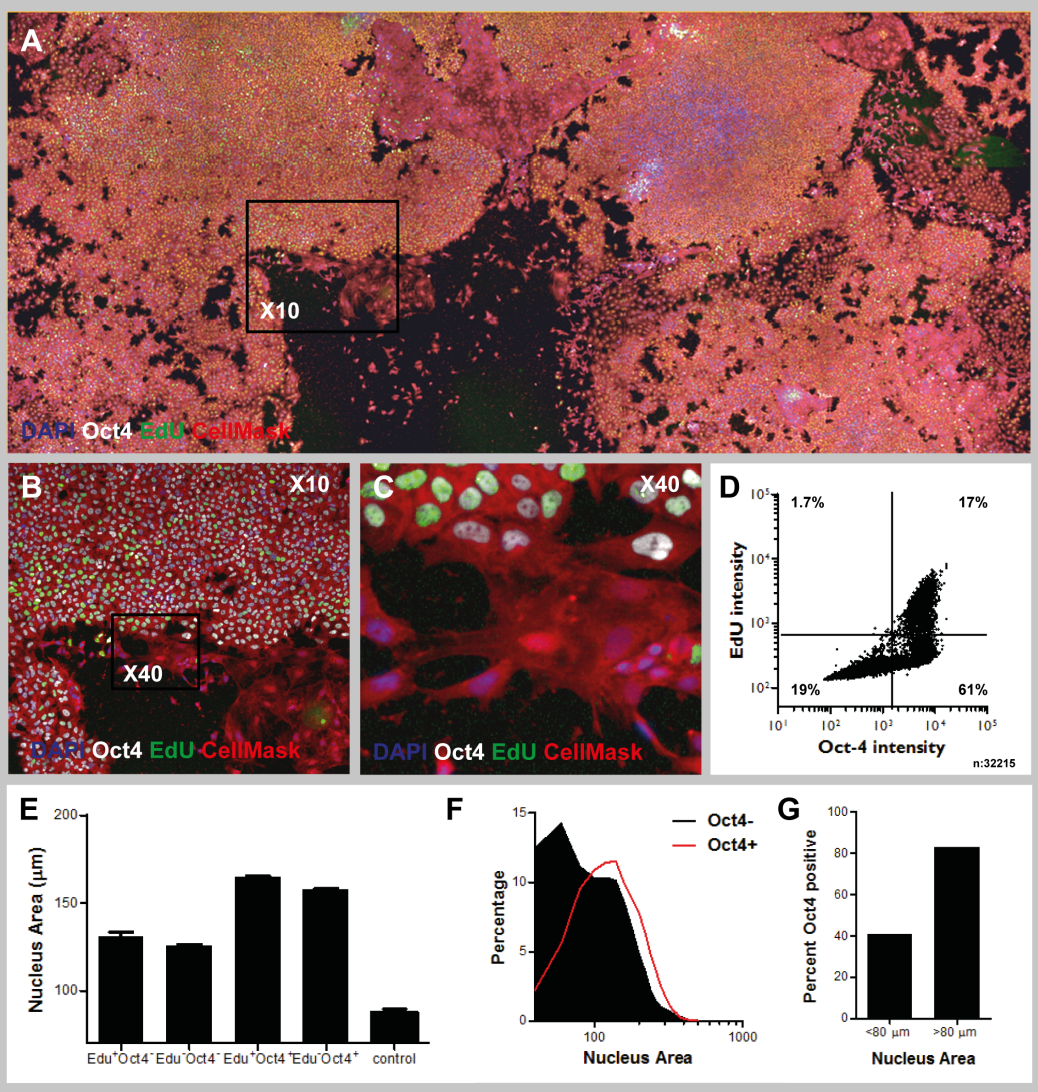

Figure 5.3: Spontaneous differentiation of human iPS cells. Human iPS cells were left without media change for 2 days to induce spontaneous differentiation. Cells were stained with DAPI, Oct-4, EdU and CellMask and images were taken using an Operetta. Shown are (A) image stitching of 32 high-resolution images with 10x magnification, (B) one representative 10x image and (C) one 40x digital magnification. (D) Quantification of EdU and Oct4 intensities. Each dot represents one cell. (E) Mean nuclear area for distinct cell populations present in the culture. (F) Histogram of nucleus area for Oct4- and Oct4+ populations. (G) Percentage of Oct4+ cells with a nucleus area smaller or larger than 80 µm.

(Figure 4.4A). After 24 hours, however, cell groups rounded up at 0.25 GX while cell groups appeared elongated on 2 GX (Figure 5.4 A).

The medium was changed after 24 hours to study the response of iPS cells to two media. KSR, which allows the control of FGF levels and therefore may be considered

differentiation medium and E8, which was used during routine passaging. On days 2 and 3 after seeding, cells were labelled with antibodies against Oct-4 and Sox-2 to detect pluripotent cells and CellMask was used to label the plasma membrane. The Operetta was used for imaging and Harmony software to process the images using high-content analysis (see chapter 5.3). The mean Oct-4 fluorescence intensity was determined for every cell in all conditions. For each condition, at least 10,000 cells were analysed.

On day 2 after seeding, no difference in Oct-4 expression was observed between E8 and KSR on all matrices (Figure 5.4 B). The Oct-4 intensity remained constant at all matrix concentrations compared to the control matrix concentration (GX 1) (Figure 5.4 B). On day 3 after seeding, the Oct-4 intensity remained constant in E8 medium compared to day 2, except at the highest matrix concentration (2 GX) which showed a reduction in the Oct-4 intensity indicating cell differentiation. Furthermore, cells cultured in KSR expressed significantly lower levels of Oct-4 compared to cells cultured in E8 at all matrix concentrations (Figure 5.4 C).

5.1.4 Quantitation of human iPS cell responses on matrices

Based on these results, I developed a high-throughput assay to further investigate the cellular response to the ECM under differentiation and self-renewal conditions. The supplement of E8 medium was reduced by 50% (1/2 E8) and 75% (1/4 E8) with the aim of limiting self-renewal factors and inducing differentiation. Furthermore, FGF, which is known to be an important self-renewal factor (Singh et al., 2012), was added to the differentiation medium KSR. An overview of all media compositions and matrix concentrations is given in Figure 5.5 A. In addition to Oct-4, the expression of the pluripotency marker Sox-2 and two cell morphology parameters (roundness and number of cells in cell groups) were also detected (Figure 5.5 B). For each condition and technical replicate 9 images were taken to make a total of 864 images

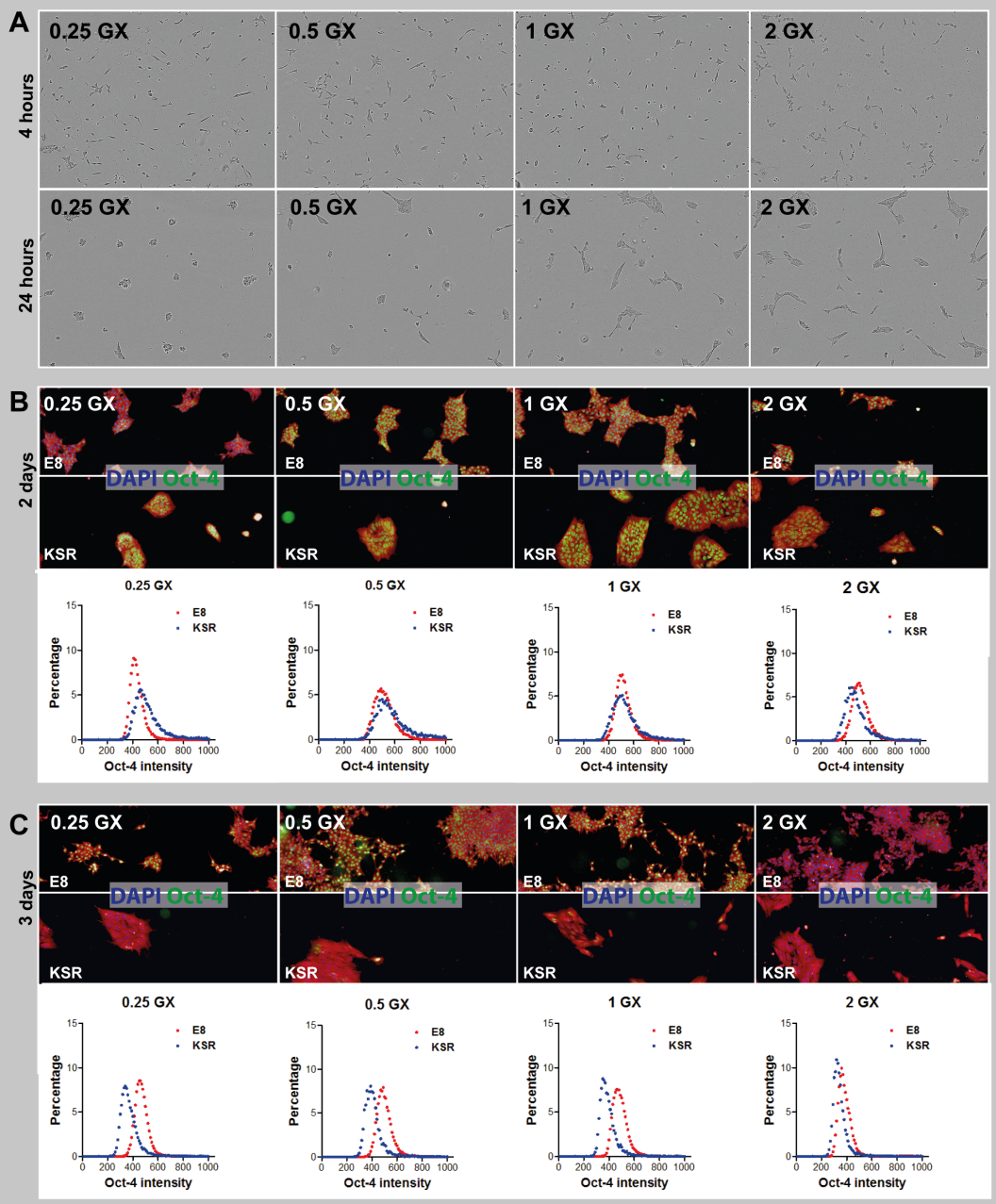

Figure 5.4: Effect of ECM on self-renewal of human iPS cells. Human iPS cells were seeded on geltrex-coated (GX) dishes in standard culture medium (E8) at a low seeding density. (A) Cells attached 4 hours after seeding (top row) and formed cell clusters after 24 hours (bottom row) in E8 medium. After 24 hours, the medium was changed into E8 or KSR. Thereafter, cells were stained for DAPI and Oct4 after (B) 2 days and (C) 3 days. The corresponding Oct4 intensities were quantified on each day (shown below).

for the screen. Harmony software was used to process all images and extract single cell data.

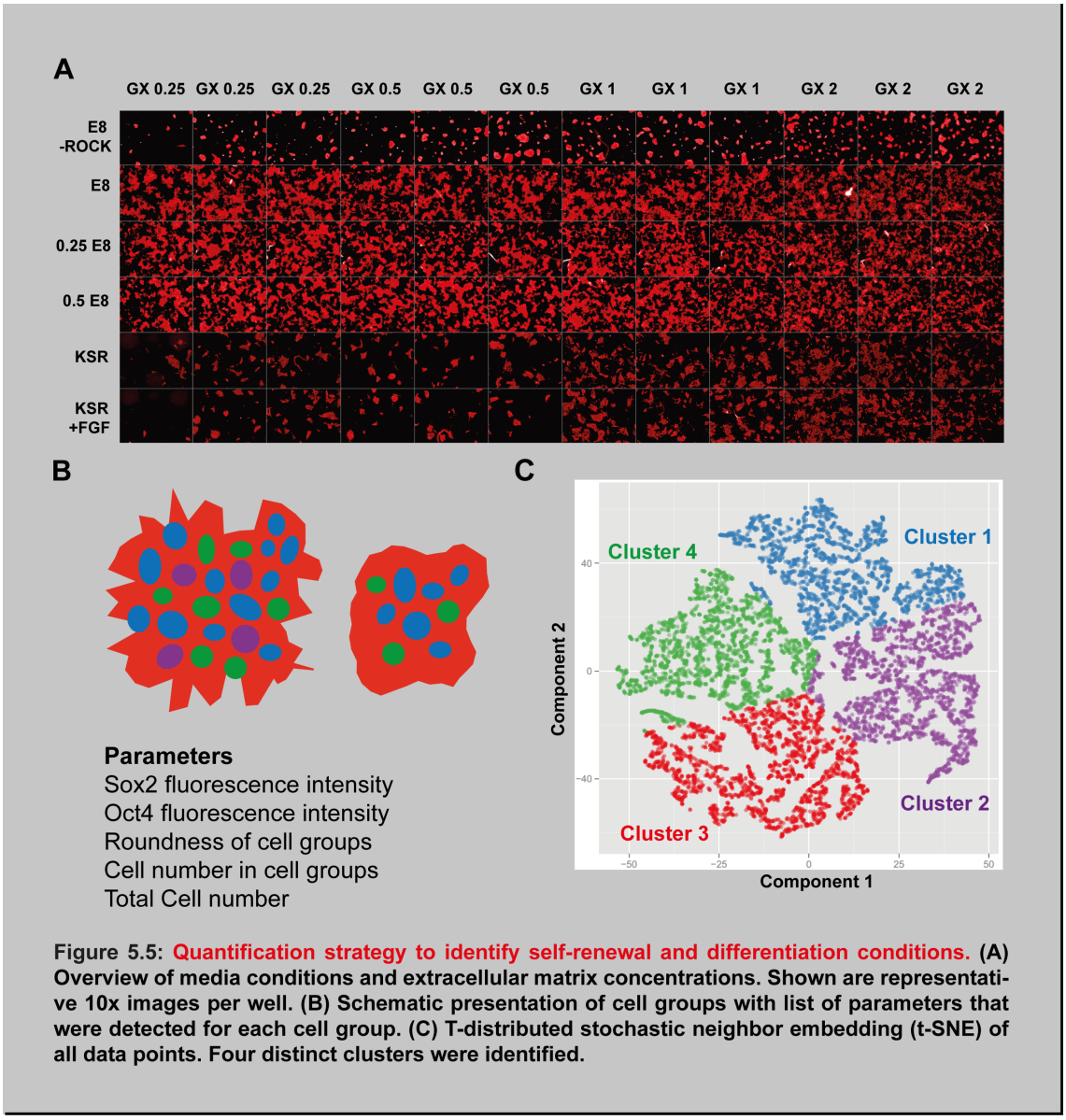

Figure 5.5: Quantification strategy to identify self-renewal and differentiation conditions. (A) Overview of media conditions and extracellular matrix concentrations. Shown are representative 10x images per well. (B) Schematic presentation of cell groups with list of parameters that were detected for each cell group. (C) T-distributed stochastic neighbor embedding (t-SNE) of all data points. Four distinct clusters were identified.

The data were analyzed using R in collaboration with Arsham Ghahramani (Grün et al., 2015). We used t-distributed stochastic neighbor embedding (t-SNE) (Grün et al., 2015) to develop an algorithm that can be used for cellular phenotyping (Figure 5.5 C). At least 60 cell groups were analysed for each technical replicate and three technical replicates (corresponding to three wells of a 96-well plate) were merged to improve the statistical power. Based on the preliminary data from Figure 5.5 we hypothesized that at least two cell states must be present in the data set as a result of self-renewing and differentiating conditions. We further speculated that

multiple media conditions might give rise to additional cell populations. Therefore, we applied k-means clustering with an input of four populations (n=4) resulting in four distinct tSNE clusters.

We treated the data from each ECM concentration separately and applied the data set to the algorithm (Figure 5.6). In the next step, we next calculated the percentages of data points (i.e. one data point represents one cell group) that lie in each cluster for every ECM concentration Figure 5.7.

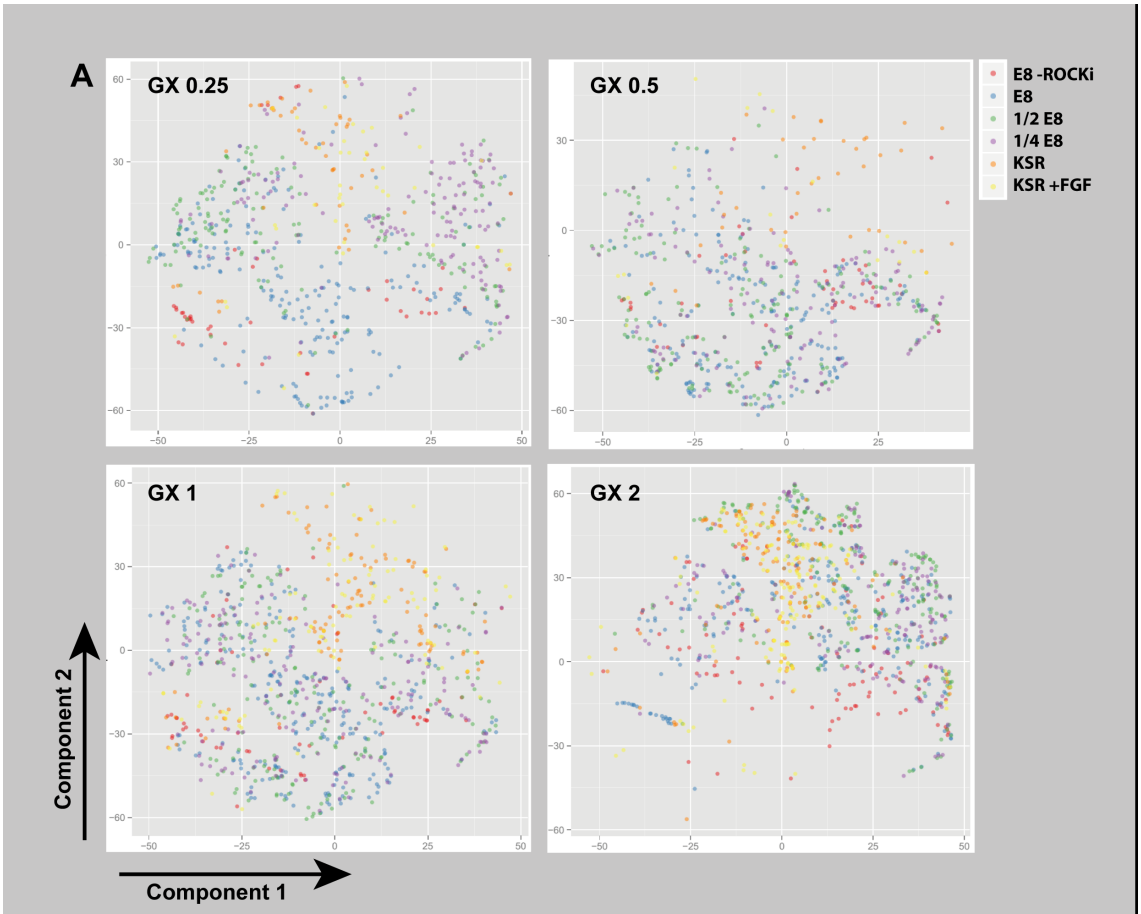

Figure 5.6: Response of iPS cells to different media conditions. t-SNE data points of all media conditions at the indicated geltrex concentrations at four distinct ECM concentrations. Shown are mergers of three technicals replicates for each condition.

The total cell number per condition was computed by taking the sum of the number of cells in all cell groups. In the absence of ROCK inhibitor, the majority of cells (50%) were found in cluster 3 at the control matrix concentration (GX 1)

and fewer than 5% of cells were in cluster 1 (Figure 5.7 A). Increasing the matrix concentration by two fold (GX2) caused a shift in cell populations to clusters 2 (51%) and 4 (26%). At the same time, few cells (6%) were found in cluster 3. The addition of ROCK inhibitor to the cells had no effect on the cell distribution between the t-SNE clusters 1 (Figure 5.7 B). However, a pronounced increase in cell number was observed at all matrix concentrations in the presence of ROCK inhibitor.

The reduction of E8 supplement (1/2 E8 and 1/4 E8) caused an effect at the highest and lowest matrix concentration (GX 0.25 and GX 2), while the intermediate matrix concentrations (GX 0.5 and GX 1) were unaffected (Figure 5.7 C and D). At GX 0.25, almost no cells were present in cluster 3 in media conditions 1/2 E8 (6%) and 1/4 E8 (2%). The overall distribution of cells amongst tSNE clusters at GX 0.25 in reduced E8 supplement is comparable to GX 2 at normal E8 supplement in the absence of ROCK inhibitor (Figure 5.7 A, C and D). Therefore, the addition of ROCK inhibitor, which is known to inhibit actin depolymerisation, induces differentiation at low matrix concentration if cells are induced to differentiate but has no effect on the cell state under self-renewal conditions. At the same time, the addition of ROCK inhibitor showed no effect on the cell differentiation state at the highest matrix concentration when E8 supplement was reduced. At standard matrix concentration (GX 1), no effect was observed if ROCK inhibitor was added, even under differentiation conditions (Figure 5.7 A-D).

In the differentiation medium KSR, an inverted phenotyping profile was observed. The majority of cells were present in cluster one with few remaining in cluster 3 (Figure 5.7 E). Changing the ECM concentration had no effect on the distribution of data points. If, however, FGF was added, the phenotyping profile shifted towards a self-renewing state. At intermediate matrix concentration and in the presence of FGF, the majority of cell groups were present in cluster 2 with an increase in cell groups in cluster 3 and a reduction in cluster 1. Therefore, the addition of FGF

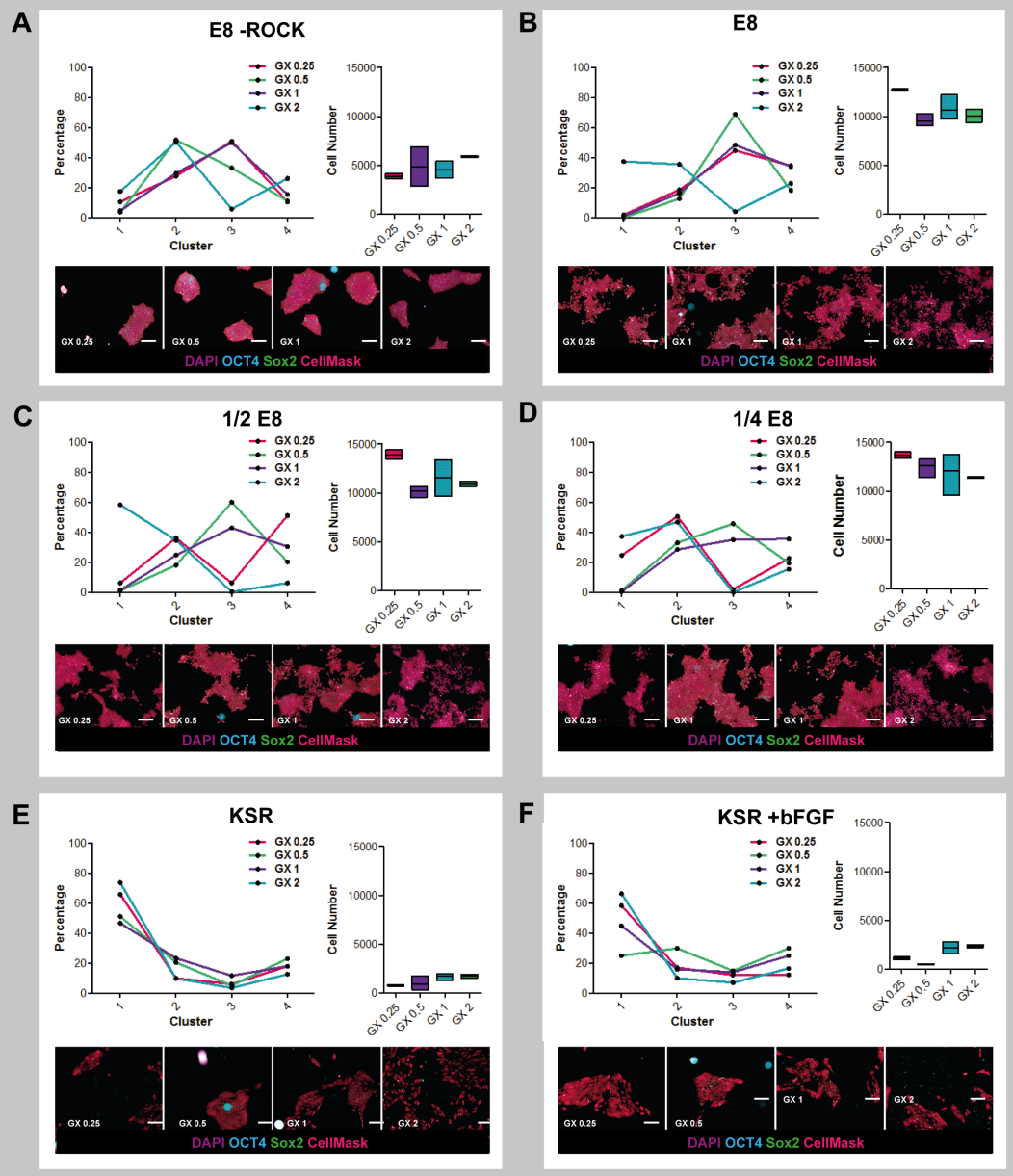

Figure 5.7: Phenotyping of human iPS cells in distinct microenvironments. Cell replication was quantified by counting the cells and changes in cellular phenotypes were shown as distribution of percentages in each t-SNE cluster. The media condition is highlighted in (A-F). Representative images for each condition are shown below.

caused a shift from a differentiation phenotype towards a self-renewing phenotype.

5.1.5 Discussion

The development of high-throughput platforms for the study of stem cell processes is of high interest for the field of regenerative biology. It has previously been shown that a single platform with multiple microenvironments can be used to study the interaction between different niche components (Ranga et al., 2014). However, it remains difficult to describe interactions between different niche components due to poor understanding of individual components of the stem cell niche. Therefore, I first evaluated the interaction of human iPS cells with the extracellular matrix (ECM) and was able to show that reducing the ECM composition caused a reduction in pluripotency gene expression. Furthermore, an increase in ECM composition caused a change in cellular morphology and a loss of pluripotency. To further validate my findings, I exposed human iPS cells to the same ECM gradients and added six different media to evaluate whether soluble components would affect the self-renewing ability of human iPS cells. 24 distinct microenvironments were generated differing in ECM composition and self-renewing components (Singh et al., 2012, Chen et al., 2011, Burdick et al., 2011).

To quantify the cellular response at the single cell level, a phenotyping tool was developed that allows the quantification of cell populations at a high resolution. Previous efforts to identify multiple cell populations in the niche have shown that it is possible to use multi-parametric analysis to isolate different stem cell populations. In my studies, I was able to show that changing the stem cell niche components induced a shift of cell populations between self-renewing and differentiating populations. I can conclude that the ECM composition was the critical determinant for the self-renewal ability of human iPS cells if media supplements were reduced. If, however, cells were subjected to the differentiation medium KSR that was shown to induce loss of Oct-4 expression, the ECM composition had no significant effect on the cell state.

The inhibition of actin depolymerisation through the addition of ROCK inhibitor had no significant effect on the self-renewal ability of human iPS cells plated on standard ECM (i.e. at the control concentration of geltrex). Interestingly, ROCK inhibition at a low ECM concentration caused a shift of cell populations towards a differentiation phenotype indicating that the actin cytoskeleton is important during the differentiation of human iPS cells. It may be interesting to investigate whether inhibition of the actin cytoskeleton using small molecules such as cytochalasin D inhibits stem cell differentiation. Furthermore, studying the mechanotransduction machinery including the translocation of YAP protein would be of high interest to understand the cell-to-substrate mechanism of action. The investigation of TGF-β signaling and the effect on the cytoskeleton tension may also be of interest to the field.

Although stem cell niche factors such as hypoxia and physical tension have not been assessed in this assay, it may be possible to implement further conditions in the assay to study the interaction of all niche factors. Furthermore, I was not able to assess the interaction of cells with their neighbors. It would be of high interest to the field to implement further analysis tools that allow the quantification of cell-to-cell interaction and the effect of niche factors thereof.

In conclusion, I have found new interactions within the stem cell environment that may be adapted for further studies and enhance the development of novel microenvironments. Furthermore, my phenotyping tool may be used for many cell types to identify the distribution of cell populations in any environment. Thus, engineering new types of stem cell niches may be facilitated using the newly developed stem cell technologies from this chapter.

5.2 Topographies to support self-renewal of human induced pluripotent stem cells

We plated cells on the previously described TopoChip library, which comprises 2,176 distinct surface topographies in duplicate on a 2 x 2 cm^2 Topochip platform (Unadkat et al., 2009). Each topography is arrayed in an area of 290 x 290 cm^2, referred to as one TopoUnit. The topographies are based on combinations of circles, squares and rectangles with a feature height of 5 μm and vary in attributes such as feature size, density and roundness (Figure 6.1 A) (Unadkat et al., 2009). Fabrication of the TopoChip platform utilizes hot embossing of standard tissue culture polystyrene, reducing the cost of manufacture and enabling future large-scale culture on selected topographies (see Chapter 2.2.2.9).

To best evaluate the ability of human iPS cells to grow as single cells, topographies were seeded at low density (100 cells/mm^2, corresponding to approximately 12 cells per TopoUnit) in E8 medium. The medium was supplemented with ROCK inhibitor, which prevents dissociation-associated apoptosis (Saha et al., 2012). An assay time of 24 hours was chosen to capture the initial cellular responses to the topographies. 5-ethynyl-2-deoxyuridine (EdU) was added for the final 30 minutes to label S phase cells (Salic et al., 2008). Following fixation, cells were labelled with antibodies to Oct-4 as a marker of pluripotency (Adachi et al., 2012). The plasma membrane dye CellMask was used to distinguish individual cells versus groups of cells. DAPI was added as a DNA label to identify individual nuclei. Four hours after seeding, the majority of attached cells were single cells (Figure 6.1 B). After 24 hours, most cells were in clusters, which formed by a combination of cell proliferation and migration (Figure 6.1 B).

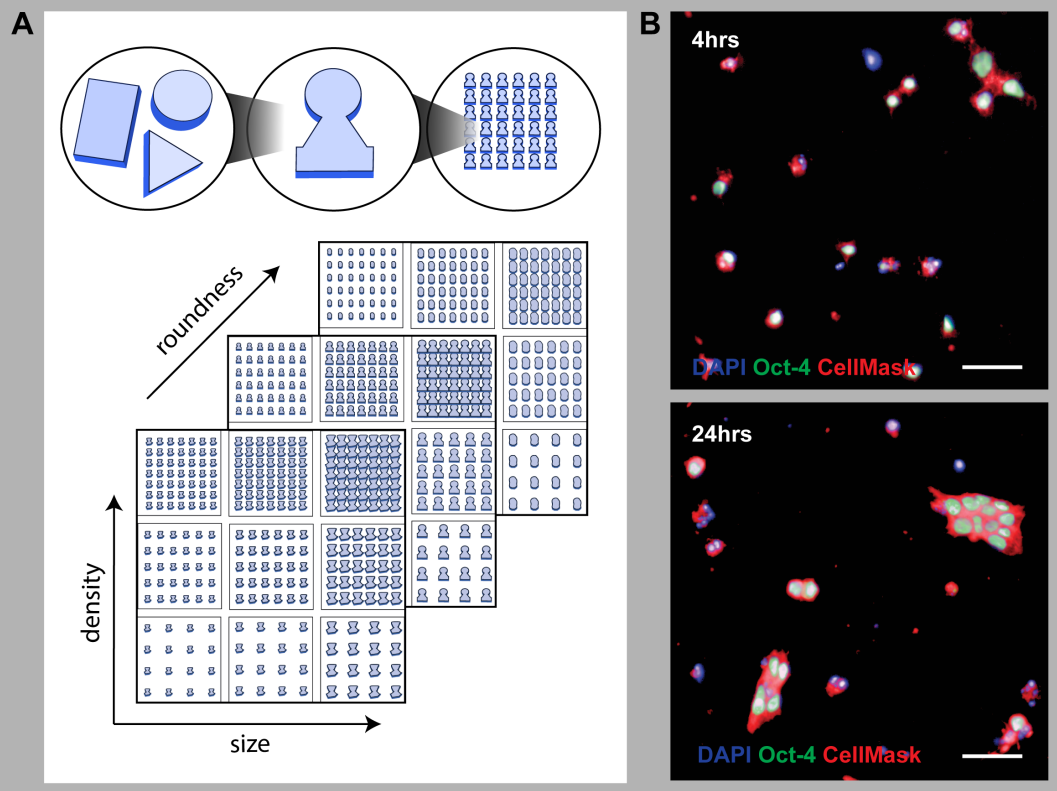

Figure 6.1: Design of TopoUnits and screen for EdU and Oct-4 labelling. (A) Schematic of the topography library. Top: combining circular, triangular and rectangular primitives into specific features that are repeated within a single TopoUnit. Bottom: differences in feature size, density and roundness between individual TopoUnits arrayed in a TopoChip. (B) Individual TopoUnits seeded for 4h (top) or 24h (bottom) then labelled for Oct-4 (green), CellMask (red) and DAPI (blue). Scale bars: 50 µm.

5.2.1 Quantitation of EdU and Oct-4 labelling

High-content images were analysed with Harmony software (Perkin Elmer) using standard algorithms. A maximum of six algorithms were tested for their ability to detect cell properties and the algorithm with the best fit was selected for further analysis. DAPI staining was used to detect cell nuclei and characterize nuclear morphology (Figure 6.2 A). Imaging noise was removed by setting thresholds for nuclear area (between 40 and 500 μm^2), nuclear roundness (higher than 0.75) and nucleus width to length ratio (higher than 0.4) (Figure 6.2 B). CellMask was used to detect cell shape and characterize cell morphology (Figure 6.2 C). Imaging noise was removed by setting thresholds for cell area (larger than 12 x 103 μm^2), cell roundness

(higher than 0.75) and cell ratio width to length (higher than 0.2) (Figure 6.2 D). Thresholds were set according to the minimum possible value for each cell property.

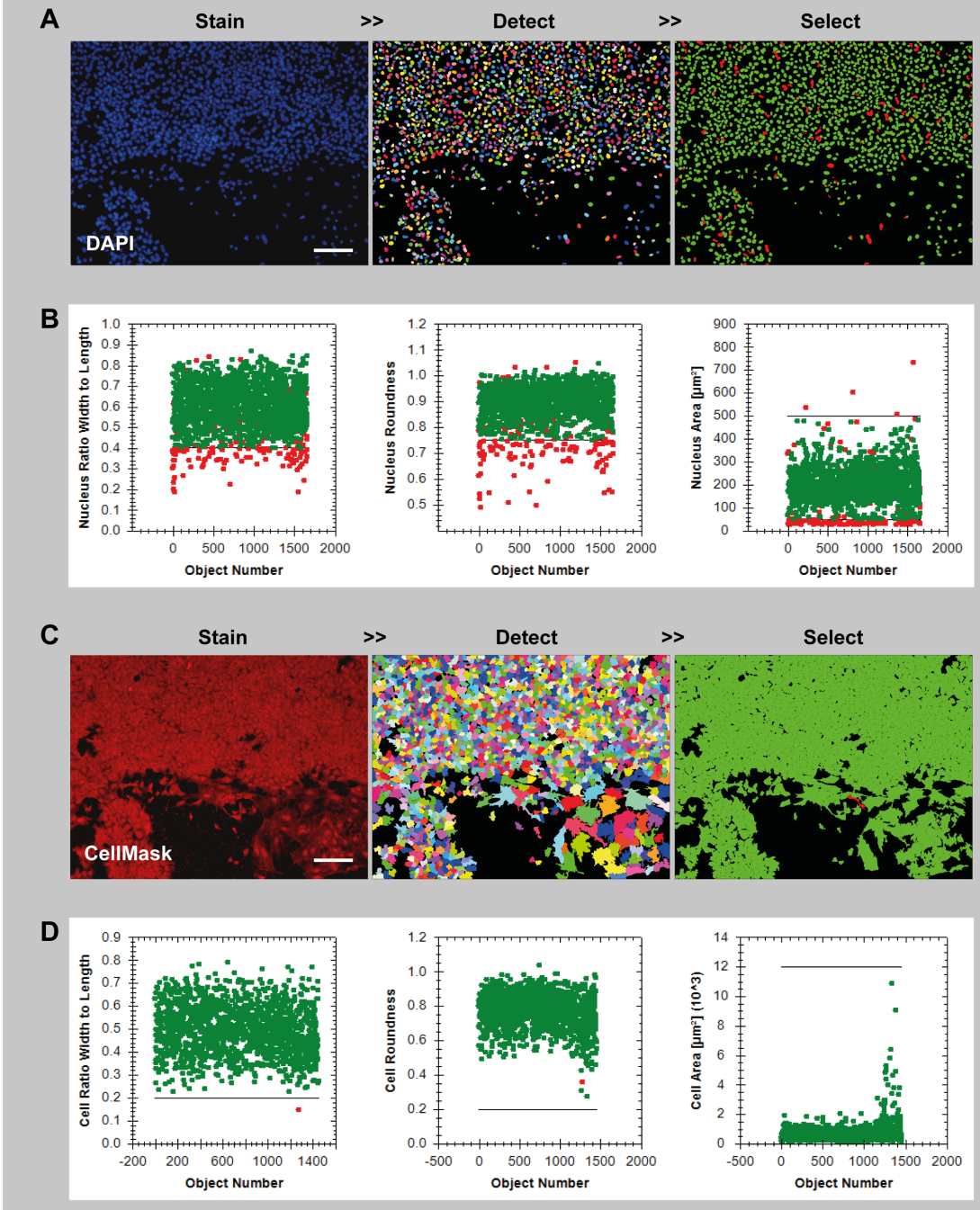

Figure 6.2.: High-content analysis to quantify molecular markers at single cell resolution (A) DAPI staining was used to detect and select nuclei according to (B) nuclei area, roundness and width to length ratio. (C) CellMask was used to label the cell membrane and select cells according to (D) cell width to length ratio, roundness and area. Individual nuclei and cells are coloured in rainbow (A and C: middle panel) and the respective selection was coloured in green with noise coloured in red (A and C: right panel). Scale bars: 100 µm.

The median fluorescence intensity of nuclear staining was calculated within the region of interest (Figure 6.3 A). Median intensity values are shown for two nuclei (Figure 6.3 B and C). The Oct-4 and EdU median intensity was calculated for all cell nuclei. To score individual cells as positive or negative, thresholds were set for each label (Figure 6.3 D and E).

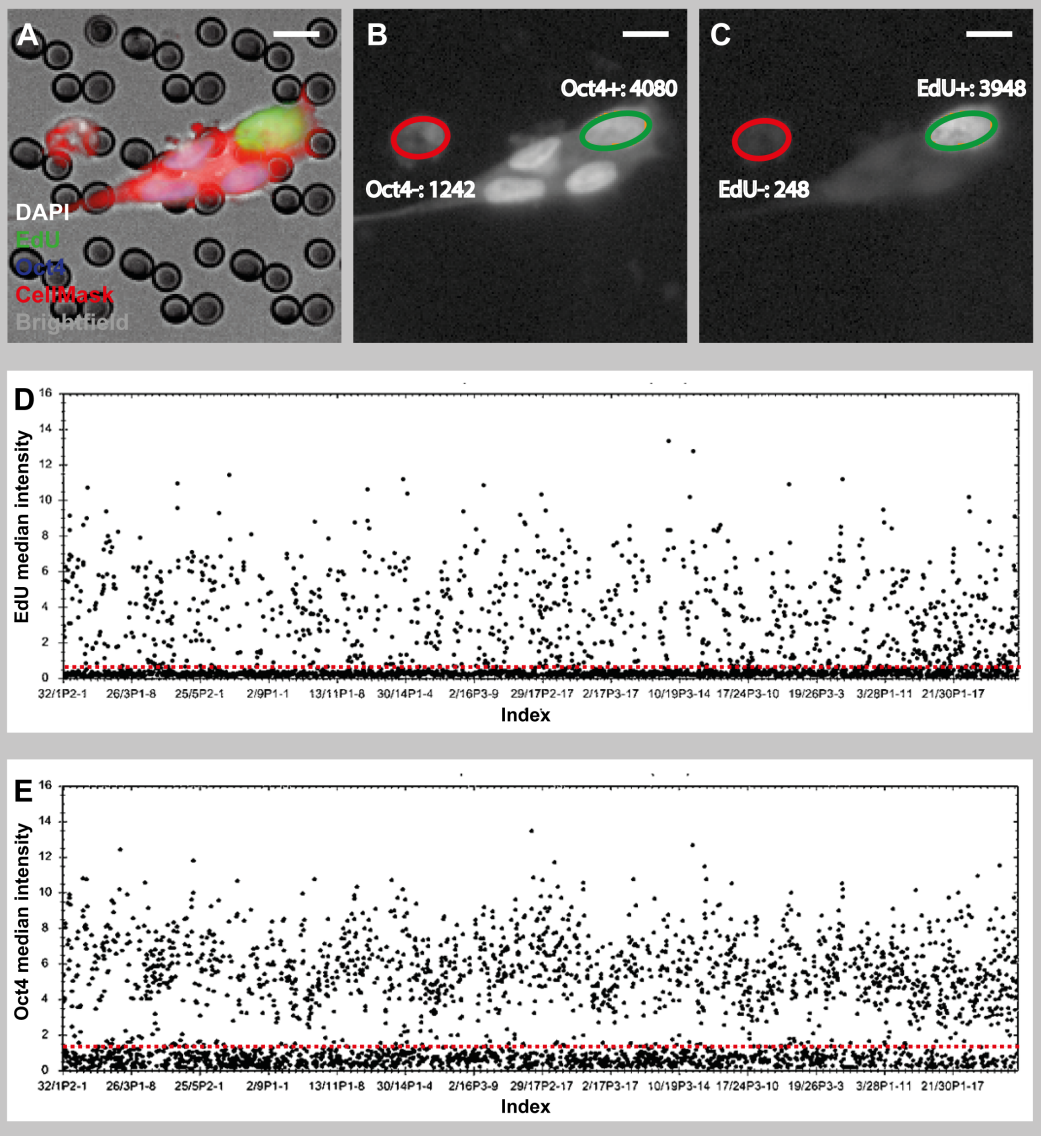

Figure 6.3: Fluorescence intensity signals. (A) Representative image of human iPS cells on one topography. (B) Fluorescence intensity for one Oct4- and one Oct4+ nuclei (circled) is shown. (C) Fluorescence intensity for one EdU- and one EdU+ nuclei (circled) is shown. Scale bar represents 10 µm. (D) EdU median intensity for all cells on the TopoChip. Dashed line represents threshold level to select EdU positive cells. (E) Oct4 median intensity for all cells on the Topochip. Dashed line represents threshold level to select Oct4 positive cells.

We then analysed 1000 topographies in detail, discarding 18 as unreadable due to defects in the manufacturing process. The effects of reducing background noise and outliers on ranking topographies according to the number of Oct-4+ cells per TopoUnit are shown in

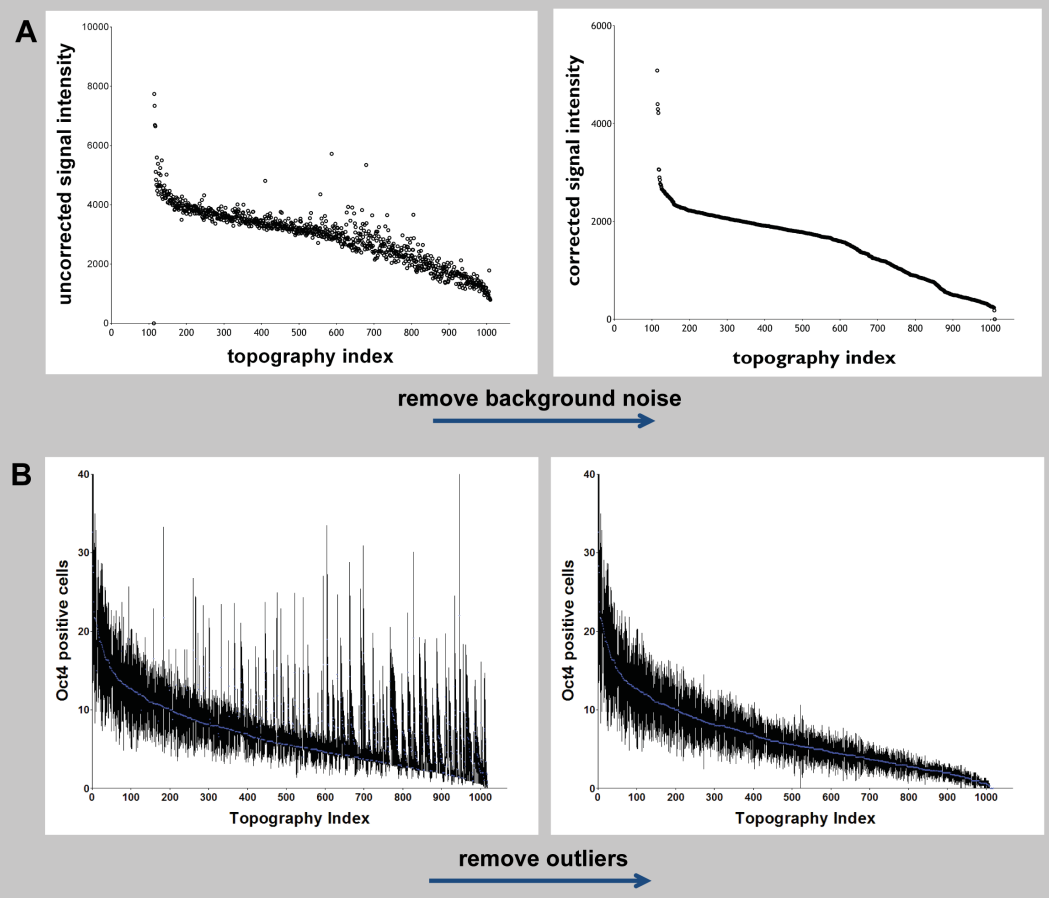

Figure 6.4: Removing background noise and outliers. (A) The fluorescence intensity signal was corrected by removing the background noise. Shown is the mean DAPI fluorescence intensity (y axis) for each topography (x axes). (B) Biological replicates were used to calculate mean values and outliers were defined as 2.5 standard deviations (STD) away from the mean.

By pooling the measurements for all cells on one TopoChip, I established that all EdU+ cells were also Oct-4+, but approximately 30% of Oct-4+ cells were EdU- (Figure 6.5 B). By plotting the total number of cells and the number of EdU+ and Oct-4+ cells per topography, I observed linear correlations between the numbers of Oct-4+ cells, EdU+ cells and total cells (Figure 6.5 B). Thus, at 24h TopoUnits with

the greatest number of cells also had the greatest number of EdU+ cells and Oct-4+ cells, indicating that they supported self-renewal and prevented differentiation of pluripotent cells.

5.2.2 Identifying topographical features that promote or decrease human iPS cell proliferation and Oct-4 expression

In order to discover how specific topographies elicited specific responses, the 100 topographies ranked top or bottom on the basis of number of Oct-4+ cells (Figure 6.5 A) were compared with each other and also with control TopoUnits that had a flat surface (polystyrene) (Figure 6.5 C-F). The 100 topographies with the highest number of Oct-4+ cells (Top 100) had three-fold more Oct-4+ and EdU+ cells compared to flat polystyrene (Figure 6.5 C). Topographies of the bottom 100 hits (Bottom 100) contained significantly fewer Oct-4+ cells and EdU+ cells than flat polystyrene (Figure 6.5 C). The percentage of Oct-4+ and EDU+ cells was also significantly higher in Top 100 compared to Bottom 100 and polystyrene substrates (Figure 6.5 D and E). Further analysis revealed that the Top 100 topographies supported formation of more cell clusters and a greater number of cells per cluster compared to the Bottom 100 topographies and flat polystyrene (Figure 6.5 F). Representative images of each type of topography are shown in (Figure 6.5 G-I).

5.2.3 Using computational tools to predict the topographical features that are most supportive of iPS cell proliferation and Oct-4 expression

In conjunction with Aliaksei Vasilevich, topographical features were analysed for their ability to support the growth of Oct-4 positive cells. Because the topographies

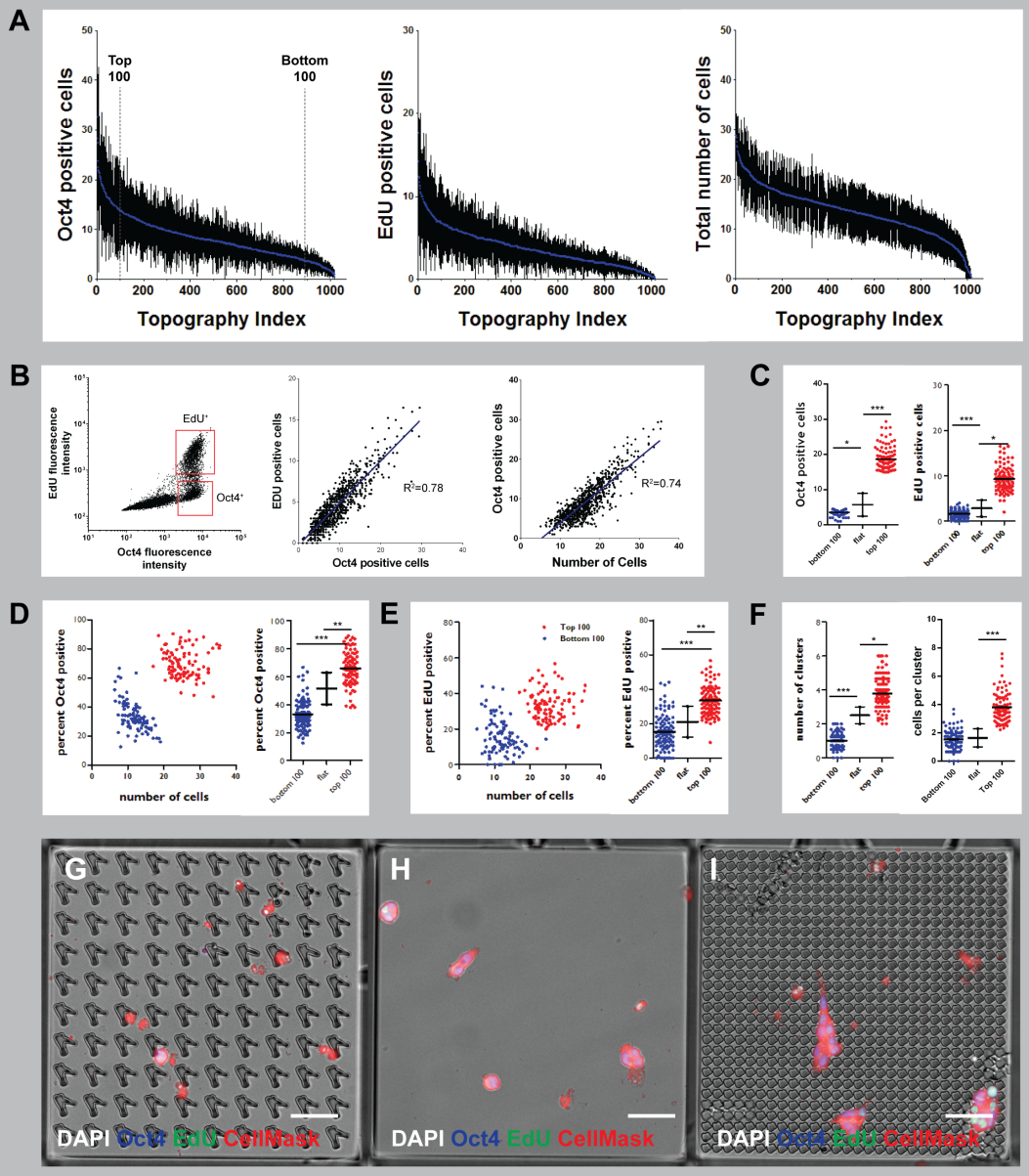

Figure 6.5: Human iPSC proliferation and Oct-4 expression on distinct topographies. (A) Topographies were ranked according to the total number of Oct-4+ (left) or EdU+ cells (middle) or the total number of attached cells (right). Cutoffs for the 100 topographies with the highest and lowest number of Oct-4 positive cells are shown. (B) Fluorescence intensity thresholds were set for Oct-4 (Oct4+) and EdU (EdU+) cells (see Fig. 3.3) and the number of positive cells for each marker was determined. Left hand panel shows all the cells (individual dots) on a single TopoChip. Top gate contains EdU+Oct-4+ cells; bottom gate contains Oct-4+EdU- cells. Middle and right hand panels show all topographies (TopoUnits) on a single TopoChip. The R2 coefficient of determination values was calculated to show positive correlations between Oct-4+ cells (right hand panel) or EdU+ cells (middle panel) and total cell

were designed from a combination of multiple parameters we used an algorithm that allows the identification and quantification of topographic cues using Classification and Regression Trees (CART) (Grajski et al., 1986, Hothorn et al., 2006) in order to define the cues that support self-renewal of human iPS cells. Characteristics evaluated by this method include the numbers of primitives (circles, triangles and lines [rectangles]) used to make each repeating feature ('building block' including surrounding space) in a TopoUnit, the area of each primitive, circle diameter, length of the shortest side of a triangle, and line length (Figure 6.6 A). We also factored in overall feature size (FeatSize: the size of the bounding square for the primitives [10, 20 or 28 μm]) and wave number [WN]. Wave number represents the fraction of the total energy in the signal in sinusoids and is computed after applying discrete Fourier transformation to the image of a single feature (Unadkat et al., 2009).

Using a regression tree of all hits from the Top 100 and Bottom 100 TopoUnits we found that small feature size was the most important determinant of pluripotency, followed by high wavenumber and high feature density (FCP) (Figure 6.6 A and B). More than 80% of the topographies in the Top 100 had a pattern area of less than 60 μm^2. Pattern area was calculated by multiplying the area of each feature and the fraction of the feature covered by primitives (FCP). More than 80% of the Bottom 100 hits had a wave number smaller than 0.008 a.u. (small number of edges per feature) (Figure 6.6 B). If pattern area was greater than 60 μm^2 and wavenumber was more than 0.008 a.u. 60% of surfaces were Oct-4 positive (Figure 6.5 A and B).

Aliaksei and I next employed a logistic regression direct probability model to identify further topographies that were predicted to support pluripotency and topographies that would not. Logistic regression enables outcomes to be predicted on the basis of binary classification, which is not possible with CART. The model we derived had an accuracy of 72%; the area under the curve for the Receiver Operating Characteristic (ROC) plot was 0.76, where randomly selected topographies

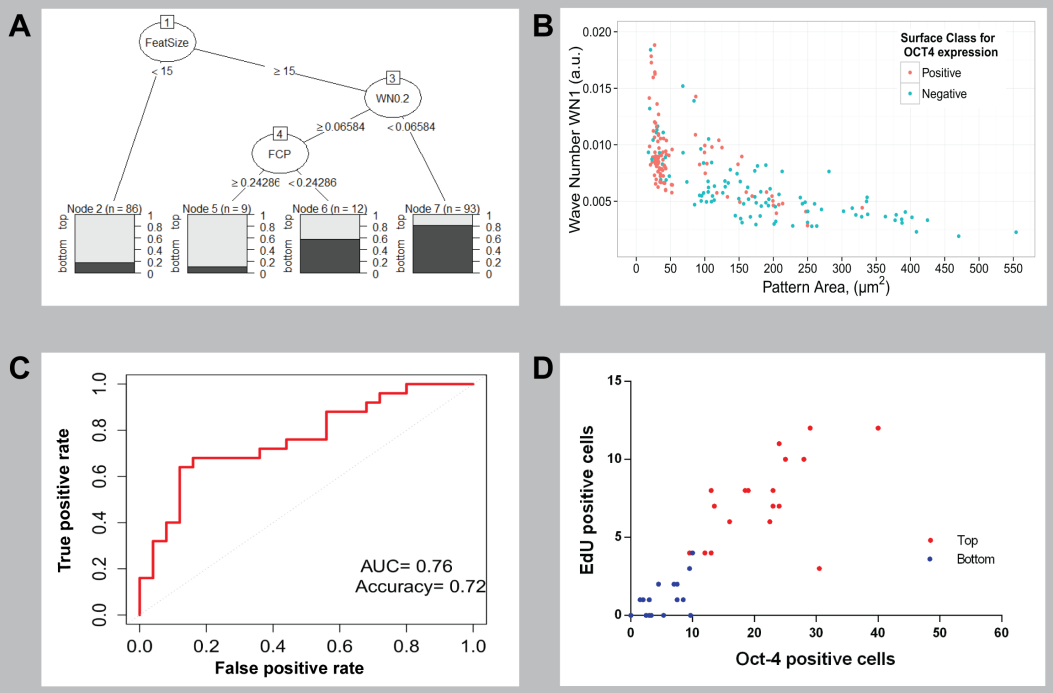

Figure 6.6: Identification of topography parameters that maintain proliferation and Oct-4 expression. (A) Regression tree showing sorting of topographies. After each node, the fraction of Positive (top 100 for Oct-4+ cells) versus Negative (bottom 100 for Oct-4+ cells) topographies is shown. (B) Scatter plot showing distribution of pattern area and wave number parameters for topographies with highest (red; top hits) and lowest (blue; bottom hits) number of Oct-4+ cells. (C) ROC plot showing prediction performance for logistic regression model. (D) 30 TopoUnits that had not been analysed previously were predicted to promote Oct4 expression and EdU labelling ('top hits') and a further 30 were predicted to be unable to support those characteristics ('bottom hits'). Of those TopoUnits, 19 in the top category and 15 in the bottom category were analysed and confirmed experimentally.

are predicted to have an area under the curve value of 0.5 and predictor with 100% accuracy equal to 1 (Figure 6.6 C). Of the 30 topographies predicted to support pluripotency, 24 were imaged and 19 proved to be top hits experimentally (Figure 6.6 D). Of the 30 topographies predicted not to support Oct-4 expression, 25 were imaged and 15 proved to be bottom hits experimentally (Figure 6.6 D). Therefore, we validated our previous finding that distinct and specific topographical features are responsible for the observed differences in human iPS cell growth.

5.2.4 Decoding surface topographies and optimising the shape

To further our analysis, I worked with Jens Kleinjung with the aim to decode the surface structures of all topographies. Phase contrast images can be used to identify unstained samples, allowing visualisation of shape and density variations (Liu et al. 2014). To characterise surface topographies phase contrast images of 1056 topographies were analysed using R. 703 topographies were pre-selected based on image quality because some surfaces contained cells and thus affected the surface structure. Input images in 8-bit gray bmp format (package 'bmp') were converted into single black-and-white image matrices by setting the lower gray range to '0' and the higher to '255' (Jefferis, 2013). Five sample images (250 x 250 pixels) with corresponding image matrices are shown in Figure 6.7 A. Black pixels represent topography elevations which correspond to feature area described in Chapter 6.4. We improved the topographical analysis by also including white pixels that were generated through convolution of the negative images to obtain a measure for the space between elevations. Using synthetic shapes and without pre-judgement all image matrices were convolved (package 'biOps') and the convolved matrices were analyzed to extract the number of matches of the synthetic shapes in the image matrix (Figure 6.7 B)(Bordese & Alini, 2013). The pixel size was 0.25 μm^2 (0.5 x 0.5 μm). To evaluate the probability to support the pluripotent state, a probability curve was calculated for three synthetic shapes (three exponential sizes for squares from 21 to 23) (Figure 6.7 C). The synthetic shape count with the highest Oct-4 probability (ie. peak value) was higher in small squares compared to large squares. Therefore, human iPS cells favour elevations with a small area and a high Oct-4 positive cell count is found at a low number of large elevations. This conclusion is in agreement with my previous finding, stating that human iPS cells grow on substrates with small pillar sizes whereas large pillar sizes do not support expansion of

human iPS cells.

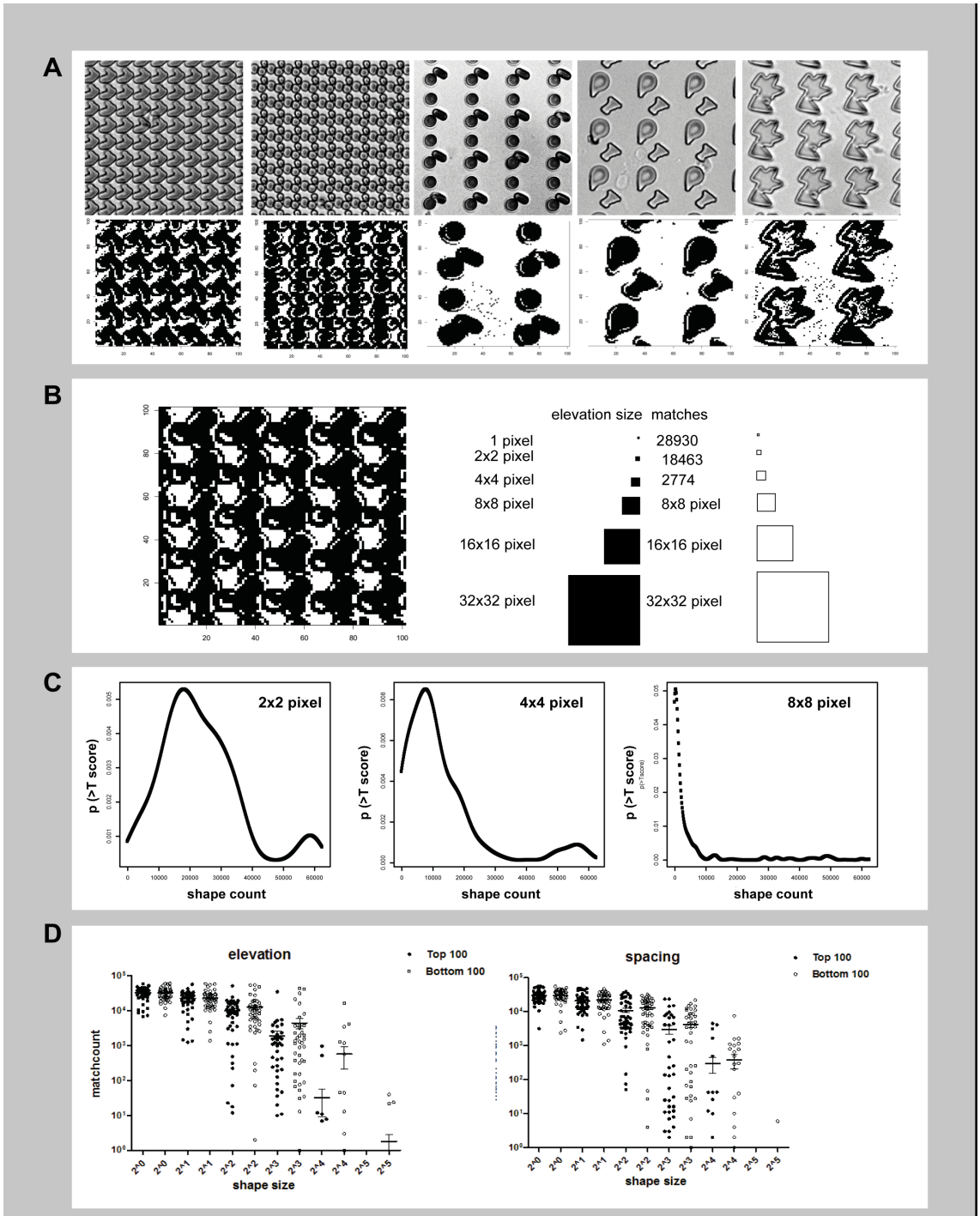

Figure 6.7: Quantification of topography spacing and elevation. (A) Representative images of topography phase contrast images (top row) with corresponding image matrices (bottom row). (B) Image matrices were convolved using synthetic shapes to extract the number of matches of synthetic shapes (C) Probability curves showing the likelyhood of high Oct4 positive cell counts for each topography.

We next considered whether the addition of further parameters would improve the resolution of the analysis. To understand the contribution of topography spacing we included the analysis of white pixels and added two further synthetic shapes (20 and 25). We ranked topographies on the basis of Oct-4+ cells as previously described (Chapter 3.2) and found that there is a significant difference in the synthetic shape counts of sizes 24 and 25 between Top 100 and Bottom 100 (Figure 6.7 D). Surprisingly, no difference in shape counts was observed in all synthetic shape counts of the negative images. This finding is in agreement with the results of Chapter 3.2, indicating that topography area and in particular topography elevation 24 (equivalent to 64 μm^2) may be a critical parameter to identify topographies that support the self-renewal of human iPS cells. To further analyze aspects of topographical parameters, we expanded the synthetic shape toolbox by adding synthetic rectangles (2^0, $16 * 2^0$) to ($2^5, 16 * 2^5$) to make a total of 12 parameters for topography elevation (six exponential sizes for squares and six exponential sizes for rectangles) and 12 parameters for topography spacing (six exponential sizes for squares and six exponential sizes for rectangles). Using the combined match counts of 703 images and their negative counterparts, principal component analysis (function 'prcomp') was performed with the match counts as features and the images as samples (Figure 6.8 A and B)(Sigg, 2014). Projection of the samples into the PC1, PC2-plane and color coding according to the quality score of the topography showed a relatively narrow area of favorable feature combinations, indicating that shape counts may identify favorable topographies (Figure 6.8 B). Thus, we are able to describe the survival or growth of human iPS cells on topographies based on sophisticated analysis of topographical parameters as also shown in Chapter 6.4. However, we now have also generated a tool that allows us to generate novel topographies with known cellular responses.

To validate our prediction model, we compared the original 703 images to 22

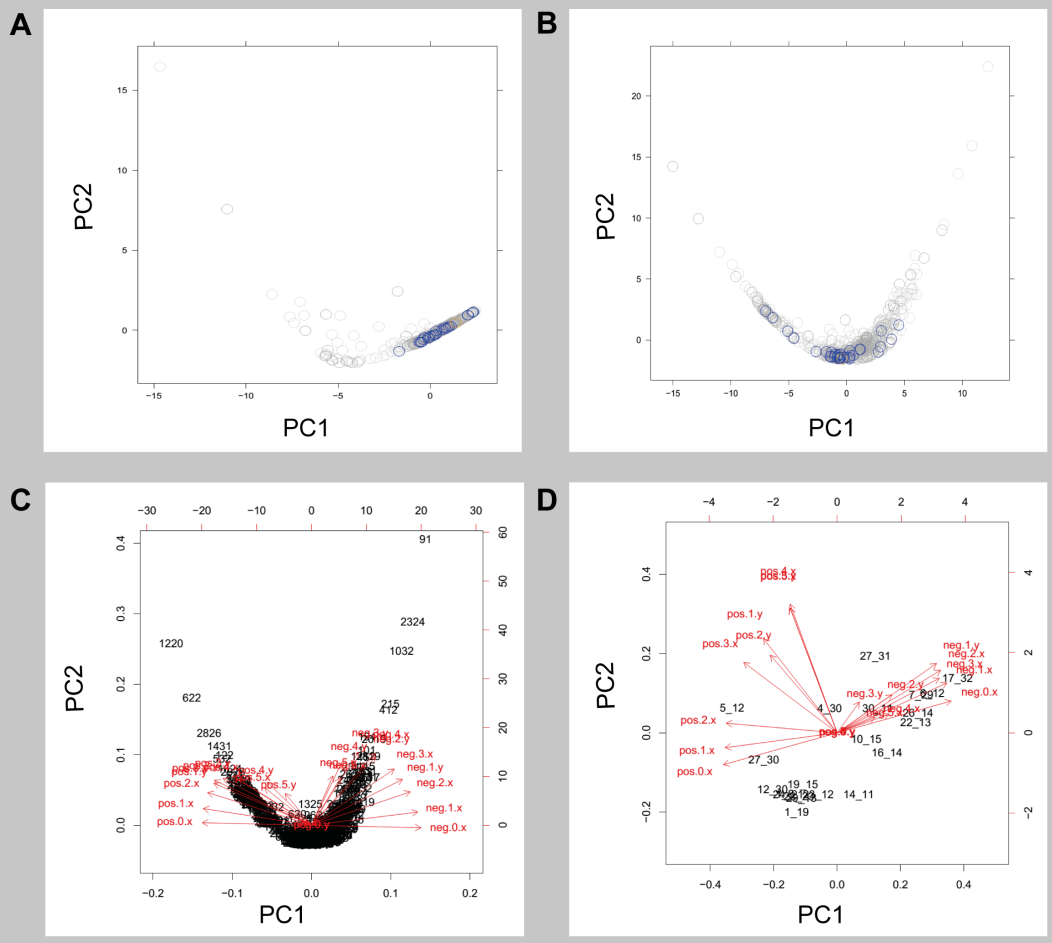

Figure 6.8: Principal component analysis to identify the optimal topography. Principal component analysis (PCA) was performed with the match counts as features and the images as samples. PCA of (A) synthetic squares and (B) synthetic squares and rectangles. Biplot analysis of (C) all 702 images and (D) 22 images that were predicted to support pluripotency.

images that were previously predicted as Top 100 hits using biplots. As expected, we found similar placements in the PC1, PC2-plane for both types of analysis, showing that our prediction model was accurate (Figure 6.8 C and D). Reverting the linear model of the PCA for the best images, allowed us to isolate a narrow area and display the best hypothetical topography (Figure 6.9 A). As before, we set a threshold with the lower gray range to '0' and the higher to '255' converting the input image into a black-and-white image matrix (Figure 6.9 B). Based on the optimised topography derived from the PCA model, a synthetic regularized topography was

created with the corresponding pillar shape and spacing (Figure 6.9 C). To confirm our prediction model, we tested the optimised topography using the established principal component analysis pipeline (Figure 6.9 D).

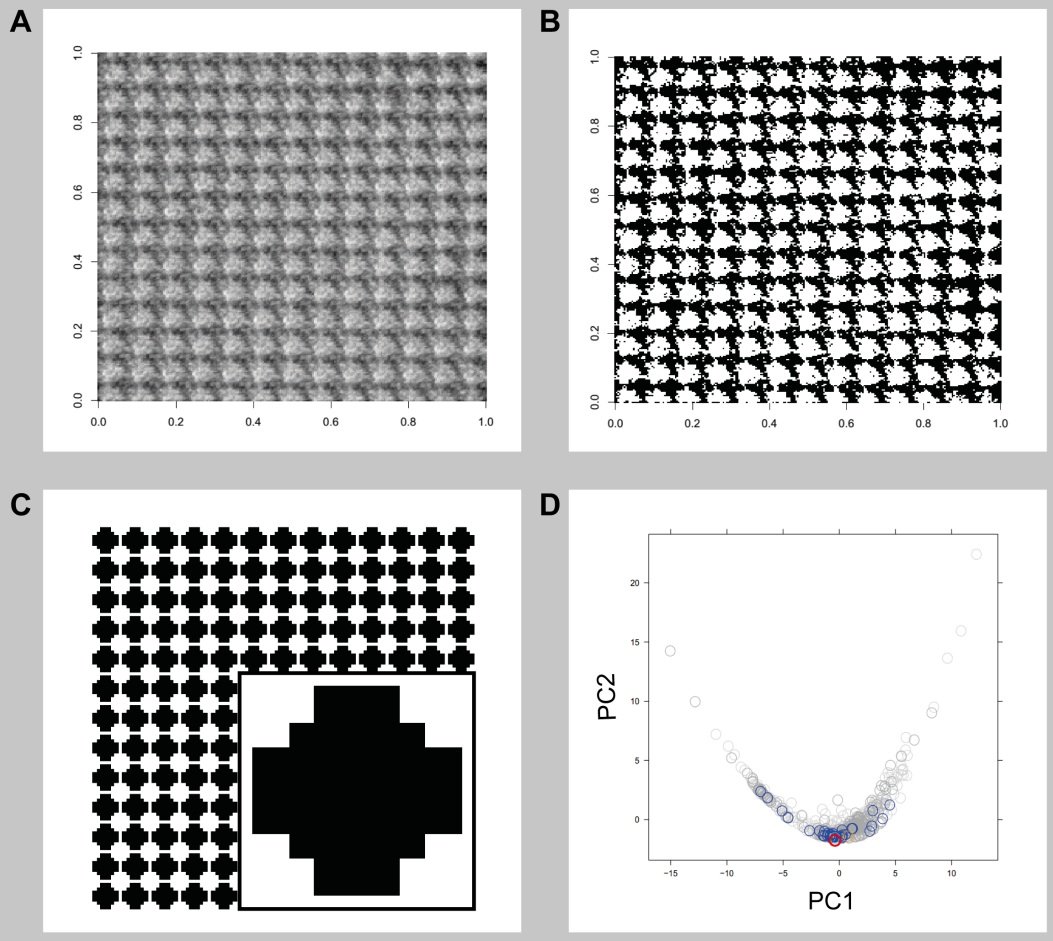

Figure 6.9: Prediction model of optimised topography. (A) Display of the best hypothetical topography by reverting the linear model of the PCA. (B) Conversion of the input image into a black-and-white image matrix. (C) A synthetic regularized topography was created with the corresponding pillar shape and spacing (magnification). (D) Location of the optimised topography in the PC1, PC2-plane (red).

5.2.5 Discussion

The interaction of stem cells with synthetic substrates has been studied extensively (Mei et al., 2010). Here, I was able to demonstrate that human iPS cells respond to topographical features of the culture substrate. Furthermore, I have defined fea-

tures that support or decrease proliferation and Oct-4 expression. Distinct cellular morphologies were observed in the Top 100 group (data not shown) and it remains unclear how human iPS cells interact with different topographies that support the pluripotent state. It may be possible that the interaction with the substrate is supported by ROCK inhibition and that subtle changes in topographical features has no effect on the cellular phenotype due to actin stabilization which may hinder the cell to adapt to topographical changes. However, the striking difference between the Top 100 group and Bottom 100 group shows the significance of surface micro-structures and how they can be used to direct stem cell behavior.

Topographical features have previously been shown to elicit responses in a variety of somatic and pluripotent cells (Mashinchian, O. et al., 2015, Unadkat et al., 2009). Topography influences both generic aspects of cell behaviour, such as adhesion, cytoskeletal organisation and migration, and cell type-specific properties, such as selection of a specific differentiated lineage. The identification of signalling pathways that integrate different extrinsic stimuli to achieve specific outcomes is of considerable interest (Watt et al., 2013). In the case of topographies, the simple parameter of cell size (Ginzberg et al., 2015) can potentially have a major impact on cellular responses, as a larger cell will have a different interface with a specific feature than a small cell, which will in turn affect cell spreading and cytoskeletal organisation.

The algorithm developed in this chapter was used to design an optimized cell culture substrate that may be used for the expansion of pluripotent stem cells. Nevertheless, it remains unclear how human iPS cells respond to the optimized substrate in an experimental setting. Further studies are required to address this along with a mechanistic study of how cells respond to the topographical features described here.

I conclude that by combining a topographical library with high content imaging

and computational analysis, it is possible to design polystyrene substrates that support maintenance of pluripotency in xeno-free medium in the absence of exogenous ECM. These findings are not only of practical importance for future clinical applications of human iPS cells but also raise interesting questions about how cells 'read' the physical constraints of their environment to select different fates.

5.3 Additional cells and substrates to study stem cell function

5.3.1 Fibroblast heterogeneity in the skin

Growth of fibroblasts in hydrogels

So far, I have described the capability of extracellular matrix components and substitutes to control the self-renewal ability of human iPS cells. The main focus of this chapter is the development of further assays for phenotyping neural progenitor cells and mesenchymal stem cells of the skin. Firstly, neural stem cells were generated from human iPS cells through an embryoid body intermediate with subsequent analysis of the self-renewing component sonic hedgehog. Secondly, fibroblasts that were isolated from neonatal mice were subjected to a 3D hydrogel assay to study the functional differences. The aim of this chapter is to compare how stem cells with a different cellular origin respond to comparable assay conditions. High-content analysis was used to screen for cellular phenotypes as described in the previous chapters.

It has previously been described that the potential to turn into fat cells is affected by the tissue of origin. The uppermost layer of the dermis, or papillary dermis, never gives rise to adipogenic cells whereas the underlying dermal layers including the reticular and hypodermis possess the ability to undergo adipogenesis. To further characterise differences in mesenchymal stem cells within the skin, I adapted and

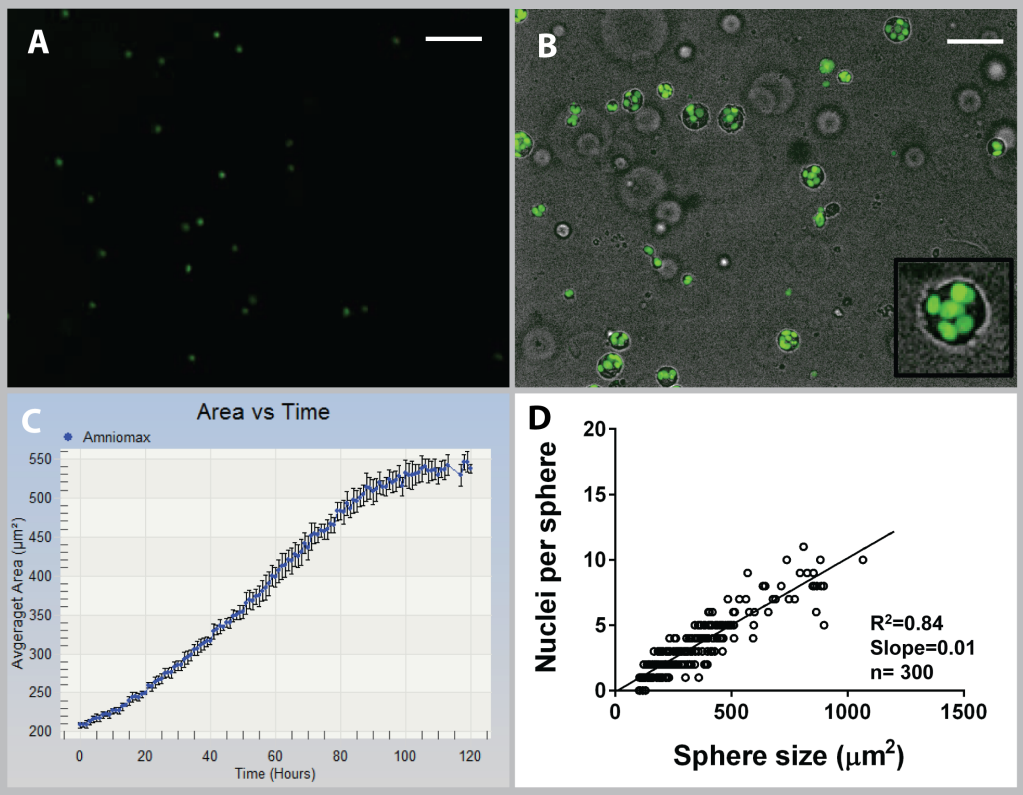

Figure 7.1: Growth of fibroblasts in 3D hydrogels. Fibroblasts isolated from postnatal (P2) mouse back skin was digested and seeded at clonal density in 3D hydrogels. Cell growth was monitored after (A) one day and (B) five days. (C) Live-cell imaging was used to capture the expansion of sphere sizes. (D) The number of nuclei was determined for each sphere and plotted against sphere size. Scale bars: 100 µm.

improved a clonal *in vitro* assay based on 3D hydrogel cultures. Firstly, fibroblasts were encapsulated in hydrogels at a clonal density and cultured in amniomax, which is known to allow fibroblast expansion. The cell density was set to 4 x 10^5/ml and the substrate volume to 50 μl to enable the acquisition of a sufficient number of clones for high-content analysis. For the set-up of assay conditions, H2B-GFP positive fibroblasts were used to allow the quantification of live cells.

GFP expression was visualised after 24 hours using the operetta high-content imaging system (Figure 7.1 A). After five days in culture, cells divided at different rates giving rise to cell spheres with different sizes and number of cells (Figure 7.1 B). The growth rate was determined by measuring the area of each sphere at an

hourly rate. A linear increase in sphere size was observed with time (Figure 7.1 C). On day 5 of the assay, the number of cells in each sphere was counted through the detection of GFP-positive nuclei. A linear correlation (R^2=0.81) was found between the number of nuclei and sphere size indicating that cell proliferation was the cause of sphere expansion (Figure 7.1 D). 100 clones were examined per condition and two technical replicates were used for each condition.

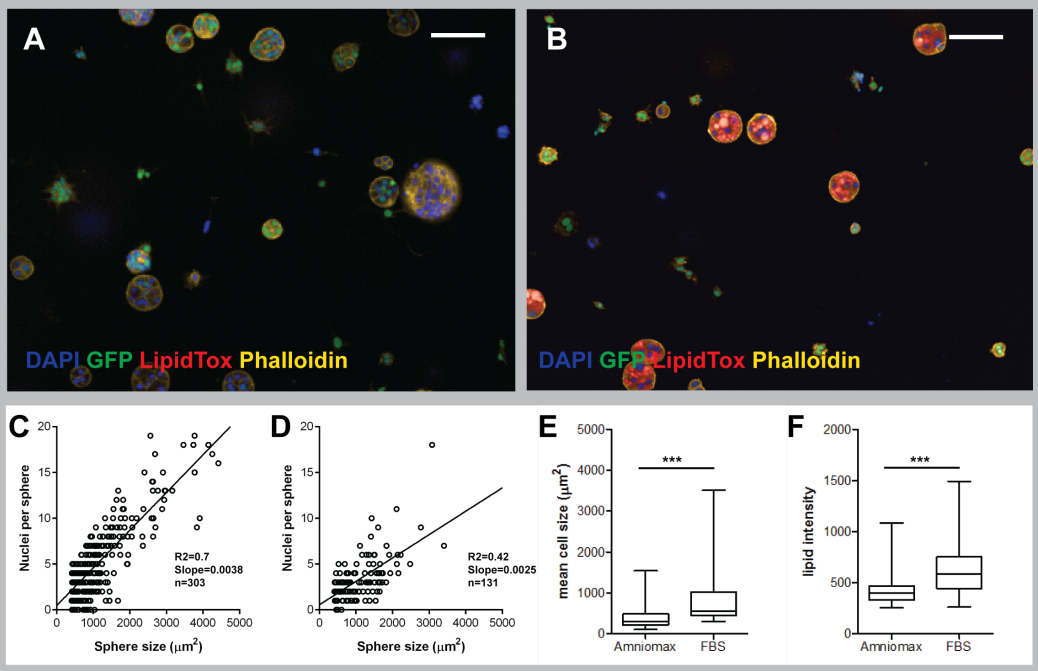

Figure 7.2.: Differentiation of fibroblasts. Fibroblasts were grown from day 5 to day 10 in (A) amniomax or (B) DMEM supplemented with FBS and stained with LipidTox to assess lipid production. (C and D) The number of nuclei per sphere was determined for each media condition and plotted against sphere size. (E) The mean cell size in each sphere was calculated by dividing sphere size by the number of nuclei. (F) The lipid intensity was determined for each sphere. Scale bars: 100 µm.

After 5 days in culture, media conditions were either changed to FBS to induce adipogenic differentiation or kept unchanged as a control (Figure 7.2 A and B). To quantify the differentiation and proliferation response, cells were labelled with DAPI to detect cell nuclei and stained with LipidTox to detect lipid production. The number of cell divisions and ability to differentiate into adipocytes was quantified using automated high-content analysis. For each clone, the number of cells

was counted and the mean lipid intensity determined. The number of nuclei per sphere was plotted against the sphere size to quantify the density of cell spheres during differentiation or proliferation (Figure 7.2 C and D). The mean cell size for each sphere was calculated by dividing sphere size by the number of nuclei. In adipogenic medium, the mean cell size and lipid intensity was significantly higher in differentiation conditions compared to the control (Figure 7.2 E and F).

Growth of fibroblasts in hydrogels

To test the adipogenic potential of mesenchymal stem cells arising from a specific location within the skin, neonatal back skin from P2 mice was digested and sorted by an Aria II according to a defined set of markers including Dlk-1, Sca-1 and CD26. The sorting strategy was adapted from work by Driskell et al. (Driskell et al., 2013). In brief, debris was removed according to cell size and granularity, singlets were isolated by cell area vs size and dead cells removed by DAPI staining (Figure 7.3 A). Papillary cells were isolated by CD26 expression and cells from the reticular dermis were Dlk-1+ and Sca-1 (Figure 7.3 A). The upper layer of the hypodermis was extracted from the lower part of the hypodermis by differential expression of Dlk-1 in a Sca-1+ population (Figure 7.3 A). After 10 days in culture, cells were assessed for their ability to divide or turn into fat cells (Figure 7.3 B). Cells were fixed and labelled with DAPI to detect cell nuclei and Phalloidin to identify the cell cytoskeleton. LipidTox was used to label fat and quantify the ability to undergo adipogenesis.

To describe the functional ability of these distinct subpopulations, single cell data was plotted on a graph highlighting the number of cell divisions and the mean fluorescence intensity of lipid staining (Figure 7.3 C). Four different clusters of cell proliferation were distinguished. If one nucleus was detected, the clone was classified as 'no cell division'. Slow proliferating clones (1-4 cell divisions) were grouped if

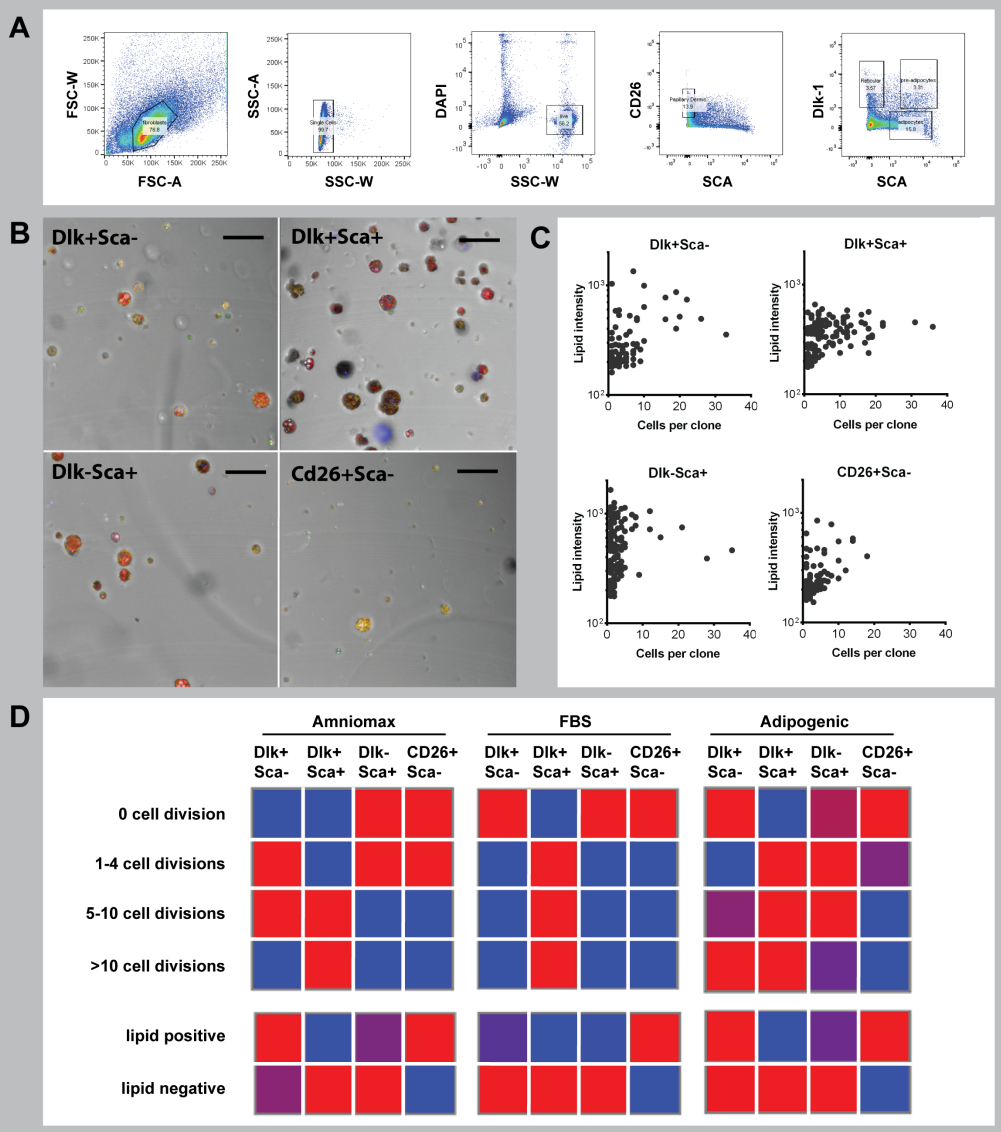

Figure 7.3: Fibroblast heterogeneity in the skin. (A) Fibroblasts isolated from prenatal mouse back skin were flow-sorted as previously described (Driskell et al., 2014). Four distinct subpopulations were isolated according to Dlk-1, Sca-1 and CD26 expression. Cells from the papillary dermis were CD26+ Sca-1- and cells from the reticular dermis Dlk-1+ Sca-1-. Two distinct pre-adipocyte populations were described and distinguished by Dlk-1 expression (Dlk-1+ Sca+ and Dlk-1- Sca+). (B) Each cell population was cultured seperately in 3D hydrogels for 10 days and stained with DAPI, LipidTox and Phalloidin. (C) The functional characterisitcs of each fibroblast subpopulation were described by the number of cell divisions and the ability to turn into fat. (D) Three different media conditions were tested and classified by their ability to divide or produce lipid. Red indicates high numbers of clones, blue indicates low numbers of clones and purple represents an intermediate number. At least 60 and a maximum of 200 cells were analysed for each population and at each condition.

two to five nuclei were counted. An intermediate class was defined as five to ten cell divisions and more than ten cell divisions was called fast proliferating (Figure 5.19D). Clones were also assessed by their ability to produce lipid and determined

lipid positive if the mean fluorescence intensity of LipidTox was greater than 250.

In self-renewal conditions the number of clones undergoing slow or intermediate cell divisions (1-4 cell divisions or 5-10 cell divisions) was higher in reticular (Dlk-1+Sca-) compared to papillary (Sca-1- Cd26+) populations. If, however, cells were induced to differentiate in adipogenic medium clones divided at a faster rate in the reticular population indicated by a greater number of clones represented in the fast proliferating class. Cells of the papillary dermis divided at a similar rate in self-renewal and differentiation conditions. Furthermore, no lipid droplets were observed in cells of the papillary dermis while cells from the reticular dermis produced high levels of lipids in adipogenic medium and lower levels in the self-renewal medium. The upper layer of the hypodermis (Dlk+Sca+) proliferated at high rates and the majority of clones turned into fat (Figure 7.3 D). Cells from the lower layer of the hypodermis (Dlk-Sca+), however, showed a much lower number of cells in the fast proliferating class with the majority of clones dividing little in self-renewal conditions and at an intermediate rate in adipogenic media. The majority of cells from both compartments of the hypodermis entered adipogenic differentiation in self-renewing and differentiation conditions (Figure 7.3 D). Thus, we can conclude that the positional identity of fibroblasts within the skin has a profound influence on the self-renewing and differentiating phenotype. To further my analysis on the interaction between different fibroblast populations, I collaborated with Maria Mastrogiannaki to study the effect of β-catenin activation in the dermis.

5.3.2 Effect of beta-catenin activation on the ability to induce lipid production in fibroblasts of the lower dermis

To establish whether β-catenin activation within pre-adipocytes resulted in an inhibition of differentiation, we analysed the differentiation capacity of Sca-1+ fibroblasts. PdgfraCreERT2, TdTomatolox/stop/lox and Ctnnb1 exon3fl/+ mice were

crossed and treated with tamoxifen on the day of birth (Figure 7.4 A). We applied a similar flow-sorting strategy as before but included ITGA6 to ensure no stem cells from the epidermal basal layer were present in culture (Figure 7.4 B and C). Activation of β-catenin did not affect the proportion of Sca1+ cells that expressed the pre-adipocyte marker CD24 (Festa et al., 2011) (Figure 7.4 D, courtesy of M. Mastrogiannaki). I encapsulated the flow-sorted SCA1+ TdTomato+ fibroblasts in hydrogels as shown previously and cultured the cells in control or adipogenic medium. After 10 days in culture individual clones were scored for cell number and the total intensity of LipidTox staining (Figure 7.4 E). As shown in Figure 7.4 F and G, β-catenin activation did not stimulate clonal growth *in vitro*. It did, however, decrease adipocyte differentiation, both in standard medium (Figure 7.4 H) and in medium supplemented with adipogenic factors (Figure 7.4 I), regardless of clone size. These findings indicate that the effect of β-catenin activation is to inhibit commitment of Sca1+ fibroblasts to undergo adipocyte differentiation.

5.3.3 Differentiation of human iPS cells into neural progenitors

For the generation of neural progenitor cells (NPCs) iPS cell line BOB and iPS cell line SPC clone 2 were induced to differentiate by the removal of FGF as previously described (Boyer et al., 2012). Embryoid bodies (EBs) were made by dissociating iPS cell colonies and culturing on low adhesive dishes. Noggin was added during the first two weeks to inhibit TGF-β signaling and induce differentiation into the neural lineage (Figure 7.5 A). After one week in culture, by which EBs developed into dense cell spheres (Figure 7.5 B), EBs were plated onto poly-L-ornithine/laminin-coated cell plates to initiate neurite outgrowth. Neural rosettes started to appear on day 10 after the start of differentiation. Neural rosette formation was three days slower with iPS cell line SPC clone 2 compared to iPS cell line BOB (data not

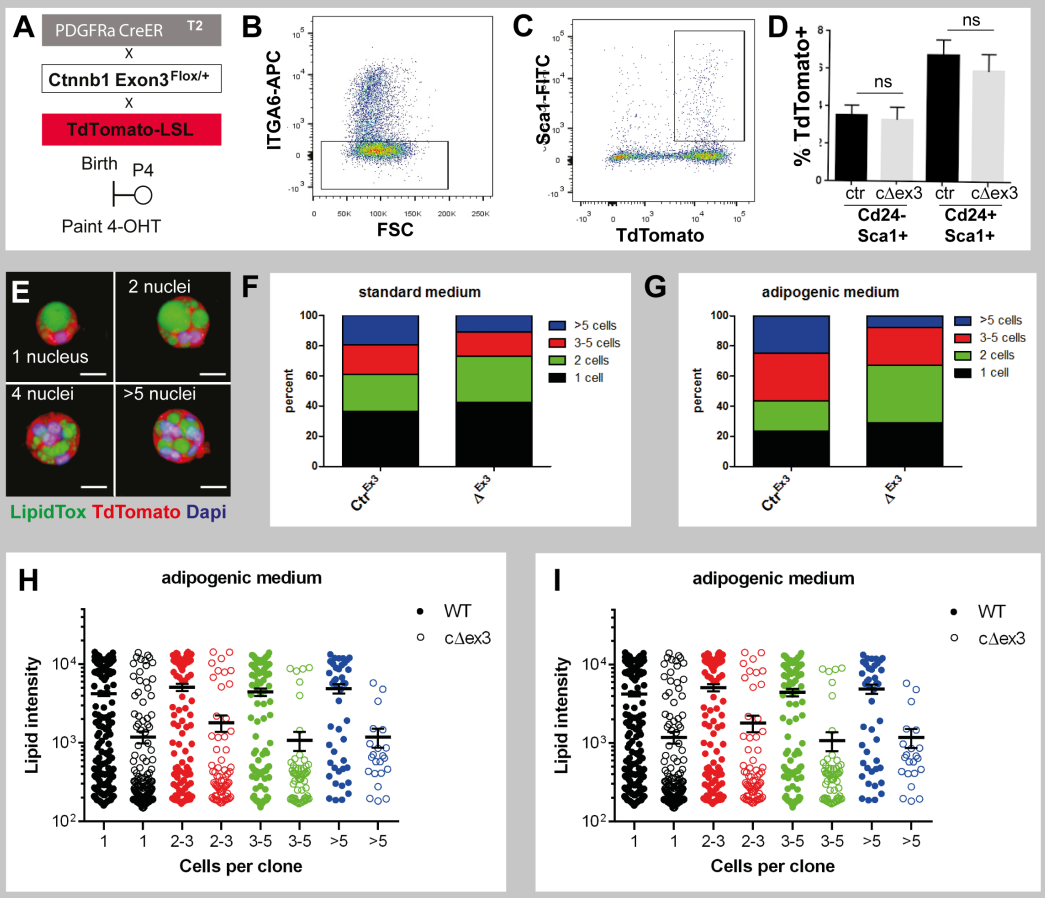

Figure 7.4: Effect of β-catenin activation on adipocyte differentiation in cultured Sca1+ fibroblasts (A) Schematic illustration of experimental strategy. (B-D) Sca1+ TdTomato+ targeted fibroblasts from dermal cell suspensions of PDGFRaCreER x Rosa26TdTomato x Ctnnb1 +/+ (Ctr) and PDGFRaCreER x Rosa26TdTomato x Ctnnb1Δex3fl/+(cΔex3) littermates were isolated by flow cytometry. (B, C) Gating out β6 integrin-positive cells (keratinocytes) (B) and positive selection for Sca1+TdTom+ cells (C). (D) Recombination efficiency (% TdTomato+ cells) in CD24+ and CD24-Sca1+ cells. Data show means with SEM of triplicate samples in a representative experiment (N=3 independent experiments) ns: difference not significant. (E) Examples of individual colonies formed by Sca1+ fibroblasts stained for LipidTox (green), TdTomato (red) and DAPI (blue). Scale bars = 10 μm. (F, G) Percentage of colonies containing 1, 2, 3-5 or more than 5 cells in standard (F) and adipogenic (G) medium. (H, I) Total LipidTox fluorescence (lipid intensity) per clone in control (ctr) and mutant (cΔex3) cultures grown in standard (H) or adipogenic (I) medium. (F-I) N = 2-3 biological replicates and 2 technical replicates. ns: no significant difference; * p≤0.05; ** p≤0.01, *** p≤0.005. F, G: two-way ANOVA with a Bonferroni post-test. H, I: 25% confidence intervals are shown.

shown). Rosettes were picked manually on day 14, reseeded and expanded in the subsequent week. After seven days, cells were expanded by passaging at a ratio of 1:2. Generated NPCs were stained for the neural stem cell markers Nestin, Sox-2 and Sox-1 to determine the differentiation efficiency (Figure 7.5 C and D). More

than 70% of cells expressed Sox-2 and almost 90% of cells were Nestin+, indicating a homogeneous population of NPCs. NPCs were passaged twice and maintained for ten days in the presence of sonic hedgehog.

5.3.4 Proliferation of neural progenitor cells after sonic hedgehog treatment

At passage 4, NPCs were treated with Accutase to make a single cell solution. Cells were seeded in the absence of sonic hedgehog at different cell densities onto poly-L-ornithine/laminin coated wells of a 96-well plate. Representative images after three days in culture are shown in Figure 7.6 A. The cell number and percentage of Sox-2 positive cells was determined for each condition on day one, two and three after plating. I was able to show that the percentage of Sox-2 positive cells declined at all densities during the 3-day interval. An increase in cell number was observed at the highest seeding density (200,000 cells/well), whereas fewer cells were counted after three days at the lowest seeding density (20,000 cells/well) (Figure 7.6 B).

To determine the effect of sonic hedgehog (SHH) on the self-renewal ability of NPCs, cells were seeded at a low density (20,000 cells/well) and treated with different concentrations of sonic hedgehog for three days (Figure 7.6 C). The number of cells declined during the three-day assay after the addition of sonic hedgehog and there was no difference between concentrations (Figure 7.6 D). However, an increase in the number of Sox-2 positive cells was observed at 200 ng/ml SHH (Figure 7.6 E). Surprisingly, fewer cells were Ki67 positive, a marker for cell cycle progression, if NPCs were stimulated with high concentrations of SHH (Figure 7.6 F). Therefore, sonic hedgehog is required to maintain Sox-2 expression in NPCs and may be considered a self-renewing factor.

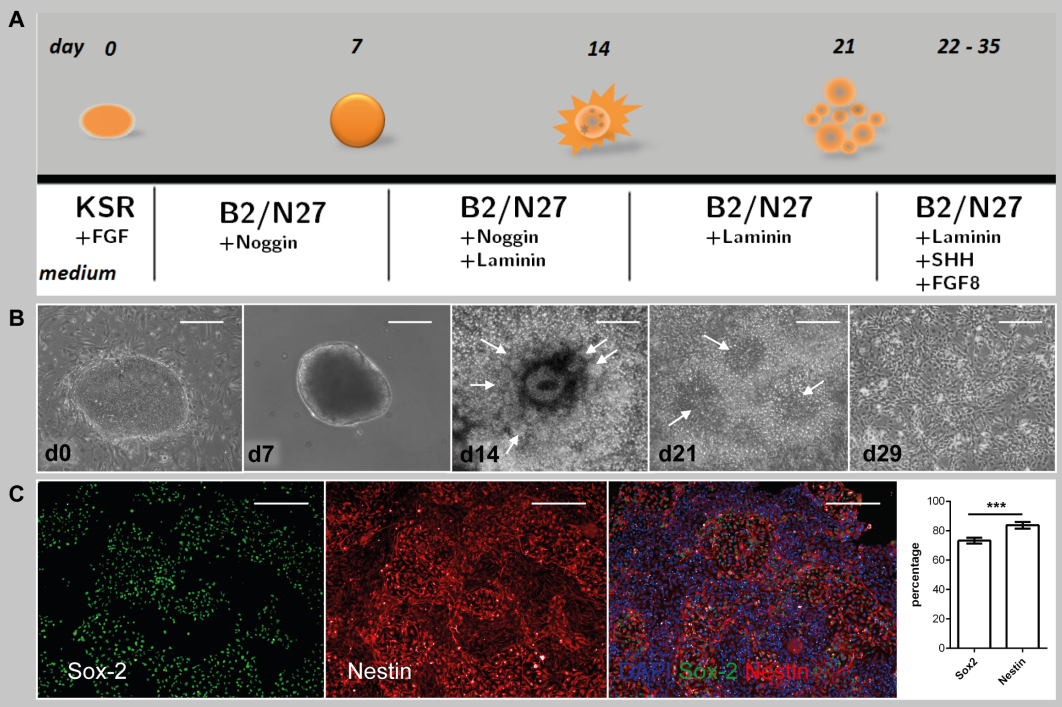

Figure 7.5: Generation of neural precursor cells from human iPS cells. hiPSC differentiation into neural progenitor cells. (A) Schematic presentation of the protocol for the generation of neural progenitor cells between the start of differentiation (day 0) and passage 4 (day 35). The applied culture medium for each week is indicated below the cartoons. (B) Morphological changes during the differentiation protocol. Images were taken on the day of passage for the first three weeks (d0-d21) and one day after the second passage (d29). (C) Immunofluoresence staining for Sox2, Sox1 and Nestin expression on the day of passage 2 (d28). Scale bar represents 200 µm.

5.3.5 Discussion

In this Chapter, I elucidated the positional identity of fibroblasts within the skin by testing whether fibroblasts from distinct dermal layers possess a pre-defined developmental program or can change their fate according to their environment. The clonal assay was previously applied by Driskell et al. (Driskell et al. 2012) and allows in-depth characterisation of cell proliferation and cell differentiation into lipid producing cells. Furthermore, previously identified fibroblast markers were used to isolate fibroblasts from different layers in the skin (Driskell et al., 2013).

It is known that cells from the papillary dermis cannot give rise to adipocytes while cells from the underlying dermis (reticular and hypodermis) undergo adipoge-

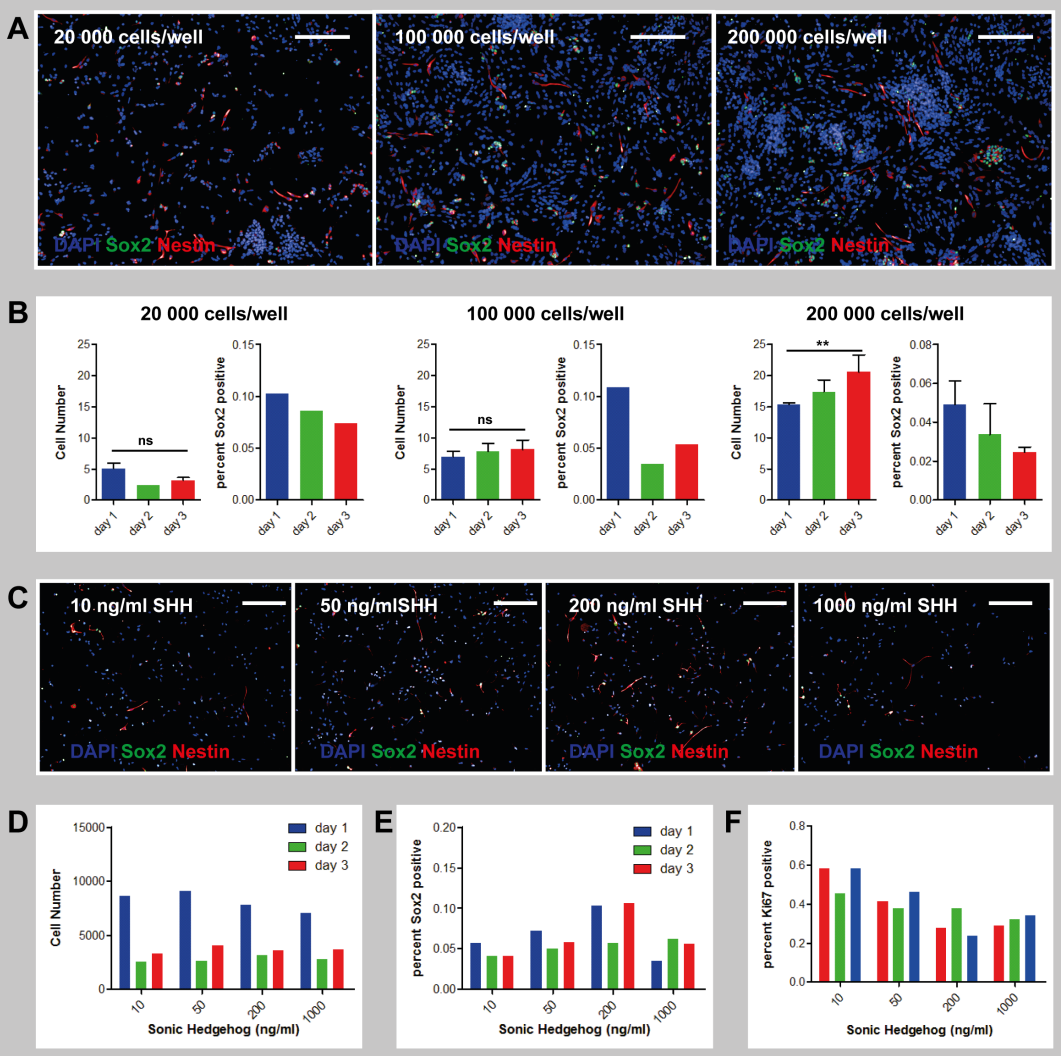

Figure 7.6: Self-renewal of neural progenitor cells. (A) Neural progenitor cells (NPCs) were grown for three days at different seeding in the absence of sonic hedgehog (SHH). (B)The cell number and Sox-2 expression was determined after one, two and three days. (C) At a low seeding density (20,000 cells/well), SHH was added at different concentrations to the medium. (D) The cell number, (E) percent Sox-2 positive cells and (F) percent Ki67 positve cells was determined at different SHH cocentrations after one, two and three days.

nesis with a variable potential depending on Dlk-1 expression (Driskell et al., 2013). Here, I was able to reproduce the original findings of Driskell et al. and further describe the functional role of papillary, reticular and hypodermal fibroblasts based on the rate of cell division and differentiation. Furthermore, I showed that activation of β-catenin has a profound effect on the differentiation capability of hypodermal fibroblasts by inhibiting adipocyte differentiation (Collins et al., 2011; Donati et al.,

2014). Therefore, the regulation of fibroblast commitment to undergo self-renewal or differentiation can be assessed using a hydrogel-based single cell assay.

In future studies, it might be interesting to study the differentiation capacity of fibroblasts to turn into multiple cell types (i.e. multipotency). At an early time point during murine development (at E12.5), fibroblasts possess the ability to turn into either mesenchymal cells of the skin or differentiate into muscle that control hair erection (also called piloerection) (Driskel et al., 2013). At a later time point, around birth, fibroblasts of the reticular dermis lose the ability to turn into muscle. However, it remains unclear how efficient the differentiation process is or how it is controlled. Therefore, it would be of high interest to the field to use the established methodology from this chapter to further analyse the differentiation capacities of fibroblasts from distinct layers of the skin.

Using a different cell type, I was also able to show that sonic hedgehog is a major self-renewal factor for neural stem cells. Depriving cells of this factor leads to differentiation and a loss of self-renewing phenotype (Koch et al., 2009; Briscoe, 2009). Therefore, neural stem cells that were produced from iPS cells rely on extrinsic cues to self-renew (Boyer et al., 2012; Chambers et al., 2009). In contrast to neural stem cells that were generated from human iPS cells, primary cells isolated from adult tissue may possess an intrinsic ability to undergo differentiation or self-renewal irrespective of extrinsic media conditions. The fibroblast subsets used in this study were ideally suited to test this hypothesis.

In conclusion, cells isolated from primary tissue possess regulatory cues that are difficult to reproduce using current *in vitro* culture methodologies. It may be possible to develop further strategies that allow more precise modelling of in vivo environments. These strategies include the reconstruction of the 3-dimensional architecture of living organs using bioengineered technologies such as 'organ on a chip' (Ertl. et al., 2014; Luni et al., 2014).

6 Conclusion

The regulation of stem cell behavior has been extensively described in distinct parts of the body (Barker et al., 2007; Melchers, 2007; Zhao et al., 2008; Watt & Hogan, 2000). However, applying basic research findings in a clinical setting has remained a challenge due to poorly described media conditions and the use of animal products which hinders the transplantation of cells into humans. Recent advancements have shown that animal products can be replaced by chemically defined substrates and media (Chen et al., 2011). My first goal was to generate a phenotyping platform that could be used to study the interaction of stem cells with the environment. In multi-well plates, a series of assays were established that were used to phenotype human iPS cells, neural progenitor cells and fibroblasts. Distinct and specific media and substrate conditions were used to generate environments that could be further adapted to investigate downstream signaling cascades involved in the self-renewal and differentiation of adult and pluripotent stem cells. It would be interesting to elucidate the interplay between cell-ECM interactions and the self-renewal signals of pluripotent stem cells. It is known that the inhibition of FGF signaling induces differentiation in ES cells (Ying et al., 2008) and that MEK-ERK signaling, which is the downstream effector cascade of bFGF, is involved in integrin-mediated signaling (Xu et al., 2010). Therefore, it would be of high interest to the field to test the possibility that FGF signaling is directly coupled to how pluripotent stem cells sense their biophysical environment. The cell-to-substrate interaction might be the critical determinant to enable the survival of human iPS cells at a single cell level. Conclusively, I have shown that human iPS cells can be used to develop a phenotyping platform that was applied to analyse cellular phenotypes of other cell types.

For the in-depth characterisation of cellular phenotypes, I developed a unique high-content analysis tool that allows the description of cell population distributions.

A sophisticated image analysis pipeline was created allowing the generation of large datasets including multiple parameters for each cell. In conjunction with Arsham Ghahramani, an algorithm based on t-Distributed Stochastic Neighbor Embedding (t-SNE) was developed to characterize the cellular behavior of pluripotent stem cells in response to the phenotyping assay (GrÃ$\frac{1}{4}$n et al., 2015). The algorithm allows the description and identification of many cell states.

My second goal was to produce an innovative surface that allows the maintenance of human iPS cells at low cost. It may be possible to commercialize this part of my thesis. The topography that I have discovered might enable the expansion of pluripotent stem cells at a large scale. Current expansion protocols include feeders or feeder-substitutes that are derived or extracted from animal tissue which is cost-ineffective and poses a high batch-to-batch variability. The plastic topographies, on the other hand, are cheap and easily reproduced by robotic technology. Furthermore, the substrate and media conditions that were used in my protocol were animal-product free possibly facilitating the development of human iPS cell-derived medicinal products. because, allowing the growth of human iPS cells under good manufacturing practice (GMP) conditions.

The topography algorithm that was used to predict the optimized topography may be used for the development of a range of topographies that allows the study of the cell-to-substrate interaction in greater detail. It is possible that topography pillars act as anchor sites and distinct pillar shapes provide different anchor sites which causes the cells to adapt a specific shape. It has previously been shown that mechanical cues can affect the shape of stem cells and direct stem cell fate decisions (Gautrot et al., 2012; McBeath et al., 2004; Trappman et al., 2012). It would be of high interest to the field if 3D substrates can reproduce these findings. Furthermore, the generation of 3D substrates may allow the production of next generation substrates with greater potential to reproduce living organs. Current

substrates used for tissue engineering constitute of scaffolds with different porosity (Viswanathan et al., 2015) but it remains unclear how cells react to patterned 3D substrates. It may be possible to introduce topographies in 3D scaffolds to allow the generation of more reproducible scaffolds with more tightly controlled stem cell attachment and regulation of cell fate.

In the third part of my thesis, I was able to show that neural progenitor cells generated from human iPS cells rely on extrinsic cues to self-renew whereas fibroblasts possess an intrinsic ability to differentiate or self-renew irrespective of media conditions. It may be possible that the cellular development *in vitro* is hampered by insufficient signals to ensure cells develop sufficiently. It would be interesting to compare other neural progenitor cells in the assay. For example, applying neural cells from different time points of the differentiation protocol would allow the identification of self-renewing phenotypes. Furthermore, the addition of morphogens such as FGF or Retinoic acid to the phenotyping platform would allow the study of signals involved in the anterior-posterior development of the brain.

The distinct fibroblast subpopulations that were isolated from neonatal back skin, however, may have been sufficiently programmed by their surrounding tissue making media conditions negligible in the subsequent assay. Fibroblasts were seeded at clonal density, allowing the description of cellular phenotypes at a clonal level. It would be of high interest to the field to describe cellular division during sphere formation in greater detail. For example, GFP-labelled nuclei could be used to study symmetric versus asymmetric cell division. Furthermore, the porosity of hydrogels could be modulated or topographies may be introduced into the gels to allow the study of different tissue architectures within the skin.

In summary, I have described how high-throughput technologies can be used to describe cellular phenotypes and discover innovative biomaterial substrates. The algorithms developed during my studies are of high interest to further research

projects in the Watt laboratory and may be applied in an industrial setting. The optimized topography will be tested thoroughly in future projects, potentially leading to further applications. The nature of my protocol allows the rapid transfer to good manufacturing practice (GMP) facilities, which would transform the industrial approach to culture human iPS cells. Finally, two distinct cell types were compared by their ability to respond to extrinsic cues. I was able to show that mesenchymal cells extracted from primary tissue possess an intrinsic ability to differentiate or self-renew independently of extrinsic cues while neural cells generated in the dish required extrinsic signals to show a self-renewal phenotype.

7 Publications

Analysis of human stem cell interactions at the single-cell resolution. Reimer, A. Drug Target Review.

A high-content platform to characterise human induced pluripotent stem cell lines. (2016) Leha, A., Moens, N., Meleckyte, R., Culley, O. J., Gervasio, M. K., Kerz, M., Reimer, A., Cain, S. A., Streeter, I., Folarin, A., Stegle, O., Kielty, C. M., Durbin, R., Watt, F. M., Danovi, D. & HipSci Consortium. Methods.

β-catenin stabilization in skin fibroblasts causes fibrotic lesions by preventing adipocyte differentiation of the reticular dermis. (2016) Mastrogiannaki, M., Lichtenberger, B. M., Reimer, A., Collins, C. A., Driskell, R. R. & Watt, F. M. Journal of Investigative Dermatology.

Scalable topographies to support proliferation and Oct4 expression by human induced pluripotent stem cells. (2016) Reimer, A., Vasilevich, A., Hulshof, F., Viswanathan, P., van Blitterswijk, C. A., de Boer, J. & Watt, F. M. Scientific Reports.

Macrophage infiltration and alternative activation during wound healing promote MEK1-induced skin carcinogenesis. (2016) Weber, C., Telerman, S. B., Reimer, A. S., Sequeira, I., Liakath-Ali, K., Arwert, E. N. & Watt, F. M. Cancer Research.

8 Acknowledgements

First and foremost, I would like to thank Fiona Watt for giving me the opportunity to help set up new methodologies and develop innovative technologies in the lab. It was great working in such a big lab with lots of freedom. The atmosphere was thoroughly good and I felt happy at work despite small difficulties that came up because of the move from Cambridge to London.

Straight after the start of my PhD, I was asked to travel regularly to Cambridge to transfer a feeder-system from Ludovic Valiers lab to our lab in London. I am grateful for his help in providing essential contacts during my PhD. Special thanks to Monica, who was in charge of the human iPS cell core in the Anne McLaren Laboratories, helping me kick-start my project by giving advice on human iPS cell culture techniques. Thanks to Sally from Cambridge CSCR for providing an initial stack of feeders that got me started with my project.

Many thanks to Chuks and his team from the Sanger Institute in Cambridge for helping and training me during the early stages of my PhD. It was great having occasional chats about the newest updates in the Human Induced Pluripotent Stem Cell Initiative (HipSci).

It was helpful to spend some time with Dusko Ilic and his team to gain insight into human ES cells. Thank you to Liani and Laureen for providing help and guidance with the feeder-free system.

Thank you to Jack Price who provided a feeder-free human iPS cell line and essential SOPs. It was very useful to collaborate and gain expertise in the neural stem cell field. Many thanks to Graham for fruitful discussions and Victoria for providing guidance on tissue culture technique.

After joining the lab, Davide Danovi, who directed HipSci phenotyping was a good mentor during my PhD and I would like to express my deepest gratitude for his patience to help and guide me throughout my course. It must have been difficult

at times to deal with my passion to drive my project and desperately find results. Big hugs to Ruta and Nathalie who helped me having some weekends off by sharing tissue culture duties.

It was amazing to be given the ability to collaborate on and off campus. Most importantly, I would like to thank Jan de Boer and his team for making my topography project possible. Thank you to Aliaksei for his mathematical expertise, Frits for showing me high-throughput analysis and his colleagues for giving me a nice time in the Netherlands. Thanks to Priya for providing me with new substrates that allowed me to finish my studies in London. It was also a great joy to go off campus in little Enschede.

Spending time away at the Ecole polytechnique federale de Lausanne (EPFL) with Vicki was a true pleasure. We learned how to make special microniches in Matthias Lutolfś lab. It was amazing to see how state-of-the-art technologies can emerge from old-fashioned instruments. The collaboration with Samy was a true success and I remember the late night exploration to Lausanne, spending a great time in shiny Swiss bars. The delicious cheese fondue on the last day was also a memory that sticks.

Working many hours with Jens Kleinjung was truly a challenge. My awe about his ability to turn an image into a binary code was truly aspiring and I enjoyed our collaborative effort to decode topography surfaces.

In the Watt laboratory, I have had positive and not so positive experiences with collaborations. But I have learned from all and am very thankful for all the help and guidance during my PhD. It was a great experience working with Ryan, who is now a group leader at the centre. We had hours of interesting discussions and it was useful to me as a young scientist to spend many hours talking about fibroblasts (no, seriously what are they actually for??). We also had a great laugh about GTA.

Big thank you to Arsham, who has done a good job in developing a new algorithm

that can make sense of millions of data points. I can imagine doing this kind of work while sharing a drink and also having a great time!

It was a great pleasure to work with Christine, who I spend most of my PhD talking German to and finding faults in anything. We are scientists after all and like to criticise at times. This goes along with the other Austrian fellows Gernot and Beate. War schön und auf jeden Fall die coolste office bay. We had lots of fun such as trying to understand British English.

Special thanks to the Cambridge crew including Marta, Vicki, Sam, Ajay, Kai and Giacomo for having joyful lunchtimes and generally being easy colleagues.

Last but not least, I want to thank my parents for providing a solid ground that helped me get through my PhD in less than three years. Big hugs and thank you also to Björn and Catrin for supporting me. I am very thankful to Laurie for being with me during most of my PhD time in London.

9 References

Adachi, K., & Schöler, H. R (2012). Directing reprogramming to pluripotency by transcription factors. Current Opinion In Genetics & Development, 22(5), 416.

Alves, H., Dechering, K., Van Blitterswijk, C., & De Boer, J (2011). High-throughput assay for the identification of compounds regulating osteogenic differentiation of human mesenchymal stromal cells. Plos One, 6(10), e26678.

Ambler, C. A., & Watt, F. M (2010). Adult epidermal Notch activity induces dermal accumulation of T cells and neural crest derivatives through upregulation of jagged 1. Development, 137(21), 3569.

Amit, M., Shariki, C., Margulets, V., & Itskovitz-Eldor, J (2004). Feeder layer- and serum-free culture of human embryonic stem cells. Biology of Reproduction, 70(3), 837.

Aoi, T., Yae, K., Nakagawa, M., Ichisaka, T., Okita, K., Takahashi, K., et al. (2008). Generation of pluripotent stem cells from adult mouse liver and stomach cells. Science, 321(5889), 699.

Appel, E. A., Larson, B. L., Luly, K. M., Kim, J. D., & Langer, R. (2014). Non-cell-adhesive substrates for printing of arrayed biomaterials. Advanced Healthcare Materials, 4(4), 501.

Appel, E. A., Tibbitt, M. W., Webber, M. J., Mattix, B. A., Veiseh, O., & Langer, R. (2015). Self-assembled hydrogels utilizing polymer-nanoparticle interactions. Nature Communications, 6, 6295.

Arnold, M., Cavalcanti-Adam, E. A., Glass, R., Blümmel, J., Eck, W., Kantlehner, M., et al. (2004). Activation of integrin function by nanopatterned adhesive interfaces. Chemphyschem, 5(3), 383.

Atala, A (2008). Advances in tissue and organ replacement. Current Stem Cell Research & Therapy, 3(1), 21.

Atit, R., Sgaier, S. K., Mohamed, O. A., Taketo, M. M., Dufort, D., Joyner, A. L.,

u. a (2006). β-catenin activation is necessary and sufficient to specify the dorsal dermal fate in the mouse. Developmental Biology, 296(1), 164.

Berge, ten, D., Kurek, D., Blauwkamp, T., Koole, W., Maas, A., Eroglu, E., u. a (2011). Embryonic stem cells require Wnt proteins to prevent differentiation to epiblast stem cells. Nature Cell Biology, 13(9), 1070.

Blanpain, C. & E. Fuchs (2009). Epidermal homeostasis: a balancing act of stem cells in the skin. Nature Review Molecular Cell Biology, 10 (3), 207-217.

Boiani, M., & Schöler, H. R (2005). Developmental cell biology: Regulatory networks in embryo-derived pluripotent stem cells. Nature Reviews Molecular Cell Biology, 6(11), 872.

Bordese, M. & Alini, W. http://www.inside-r.org/packages/cran/biOps (2013). Boyer, L. F., Campbell, B., Larkin, S., & Mu, Y (2012). Dopaminergic differentiation of human pluripotent cells. Current Protocols In Stem Cell Biology. Chapter 1:Unit1H.6.

Braam, S. R., Zeinstra, L., Litjens, S., Oostwaard, D. W., van den Brink, S., van Laake, L., et al. (2008). Recombinant vitronectin is a functionally defined substrate that supports human embryonic stem cell self-renewal via $\alpha 1\beta 5$ integrin. Stem Cells, 26 (9), 2257.

Brawley, C., & Matunis, E (2004). Regeneration of male germline stem cells by spermatogonial dedifferentiation in vivo. Science, 304(5675), 1331.

Brons, I. G. M., Smithers, L. E., Trotter, M. W. B., Rugg-Gunn, P., Sun, B., de Sousa Lopes, S. M. C., et al. (2007). Derivation of pluripotent epiblast stem cells from mammalian embryos. Nature, 448(7150), 191.

Calder, E. L., Tchieu, J., Steinbeck, J. A., Tu, E., Keros, S., Ying, S.-W., et al. (2015). Retinoic Acid-Mediated Regulation of GLI3 Enables Efficient Motoneuron Derivation from Human ESCs in the Absence of Extrinsic SHH Activation. Journal of Neuroscience, 35(33), 11462.

Chambers, I., Colby, D., Robertson, M., Nichols, J., Lee, S., Tweedie, S., & Smith,

A (2003). Functional expression cloning of nanog, a pluripotency sustaining factor in embryonic stem cells. Cell, 113(5), 643.

Chan, Y., Göke, J., Ng, J., Lu, X., Gonzales, K. A. U., Tan, C., et al. (2013). Induction of a human pluripotent state with distinct regulatory circuitry that resembles preimplantation epiblast. Cell Stem Cell, 13(6), 663.

Chen, G., Gulbranson, D. R., Hou, Z., Bolin, J. M., Ruotti, V., Probasco, M. D., et al. (2011). Chemically defined conditions for human iPS cell derivation and culture. Nature Methods, 8(5), 424.

Chen, L., Acciani, T., Le Cras, T., Lutzko, C., & Perl, A.-K. T. (2012). Dynamic regulation of platelet-derived growth factor receptor α expression in alveolar fibroblasts during realveolarization. American Journal of Respiratory Cell and Molecular Biology, 47(4), 517.

Chowdhury, F., Na, S., Li, D., Poh, Y., Tanaka, T. S., Wang, F., & Wang, N (2009). Material properties of the cell dictate stress-induced spreading and differentiation in embryonic stem cells. Nature Materials, 9(1), 82.

Cimetta, E., Sirabella, D., Yeager, K., Davidson, K., Simon, J., Moon, R. T., & Vunjak-Novakovic, G (2013). Microfluidic bioreactor for dynamic regulation of early mesodermal commitment in human pluripotent stem cells. Lab Chip, 13(3), 355.

Cocks, G., Curran, S., Gami, P., Uwanogho, D., Jeffries, A. R., Kathuria, A., et al. (2013). The utility of patient specific induced pluripotent stem cells for the modelling of Autistic Spectrum Disorders. Psychopharmacology, 231(6), 1079.

Coleman, M. A., Bridge, J. A., Lane, S. W., Dixon, C. M., Hill, G. R., Wells, J. W., u. a (2012). Tolerance induction with gene-modified stem cells and immune-preserving conditioning in primed mice: restricting antigen to differentiated antigen-presenting cells permits efficacy. Blood, 121(6), 1049.

Collins, C. A., Kretzschmar, K., & Watt, F. M (2011). Reprogramming adult dermis to a neonatal state through epidermal activation of β-catenin. Development,

138(23), 5189.

Connelly, J. T., Gautrot, J. E., Trappmann, B., Tan, D. W., Donati, G., Huck, W. T. S., & Watt, F. M (2010). Actin and serum response factor transduce physical cues from the microenvironment to regulate epidermal stem cell fate decisions. Nature Cell Biology, 12(7), 711.

Consiglio, A., Gritti, A., Dolcetta, D., Follenzi, A., Bordignon, C., Gage, F. H., et al. (2004). Robust in vivo gene transfer into adult mammalian neural stem cells by lentiviral vectors. Proceedings Of The National Academy Of Sciences, 101(41), 14835.

Cotsarelis, G., Sun, T., & Lavker, R. M (1990). Label-retaining cells reside in the bulge area of pilosebaceous unit: Implications for follicular stem cells, hair cycle, and skin carcinogenesis. Cell, 61(7), 1329.

Dalby, M. J., Gadegaard, N., & Oreffo, R. O. C. (2014). Harnessing nanotopography and integrin-matrix interactions to influence stem cell fate. Nature Materials, 13(6), 558.

Dalby, M. J., Gadegaard, N., Tare, R., Andar, A., Riehle, M. O., Herzyk, P., et al. (2007). The control of human mesenchymal cell differentiation using nanoscale symmetry and disorder. Nature Materials, 6(12), 997.

Dang, L., Feric, N., Laschinger, C., Chang, W., Zhang, B., Wood, G. et al., (2014) Inhibition of apoptosis in human induced pluripotent stem cells during expansion in a defined culture using angiopoietin-1 derived peptide QHREDGS. Biomaterials, 35 (27), 7786.

Desbordes, S. C., Placantonakis, D. G., Ciro, A., Socci, N. D., Lee, G., Djaballah, H., & Studer, L (2008). High-throughput screening assay for the identification of compounds regulating self-renewal and differentiation in human embryonic stem cells. Cell Stem Cell, 2(6), 602.

Donati, G., Proserpio, V., Lichtenberger, B. M., Natsuga, K., Sinclair, R., Fujiwara,

H., & Watt, F. M (2014). Epidermal Wnt/β-catenin signaling regulates adipocyte differentiation via secretion of adipogenic factors. Proceedings Of The National Academy Of Sciences, 111(15), 1501.

Driskell, R. R., & Watt, F. M (2015). Understanding fibroblast heterogeneity in the skin. Trends In Cell Biology, 25(2), 92.

Driskell, R. R., Giangreco, A., Jensen, K. B., Mulder, K. W., & Watt, F. M (2009). Sox2-positive dermal papilla cells specify hair follicle type in mammalian epidermis. Development, 136(16), 2815.

Driskell, R. R., Juneja, V. R., Connelly, J. T., Kretzschmar, K., Tan, D. W. M., & Watt, F. M (2011). Clonal growth of dermal papilla cells in hydrogels reveals intrinsic differences between Sox-2-positive and -negative cells in vitro and in vivo. Journal Of Investigative Dermatology, 132(4), 1084.

Driskell, R. R., Lichtenberger, B. M., Hoste, E., Kretzschmar, K., Simons, B. D., Charalambous, M., et al. (2013). Distinct fibroblast lineages determine dermal architecture in skin development and repair.

Driskell, R. R., Lichtenberger, B. M., Hoste, E., Kretzschmar, K., Simons, B. D., Charalambous, M., et al. (2013). Distinct fibroblast lineages determine dermal architecture in skin development and repair. Nature, 504(7479), 277.

Driskell, R. R., Lichtenberger, B. M., Hoste, E., Kretzschmar, K., Simons, B. D., Charalambous, M., et al. (2013). Distinct fibroblast lineages determine dermal architecture in skin development and repair. Nature, 504(7479), 277.

Editors. Can biological phenomena be understood by humans? Nature 403, 345 (2000).

Elisseeff, J., Ferran, A., Hwang, S., Varghese, S., & Zhang, Z (2006). The role of biomaterials in stem cell differentiation: Applications in the musculoskeletal system. Stem Cells And Development, 15(3), 295.

Enshell-Seijffers, D., Lindon, C., Wu, E., Taketo, M. M., & Morgan, B. A (2010).

-Catenin activity in the dermal papilla of the hair follicle regulates pigment-type switching. Proceedings Of The National Academy Of Sciences, 107(50), 21564.

Ertl, P., Sticker, D., Charwat, V., Kasper, C., & Lepperdinger, G. (2014). Lab-on-a-chip technologies for stem cell analysis. Trends in Biotechnology, 32(5), 245.

Falk, S., Wurdak, H., Ittner, L. M., Ille, F., Sumara, G., Schmid, M.-T., et al. (2008). Brain area-specific effect of TGF-beta signaling on Wnt-dependent neural stem cell expansion. Cell Stem Cell, 2(5), 472.

Forristal, C. E., Winkler, I. G., Nowlan, B., Barbier, V., Walkinshaw, G., & Levesque, J. P (2012). Pharmacologic stabilization of HIF-1 increases hematopoietic stem cell quiescence in vivo and accelerates blood recovery after severe irradiation. Blood, 121(5), 759.

Fuchs, E (2014). Stem cell paradigms in tissue regeneration and cancer. Blood, 124(21), SCI-41.

Fukuda, S., Kato, F., & Tozuka, Y (2003). Two distinct subpopulations of nestin-positive cells in adult mouse dentate gyrus. 23(28): 9357.

Gafni, O., Weinberger, L., Mansour, A. A., Manor, Y. S., Chomsky, E., Ben-Yosef, D., et al. (2013). Corrigendum: Derivation of novel human ground state naive pluripotent stem cells. Nature, 520(7549), 710.

Gage, F. H (2000). Mammalian neural stem cells. Science, 287(5457), 1433. Garcia, A. D. R., Doan, N. B., Imura, T., Bush, T. G., & Sofroniew, M. V (2004). GFAP-expressing progenitors are the principal source of constitutive neurogenesis in adult mouse forebrain. Nature Neuroscience, 7(11), 1233.

Gautrot, J. E., Wang, C., Liu, X., Goldie, S. J., Trappmann, B., Huck, W. T. S., & Watt, F. M (2012). Mimicking normal tissue architecture and perturbation in cancer with engineered micro-epidermis. Biomaterials, 33(21), 5221.

Ginzberg, M.B., Kafri, R. & Kirschner, M. On being the right (cell) size. Science 348, 1245075 (2015).

Gobaa, S., Hoehnel, S., Roccio, M., Negro, A., & Kobel, S (2011). Artificial niche microarrays for probing single stem cell fate in high throughput. Nature Methods, 8(11), 949.

Götz, M., & Huttner, W. B. (2005). The cell biology of neurogenesis. Nature Reviews Molecular Cell Biology, 6(10), 777.

Grajski, K. A., Breiman, L., Di Prisco, G. V., & Freeman, W. J (1986). Classification of EEG Spatial Patterns with a Tree-Structured Methodology: CART. IEEE Transactions On Biomedical Engineering, BME-33(12), 1076.

Guilak, F., Cohen, D. M., Estes, B. T., Gimble, J. M., Liedtke, W., & Chen, C. S (2009). Control of stem cell fate by physical interactions with the extracellular matrix. Cell Stem Cell, 5(1), 17.

Hamburg-Shields, E., & DiNuoscio, G. J (2015). Sustained β-catenin activity in dermal fibroblasts promotes fibrosis by up-regulating expression of extracellular matrix protein-coding genes. The Journal Of Pathology, 235(5), 686.

Harb, N., Archer, T. K., & Sato, N (2008). The Rho-Rock-Myosin signaling axis determines cell-cell integrity of self-renewing pluripotent stem cells. Plos One, 3(8), e3001.

He, S., Nakada, D. and Morrison, S.J. (2009) Mechanisms of stem cell self-renewal. Annual Review Cell Developmental Biology, 25: 377.

Hogan, B., Barkauskas, C. E., Chapman, H. A., Epstein, J. A. & Jain, R. Hsia, C. et al. (2014). Repair and regeneration of the respiratory system: Complexity, plasticity, and mechanisms of lung stem cell function. Cell Stem Cell, 15(2), 123.

Hothorn, T., Bühlmann, P., Dudoit, S., Molinaro, A. & van der Laan, M.J. (2005). Survival ensembles. Biostatistics, 7(3), 355.

Hothorn, T., Hornik, K. & Zeileis, A. Unbiased Recursive Partitioning: A Conditional Inference Framework J. Comput. Graphical Statistics 15, 651-674 (2006).

Hsu, H., LaFever, L., & Drummond-Barbosa, D (2008). Diet controls normal and

tumorous germline stem cells via insulin-dependent and -independent mechanisms in Drosophila. Developmental Biology, 313(2), 700.

Hulsman M. et al. Acta Biomater. 15, 29-38 (2015).

Hulsman, M., Hulshof, F., Unadkat, H., Papenburg, B. J., Stamatialis, D. F., Truckenmüller, R., et al. (2015). Analysis of high-throughput screening reveals the effect of surface topographies on cellular morphology. Acta Biomaterialia, 15, 29.

Hynes, R. O (2009). The extracellular matrix: not just pretty fibrils. Science, 326(5957), 1216.

James, D (2005). TGF-β/activin/nodal signaling is necessary for the maintenance of pluripotency in human embryonic stem cells. Development, 132(6), 1273.

Jefferis, G. http://CRAN.R-project.org/package=caret (2013).

Jinno, H., Morozova, O., Jones, K. L., Biernaskie, J. A., Paris, M., Hosokawa, R., et al. (2010). Convergent genesis of an adult neural crest-like dermal stem cell from distinct developmental origins. Stem cells, 28(11), 2027.

Kalaskar, D. M., Downes, J. E., Murray, P., Edgar, D. H., & Williams, R. L. (2013). Characterization of the interface between adsorbed fibronectin and human embryonic stem cells. Journal of the Royal Society Interface, 10(83), 20130139.

Katon, W., Kleinman, A., & Rosen, G (1982). Depression and somatization: a review. The American Journal Of Medicine, 72(1), 127.

Kaushal, G. S., Rognoni, E., Lichtenberger, B. M., Driskell, R. R., Kretzschmar, K., Hoste, E., & Watt, F. M (2015). Fate of Prominin-1 Expressing Dermal Papilla Cells during Homeostasis, Wound Healing and Wnt Activation.

Kilian, K. A., Bugarija, B., Lahn, B. T., & Mrksich, M (2010). Geometric cues for directing the differentiation of mesenchymal stem cells. Proceedings Of The National Academy Of Sciences, 107(11), 4872.

Kim, K., Doi, A., Wen, B., Ng, K., Zhao, R., Cahan, P., u. a (2010).

Epigenetic memory in induced pluripotent stem cells. Nature, 467(7313), 285.

Kimura, W., & Sadek, H. A (2012). The cardiac hypoxic niche: emerging role of hypoxic microenvironment in cardiac progenitors. Cardiovascular Diagnosis and Therapy, 2(4), 278.

Kitsberg, D (2007). Human embryonic stem cells for tissue engineering. Tissue Engineering 140. 33.

Klim, J. R., Li, L., Wrighton, P. J., Piekarczyk, M. S., & Kiessling, L. L (2010). A defined glycosaminoglycan-binding substratum for human pluripotent stem cells. Nature Methods, 7(12), 989.

Kobel, S., Limacher, M., Gobaa, S., Laroche, T., & Lutolf, M. P (2009). Micropatterning of hydrogels by soft embossing. Langmuir, 25(15), 8774.

Kojima, Y., Kaufman-Francis, K., Studdert, J. B., Steiner, K. A., Power, M. D., Jones, V., u. a (2014). The transcriptional and functional properties of mouse epiblast stem cells resemble the anterior primitive streak. Cell Stem Cell, 14(1), 107.

Kuang, S., Kuroda, K., Le Grand, F., & Rudnicki, M. A (2007). Asymmetric self-renewal and commitment of satellite stem cells in muscle. Cell, 129(5), 999.

Kuhn, M. http://CRAN.R-project.org/package=caret (2014). Lander, E. S (2011). Initial impact of the sequencing of the human genome. Nature, 470(7333), 187.

Lane, S. W., Williams, D. A., & Watt, F. M (2014). Modulating the stem cell niche for tissue regeneration. Nature Biotechnology, 32(8), 795.

Lang, P., Yeow, K., Nichols, A., & Scheer, A (2006). Cellular imaging in drug discovery. Nature Reviews Drug Discovery, 5(4), 343.

Larue, L., Ohsugi, M., Hirchenhain, J., & Kemler, R (1994). E-cadherin null mutant embryos fail to form a trophectoderm epithelium. Proceedings Of The National Academy Of Sciences, 91(17), 8263.

Li, D., Zhou, J., Wang, L., Shin, M. E., Su, P., Lei, X., et al. (2010). Integrated biochemical and mechanical signals regulate multifaceted human embry-

onic stem cell functions. The Journal Of Cell Biology, 191(3), 631. Li, L., & Clevers, H (2010). Coexistence of quiescent and active adult stem cells in mammals. Science, 327(5965), 542.

Liu, H., & Zhang, S (2011). Specification of neuronal and glial subtypes from human pluripotent stem cells. Cellular And Molecular Life Sciences, 68(24), 3995.

Liu, Z., Tian, L., Liu, S., & Waller, L (2014). Real-time brightfield, darkfield, and phase contrast imaging in a light-emitting diode array microscope. Journal Of Biomedical Optics, 19(10), 106002.

Loh, K. M., Ang, L. T., Zhang, J., Kumar, V., Ang, J., Auyeong, J. Q., u. a (2014). Efficient endoderm induction from human pluripotent stem cells by logically directing signals controlling lineage bifurcations. Cell Stem Cell, 14(2), 237.

Lü, D., Luo, C., Zhang, C., Li, Z., & Long, M (2014). Differential regulation of morphology and stemness of mouse embryonic stem cells by substrate stiffness and topography. Biomaterials, 35(13), 3945.

Luni, C., Serena, E., & Elvassore, N. (2013). Human-on-chip for therapy development and fundamental science. Current Opinion in Biotechnology, 25, 45.

Markert, L., Lovmand, J., & Foss, M (2009). Identification of distinct topographical surface microstructures favoring either undifferentiated expansion or differentiation of murine embryonic stem cells. Stem Cells And Development, 18(9), 1331.

Martí, M., Mulero, L., Pardo, C., Morera, C., Carrió, M., Laricchia-Robbio, L., et al. (2013). Characterization of pluripotent stem cells. Nature Protocols, 8(2), 223.

MartÃ, M., Mulero, L., Pardo, C., Morera, C., Carrió, M., Laricchia-Robbio, L., et al. (2013). Characterization of pluripotent stem cells. Nature Protocols, 8(2), 223.

Martin, G. R (1981). Isolation of a pluripotent cell line from early mouse embryos cultured in medium conditioned by teratocarcinoma stem cells Proceedings Of The National Academy Of Sciences, 78(12), 7634.

Martino, M. M., Briquez, P. S., Maruyama, K., & Hubbell, J. A. (2015).

Extracellular matrix-inspired growth factor delivery systems for bone regeneration. Advanced Drug Delivery Reviews, S0169-409X(15).

Mashinchian, O., Turner, L., Dalby, M. J., Laurent, S., Shokrgozar, M.A. et al. (2015) Regulation of stem cell fate by nanomaterial substrates. Nanomedicine (Lond). 10, 829-847 (2015).

Mashinchian, O., Turner, L., Dalby, M. J., Laurent, S., Shokrgozar, M. A., Bonakdar, S., et al. (2015). Regulation of stem cell fate by nanomaterial substrates. Nanomedicine, 10(5), 829.

McBeath, R., Pirone, D. M., Nelson, C. M., Bhadriraju, K., & Chen, C. S (2004). Cell shape, cytoskeletal tension, and RhoA regulate stem cell lineage commitment. Developmental Cell, 6(4), 483.

McKernan, R., & Watt, F. M (2013). What is the point of large-scale collections of human induced pluripotent stem cells. Nature Biotechnology, 31(12), 1148.

McNeish, J., Gardner, J. P., Wainger, B. J., Woolf, C. J., & Eggan, K (2015). From dish to bedside: lessons learned while translating findings from a stem cell model of disease to a clinical trial. Cell Stem Cell, 17(1), 8.

Mei, Y., Goldberg, M., & Anderson, D (2007). The development of high-throughput screening approaches for stem cell engineering. Current Opinion In Chemical Biology, 11(4), 388.

Mei, Y., Saha, K., Bogatyrev, S. R., Yang, J., Hook, A. L., Kalcioglu, Z. I., et al. (2010). Combinatorial development of biomaterials for clonal growth of human pluripotent stem cells. Nature Materials, 9(9), 768.

Merkle, F. T. & Eggan, K (2013). Modeling human disease with pluripotent stem cells: from genome association to function. Cell Stem Cell, 12(6), 656.

Miklas, J. W., Dallabrida, S. M., Reis, L. A., Ismail, N., Rupnick, M., & Radisic, M (2013). QHREDGS enhances tube formation, metabolism and survival of endothelial cells in collagen-chitosan hydrogels. Plos One, 8(8).

Mogilner, A., Allard, J., & Wollman, R (2012). Cell Polarity: Quantitative Modeling as a Tool in Cell Biology. Science, 336(6078), 175.

Morrison, S. J., & Spradling, A. C (2008). Stem cells and niches: Mechanisms that promote stem cell maintenance throughout life. Cell, 132(4), 598.

Muscari, C., Giordano, E., BonafÃ¨, F., Govoni, M., Pasini, A., & Guarnieri, C (2013). Priming adult stem cells by hypoxic pretreatments for applications in regenerative medicine. Journal Of Biomedical Science, 20(1), 63.

Nagy, A., Gocza, E., Diaz, E. M., Prideaux, V. R., & Ivanyi, E (1990). Embryonic stem cells alone are able to support fetal development in the mouse. Development, 110 (3). 815.

Nakagawa, M., Koyanagi, M., Tanabe, K., Takahashi, K., Ichisaka, T., Aoi, T., et al. (2008). Generation of induced pluripotent stem cells without Myc from mouse and human fibroblasts. Nature Biotechnology, 26(1), 101.

Nampe, D., & Tsutsui, H (2013). Engineered micromechanical cues affecting human pluripotent stem cell regulations and fate. Journal Of Laboratory Automation, 18(6), 482.

Nat. Rev. Mol. Cell Biol. 14, 467-473 (2013).

Nguyen, P. K., Riegler, J., & Wu, J. C (2014). Stem cell imaging: From bench to bedside. Cell Stem Cell, 14(4), 431.

Nichols, J., & Smith, A (2012). Pluripotency in the Embryo and in Culture. Cold Spring Harbor Perspectives In Biology, 4(8), a008128.

Niwa, H (2007). How is pluripotency determined and maintained. Development, 134(4), 635.

Ohtola, J., Myers, J., Akhtar-Zaidi, B., Zuzindlak, D., Sandesara, P., Yeh, K., u. a (2008). -Catenin has sequential roles in the survival and specification of ventral dermis. Development, 135(13), 2321.

Pan, F., Zhang, M., Wu, G., Lai, Y., Greber, B., Schöler, H. R., & Chi, L (2013).

Topographic effect on human induced pluripotent stem cells differentiation towards neuronal lineage. Biomaterials, 34(33), 8131.

Park, I., Zhao, R., West, J. A., Yabuuchi, A., Huo, H., Ince, T. A., et al. (2008). Reprogramming of human somatic cells to pluripotency with defined factors. Nature, 451(7175), 141.

Patel, A. K., Celiz, A. D., Rajamohan, D., Anderson, D. G., Langer, R., Davies, M. C., et al. (2015). A defined synthetic substrate for serum-free culture of human stem cell derived cardiomyocytes with improved functional maturity identified using combinatorial materials microarrays. Biomaterials, 61, 257.

R Core Team. http://www.R-project.org/ (2014).

Ranga, A., Gobaa, S., Okawa, Y., Mosiewicz, K., Negro, A., & Lutolf, M. P (2014). 3D niche microarrays for systems-level analyses of cell fate. Nature Communications, 5.

Reardon, S. (2015). 'Organs-on-chips' go mainstream. Nature, 523(7560), 266.

Recknor, J. B., Sakaguchi, D. S., & Mallapragada, S. K (2006). Directed growth and selective differentiation of neural progenitor cells on micropatterned polymer substrates. Biomaterials, 27(22), 4098.

Reimer A, Seiler K, Tornack J, Tsuneto M & Melchers F (2012). Reprogramming to iPS cells and their subsequent hematopoietic differentiation is more efficient from MEFs than from preB cells. Immunology Letters, 143(1), 70.

Reya, T., Duncan, A. W., Ailles, L., Domen, J., Scherer, D. C., Willert, K., et al. (2003). A role for Wnt signalling in self-renewal of haematopoietic stem cells. Nature, 423(6938), 409.

Rinn, J. L., Bondre, C., Gladstone, H. B., Brown, P. O., & Chang, H. Y (2006). Anatomic demarcation by positional variation in fibroblast gene expression programs. Plos Genetics, 2(7), 119.

Rompolas, P., Mesa, K. R., & Greco, V (2013). Spatial organization within a niche

as a determinant of stem-cell fate. Nature, 502(7472), 513.

Rowland, T. J., Miller, L. M., Blaschke, A. J., Doss, E. L., Bonham, A. J., Hikita, S. T., et al. (2010). Roles of integrins in human induced pluripotent stem cell growth on matrigel and vitronectin. Stem Cells And Development, 19(8), 1231.

Ruoslahti, E (1991). Integrins. Journal Of Clinical Investigation, 87(1), 1. Russell, E (1985). A history of mouse genetics. Annual Review Of Genetics, 19(1), 1.

Saha, K., Mei, Y., Reisterer, C. M., Pyzocha, N. K., Yang, J., Muffat, J., et al. (2011). Surface-engineered substrates for improved human pluripotent stem cell culture under fully defined conditions. Proceedings Of The National Academy Of Sciences, 108(46), 18714.

Saha, K., Mei, Y., Reisterer, C. M., Pyzocha, N. K., Yang, J., Muffat, J., et al. (2011).

Sahai, E., & Marshall, C. J (2002). ROCK and Dia have opposing effects on adherens junctions downstream of Rho. Nature Cell Biology, 4(6), 408.

Sailem, H., Bousgouni, V., Cooper, S., & Bakal, C (2014). Cross-talk between Rho and Rac GTPases drives deterministic exploration of cellular shape space and morphological heterogeneity. Open Biology, 4(1), 130132.

Salic, A., & Mitchison, T. J (2008). A chemical method for fast and sensitive detection of DNA synthesis in vivo. Proceedings Of The National Academy Of Sciences, 105(7), 2415.

Samavarchi-Tehrani, P., Golipour, A., David, L., Sung, H., Beyer, T. A., Datti, A., et al. (2010). Functional genomics reveals a BMP-driven mesenchymal-to-epithelial transition in the initiation of somatic cell reprogramming. Cell Stem Cell, 7(1). 64.

Scadden, D. T (2014). Nice neighborhood: emerging concepts of the stem cell niche. Cell, 157(1), 41.

Schofield, R. (1978). The relationship between the spleen colony-forming cell and the haemopoietic stem cell. Blood Cells 4, 7.

Shahzad, K., & Loor, J. J (2012). Application of Top-Down and Bottom-up Systems Approaches in Ruminant Physiology and Metabolism. Current Genomics, 13(5), 379.

Sigg, C. https://cran.r-project.org/web/packages/nsprcomp/index.html (2014).

Silva-Vargas, V., Celso, Lo, C., Giangreco, A., Ofstad, T., Prowse, D. M., Braun, K. M., & Watt, F. M (2005). β-Catenin and hedgehog signal strength can specify number and location of hair follicles in adult epidermis without recruitment of bulge stem cells. Developmental Cell, 9(1), 121.

Singh, A. M., Reynolds, D., Cliff, T., Ohtsuka, S., Mattheyses, A. L., Sun, Y., et al. (2012). Signaling network crosstalk in human pluripotent cells: A smad2/3-regulated switch that controls the balance between self-renewal and differentiation. Cell Stem Cell, 10(3), 312.

Speth, J.M., Hoggatt, J., Singh, P. & Pelus, L.M (2014). Pharmacologic increase in HIF1alpha enhances hematopoietic stem and progenitor homing and engraftment. Blood 123, 203.

Stadtfeld, M., Brennand, K., & Hochedlinger, K (2008). Reprogramming of pancreatic β cells into induced pluripotent stem cells. Current Biology, 18(12), 890.

Suh, H., Consiglio, A., Ray, J., Sawai, T., D'Amour, K. A., & Gage, F. H (2007). In vivo fate analysis reveals the multipotent and self-renewal capacities of Sox-2+ neural stem cells in the adult hippocampus. Cell Stem Cell, 1(5), 515.

Surface-engineered substrates for improved human pluripotent stem cell culture under fully defined conditions. Proceedings Of The National Academy Of Sciences, 108(46), 18714.

Takahashi, K., & Yamanaka, S (2006). Induction of pluripotent stem cells from mouse embryonic and adult fibroblast cultures by defined factors. Cell, 126(4), 663.

Takashima, Y., Guo, G., Loos, R., Nichols, J., Ficz, G., Krueger, F., et al. (2014). Resetting transcription factor control circuitry toward ground-state pluripotency in

human. Cell, 158(6), 1254.

Tan, J. L., Tien, J., Pirone, D. M., Gray, D. S., Bhadriraju, K., & Chen, C. S. (2003). Cells lying on a bed of microneedles: an approach to isolate mechanical force. Proceedings of the National Academy of Sciences, 100(4), 1484.

Tan, J. L., Tien, J., Pirone, D. M., Gray, D. S., Bhadriraju, K., & Chen, C. S (2003). Cells lying on a bed of microneedles: An approach to isolate mechanical force. Proceedings Of The National Academy Of Sciences, 100(4), 1484.

Tanimura, S., Tadokoro, Y., Inomata, K., Binh, N. T., Nishie, W., Yamazaki, S., u. a (2011). Hair Follicle Stem Cells Provide a Functional Niche for Melanocyte Stem Cells. Cell Stem Cell, 8(2).

Tesar, P. J., Chenoweth, J. G., Brook, F. A., Davies, T. J., Evans, E. P., Mack, D. L., et al. (2007). New cell lines from mouse epiblast share defining features with human embryonic stem cells. Nature, 448(7150), 196. Thernea, T., Atkinson, B. & Ripley, B. http://CRAN.R-project.org/package=rpart (2014).

Thiers, B. H (2008). Induced pluripotent stem cell lines derived from human somatic cells. Yearbook Of Dermatology And Dermatologic Surgery, 2008, 301. Thomson, J. A (1998). Embryonic Stem Cell Lines Derived from Human Blastocysts. Science, 282(5391), 1145.

Toh, Y., Xing, J., & Yu, H (2015). Modulation of integrin and E-cadherin-mediated adhesions to spatially control heterogeneity in human pluripotent stem cell differentiation. Biomaterials, 50, 87.

Tomlin, C. J., & Axelrod, J. D (2007). Biology by numbers: mathematical modelling in developmental biology. Nature Reviews Genetics, 8(5), 331.

Torres, J., & Watt, F. M (2008). Nanog maintains pluripotency of mouse embryonic stem cells by inhibiting NFÎºB and cooperating with Stat3. Nature Cell Biology, 10(2), 194.

Trappmann, B., Gautrot, J. E., Connelly, J. T., Strange, D. G. T., Li, Y., Oyen,

M. L., et al. (2012). Extracellular-matrix tethering regulates stem-cell fate. Nature Materials, 11(7), 642.

Treiser, M. D., Yang, E. H., Gordonov, S., Cohen, D. M., Androulakis, I. P., Kohn, J., et al. (2010). Cytoskeleton-based forecasting of stem cell lineage fates. Proceedings Of The National Academy Of Sciences, 107(2), 610.

Tsakiridis, A., Huang, Y., Blin, G., Skylaki, S., Wymeersch, F., Osorno, R., et al. (2014). Distinct Wnt-driven primitive streak-like populations reflect in vivo lineage precursors. Development, 141(6), 1209.

Turing, A. M (1952). The chemical basis of morphogenesis. Transactions Of The Royal Society Of London. 237 (641): 37.

Unadkat, H. V., Hulsman, M., Cornelissen, K., Papenburg, B. J., Truckenmuller, R. K., Carpenter, A. E., et al. (2011). An algorithm-based topographical biomaterials library to instruct cell fate. Proceedings Of The National Academy Of Sciences, 108(40), 16565.

Unadkat, H. V., Hulsman, M., Cornelissen, K., Papenburg, B. J., Truckenmuller, R. K., Carpenter, A. E., et al. (2011). An algorithm-based topographical biomaterials library to instruct cell fate. Proceedings Of The National Academy Of Sciences, 108(40), 16565.

Unadkat, H. V., Hulsman, M., Cornelissen, K., Papenburg, B. J., Truckenmuller, R. K., Carpenter, A. E., et al. (2011). An algorithm-based topographical biomaterials library to instruct cell fate. Proceedings Of The National Academy Of Sciences, 108(40), 16565.

Vaziri, C., & Faller, D. V. (1996). Down-regulation of platelet-derived growth factor receptor expression during terminal differentiation of 3T3-L1 pre-adipocyte fibroblasts. Journal of Biological Chemistry, 272(5), 2762.

Villa-Diaz, L. G., Torisawa, Y., Uchida, T., Ding, J., Nogueira-de-Souza, N. C., O'Shea, K. S., et al. (2009). Microfluidic culture of single human embryonic stem

cell colonies. Lab Chip, 9(12), 1749.

Wagers, A. J (2012). The ctem cell niche in regenerative medicine. Cell Stem Cell, 10(4), 362.

Ware, C. B., Nelson, A. M., Mecham, B., Hesson, J., Zhou, W., Jonlin, E. C., et al. (2014). Derivation of naive human embryonic stem cells. Proceedings Of The National Academy Of Sciences, 111(12), 4484.

Watt, F. M (2000). Out of Eden: Stem Cells and Their Niches. Science, 287(5457), 1427.

Watt, F. M (2002). Role of integrins in regulating epidermal adhesion, growth and differentiation. The EMBO Journal, 21(15), 3919.

Watt, F. M (2014). Mammalian skin cell biology: At the interface between laboratory and clinic. Science, 346(6212), 937.

Watt, F. M., & Huck, W (2013). Role of the extracellular matrix in regulating stem cell fate. Nature Reviews Molecular Cell Biology. 14, 467.

Watt, F. M., Estrach, S., & Ambler, C. A (2008). Epidermal Notch signaling: differentiation, cancer and adhesion. Current Opinion In Cell Biology, 20(2), 171.

Watt, F. M., Jordan, P. W., & O'Neill, C. H (1988). Cell shape controls terminal differentiation of human epidermal keratinocytes. Proceedings Of The National Academy Of Sciences, 85(15), 5576.

Watt, F.M. & Huck, W.T. Role of the extracellular matrix in regulating stem cell fate.

Watt, F.M. (1998) Epidermal stem cells: markers, patterning and the control of stem cell fate. Philosophical Transactions of the Royal Society B: Biological Sciences, 353(1370), 831.

Weber, G. F., Bjerke, M. A., & DeSimone, D. W (2011). Integrins and cadherins join forces to form adhesive networks. Journal Of Cell Science, 124(8), 1183.

Wong, C. E., Paratore, C., Dours-Zimmermann, M. T., Rochat, A., Pietri, T., Suter,

U., et al. (2006). Neural crest-derived cells with stem cell features can be traced back to multiple lineages in the adult skin. The Journal Of Cell Biology, 175(6), 1005.

Wong, S., Shim, M. S., & Kwon, Y. J (2014). Synthetically designed peptide-based biomaterials with stimuli-responsive and membrane-active properties for biomedical applications. J. Mater. Chem. B, 2(6), 595.

Yamanaka, S (2012). Induced Pluripotent Stem Cells: Past, Present, and Future. Cell Stem Cell, 10(6), 678.

Yin, Z., Sadok, A., Sailem, H., McCarthy, A., Xia, X., Li, F., et al. (2013). A screen for morphological complexity identifies regulators of switch-like transitions between discrete cell shapes. Nature Cell Biology, 15(7), 860.

Ying, Q., Nichols, J., Chambers, I., & Smith, A (2003). BMP induction of Id proteins suppresses differentiation and sustains embryonic stem cell self-renewal in collaboration with STAT3. Cell, 115(3), 281.

Yu, J., Vodyanik, M. A., & Smuga, K (2007). Induced pluripotent stem cell lines derived from human somatic cells. Science. 318 (5858), 1917.

Yusa, K., Rashid, S. T., Strick-Marchand, H., Varela, I., Liu, P., Paschon, D. E., et al. (2011). Targeted gene correction of α1-antitrypsin deficiency in induced pluripotent stem cells. Nature, 478(7369), 391.

Zambrowicz, B. P., & Sands, A. T (2003). Knockouts model the 100 best-selling drugs-will they model the next 100. Nature Reviews Drug Discovery. 2, 38.

Zhao, C., Deng, W., & Gage, F. H (2008). Mechanisms and functional implications of adult neurogenesis. Cell, 132(4), 645.